A global analysis of controls on submarine-canyon geomorphology

Laura H. Bührig*, Luca Colombera, Marco Patacci, Nigel P. Mountney and William D. McCaffrey

School of Earth and Environment, University of Leeds, LS2 9JT, United Kingdom

*corresponding author: lhbuehrig@gmail.com

Twitter handle:

Laura H. Bührig @BuehrigLaura

This manuscript is a non-peer reviewed EarthArXiv preprint submitted for publication in Earth-Science Reviews.

A global analysis of controls on submarine-canyon geomorphology

Laura H. Bührig, Luca Colombera, Marco Patacci, Nigel P. Mountney and William D. McCaffrey

School of Earth and Environment, University of Leeds, LS2 9JT, United Kingdom (Email: lhbuehrig@gmail.com)

ABSTRACT

The role of possible controlling factors in influencing the geomorphology of submarine canyons has been investigated using a database of 282 globally distributed modern examples collated from the literature, open-source worldwide bathymetry and satellite imagery. Canyon geomorphology has been characterized quantitatively in terms of maximum and average canyon dimensions, canyon sinuosity, the average canyon thalweg gradient, and maximum canyon sidewall steepness. Geomorphological variations with respect to position of the canyon apex relative to the shelf break, continental-margin type, terrestrial source-to-sink system setting, oceanographic environment, and climate zones have been assessed. Scaling relationships between canyon morphometric parameters, and between them and attributes of their physiographic setting, their terrestrial catchments, and attributes of continental shelves and slopes have been quantified.

Key findings are as follows: (i) a number of scaling relationships describing canyon morphometry (e.g. scaling between maximum canyon dimensions, relationships of maximum canyon sidewall steepness with maximum canyon width and depth) can be recognized globally, suggesting their general predictive value; (ii) possible causal links are identified between hydrodynamic processes (e.g. upwelling, longshore- and along-slope currents) and

canyon morphology; (iii) potential predictors of canyon geomorphology include whether a canyon is incised into the shelf or confined to the slope, the continental-margin type, the oceanographic environment, latitude, and shelf-break depth; (iv) similarity in maximum width-to-maximum depth ratios across all settings suggests that the relative magnitudes of canyon-margin erosion and intra-canyon deposition do not vary greatly depending on setting or canyon size.

The relationships between canyon geomorphology and environmental variables identified in this study may be incorporated into conceptual models describing canyon geomorphology and its relationship to other elements of deep-water systems, and into its broader source-to-sink context.

Keywords: Quantitative analysis, scaling relationships, geometry, source-to-sink, deep marine, continental slope

1 Introduction

Submarine canyons constitute conduits for the transfer of water masses, sediment, nutrients, organic matter and pollutants between shallow- and deep-marine environments, across continental slopes (Harris and Whiteway, 2011; Fildani, 2017). As such, they are important parts of sediment routing systems, facilitating the transport of sediment across continental margins to slope and basin-floor settings. Submarine canyons form large-scale erosional features through which flows pass in a manner that enables the sorting and segregation of sediments that are ultimately deposited in deep-marine environments (Sweet et al., 2020); they intercept and influence oceanic currents along shelves (e.g. Jordi et al., 2008) and slopes (e.g. Marchès et al., 2007; Voigt et al., 2013), and can modify hydrodynamic conditions on continental shelves in vicinity of their location (e.g. Allen et al., 2001; Connolly and Hickey, 2014); they can increase salinity of shelf waters via upwelling of deeper slope waters (e.g. Connolly and Hickey, 2014); they can influence the formation of gas hydrates

(Crutchley et al., 2017) and the associated processes of trapping and release of hydrocarbons (e.g. Davies et al., 2012, Benjamin et al., 2015); they can promote salt migration within the subsurface and impact the geometry of salt bodies (Fiduk, 1995); and they can tap into groundwater aquifers (e.g. Paldor et al., 2020). The association of submarine canyons with hydrocarbon-bearing deposits can promote vertical hydrocarbon migration and its expulsion, which can generate trains of pockmarks in younger canyons (e.g. Benjamin et al., 2015). Pockmarks can also form atop of canyon fills as a result of sediment compaction (e.g. Jobe et al., 2011). Given that these structures can reach diameters of several hundred metres and depths of tens of metres (e.g. Jobe et al., 2011; Benjamin et al., 2015), their presence might affect canyon internal flows and flow pathways on the seafloor.

Submarine canyons can impact the formation and evolution of slope systems by reducing local gradients (Orange et al., 1994), capturing and redirecting sediment pathways from adjacent canyons (e.g. Bernhardt et al., 2015), and functioning as tributaries to other canyons (e.g. Mountjoy et al., 2009). Buried canyons that are partially infilled can influence the pathways of younger ones by forming negative seafloor topography that can confine sediment transport (e.g. Pratson et al., 1994).

Submarine canyons are also important for faunal communities, for which they provide significant habitats. Aspects related to their physiography have been suggested to exert control on the biodiversity and abundance of faunal assemblages; these aspects include canyon spacing, gradient, dendricity and sinuosity (Fanelli et al., 2018), canyon size and magnitude of incision of the shelf (Santora et al., 2018). The effect of submarine-canyon geomorphology on hydrodynamic processes also impacts the spatial distribution of faunal communities like zooplankton (Allen et al., 2001).

Submarine canyons are linked to potential geohazards, due to the ability of intra-canyon slope failures to trigger tsunamis (e.g. Orange et al., 1994; Power et al., 2016), and to the influence of canyon geomorphology on tsunami propagation (e.g. Aranguiz and Shibayama,

2013; Iglesias et al., 2014). Moreover, canyon-crossing seafloor telecommunication cables are at risk of breakage from canyon-margin failure and sediment gravity flows passing through canyons (e.g. Heezen and Ewing, 1952; Hsu et al., 2008; Carter et al., 2014). Such flows are also considered responsible for the displacement of marine pipelines (e.g. Porcile et al., 2020), hence posing a hazard for hydrocarbon leakages.

The sedimentary fills of submarine canyons, and their linkage to down-system submarine fans (e.g. Covault, 2011b; Jobe et al., 2011) and contourite-drift systems (e.g. Wang et al., 2018; Warratz et al., 2019), make them important references and targets for hydrocarbon exploration. Canyons can represent significant sinks for both macro- (e.g. Zhong & Peng, 2021) and micropollutants (e.g. Azaroff et al., 2020).

The study of submarine canyons represents a key area of interest for research linked to a broad range of scientific disciplines (Matos et al., 2018). However, the relative importance of environmental factors on canyon geomorphology has hitherto not been investigated in a comparative study of global scale (see section 2.2).

Quantified insights on canyon geomorphologies from the study of modern systems can aid in the reconstruction of ancient deep-water sedimentary successions and in predicting canyon evolution in modern systems. Given the important role of modern submarine canyons for marine ecosystems, and their potential geohazard risk, a better understanding of how canyon systems respond to external forcings is important in the development of strategies for canyon conservation (see Fernandez-Arcaya et al., 2017), and assessment of their geohazard risk.

The aim of this study is to improve our understanding of controlling factors on submarine-canyon geomorphology. A database has been built to support the following research objectives: (i) to characterize the morphometric parameters of submarine canyons, both globally and with consideration of the role of environmental factors (canyon-apex location relative to the shelf-break, continental-margin type, source-to-sink system setting, oceanographic environment and climate zones); (ii) to establish relationships between

canyon morphometric parameters; (iii) to elucidate, demonstrate and explain relationships between canyon morphometric parameters and external parameters, including canyon bathymetry, distance between the canyon apex and the shoreline, parameters of the catchment, shelf and slope, and latitude of the canyon.

2 Background

2.1 Controls on submarine canyon evolution

Submarine canyons are highly complex sedimentary systems whose evolution is influenced by a wide range of processes and environmental factors (e.g. Shepard, 1936, 1981; Pratson and Coakley, 1996; Pratson et al., 2007; Puig et al., 2014 and references therein).

Various physiographic and environmental factors are known to influence canyon evolution by exerting controls on connectivity to sediment sources, on mechanisms of sediment distribution, and on types of canyon evolutionary processes. Physiographic factors that have been invoked include the distance of the canyon to fluvial outlets and littoral cells (e.g. Sweet and Blum, 2016; Sweet et al., 2020), shelf width in the vicinity of the canyon (e.g. Covault and Graham, 2010; Jipa and Panin, 2020), and continental-slope gradients (e.g. McGregor, 1983; Orange et al., 1994; Lo Iacono et al., 2014). Environmental factors comprise local- and regional-scale tectonics (e.g. Ratzov et al., 2012; Micallef et al., 2014; Almeida et al., 2015), sea-level fluctuations (e.g. Rasmussen, 1994; Mitchell et al., 2007), and climate (e.g. Henrich et al., 2010).

It has been shown that anthropogenic influence can variously affect the evolution of modern submarine canyons. Sediment gravity flows can be triggered by trawling (e.g. Palanques et al., 2006; Lopez-Fernandez et al., 2013). Farming and deforestation (e.g. Milliman and Farnsworth, 2011), artificial diversion (e.g. Higgins et al., 2018) or damming of rivers (e.g. Sheng et al., 2019) may impact catchments and fluvial discharge rates, which in turn can govern mechanisms of sediment distribution to submarine canyons (e.g. Mazières et al., 2014; Puig et al., 2017).

2.2 Submarine canyon studies

Submarine canyons have been the subject of many prior studies: Matos et al. (2018) conducted a review of the scientific literature on submarine canyons published between 1929 and 2016, considering 1,968 publications. These authors identified a geographical bias in prior canyon research: less than 10% of the canyons mapped globally by Harris et al. (2014) are covered by the literature, and almost half of the 1,968 publications concentrate exclusively on 11 intensively studied submarine canyons. Consequently, research efforts have largely been directed towards the particular environmental conditions and set of controls associated with a limited subset of canyons. However, the rate at which studies on submarine canyons are published has further accelerated in recent years (Matos et al., 2018), likely due in part to technological advances in data acquisition and processing (e.g. Xu, 2011; Urías Espinosa et al., 2016; Simmons et al., 2020; Bailey et al., 2021).

Despite being well studied, the genesis and long-term evolution of submarine canyons remain topics of ongoing debate and require further understanding (e.g. Pratson et al., 2007 and references therein; Baztan et al., 2005; Puig et al., 2014; Smith et al., 2017, 2018). Canyon classification schemes based on case studies from specific regions have been proposed to be universally applicable, for example where specific sets of controls are associated with a canyon (canyon-head location relative to the shelf break, type of intracanyon sedimentary processes, sediment sources and sediment characteristics; cf. Jobe et al., 2011), and models for canyon evolution have been considered relevant to canyons that developed under similar external controls, as for canyons associated with active margins (e.g. Micallef et al., 2014). A quantitative assessment of canyon geomorphology on a global scale can augment the findings of these studies.

For the interpretation of autogenic and allogenic controls on canyon geomorphology, an improved understanding of the sensitivity of canyon morphometric parameters to seafloor processes and environmental factors is required. Previous global-scale studies that investigated submarine canyon geomorphology (e.g. Nelson, 1970; De Pippo et al., 1999;

Sømme et al. 2009; Covault et al. 2011a; Harris and Whiteway, 2011) constitute important contributions to a fuller understanding of submarine canyon evolution. Nevertheless, global investigations of the geomorphology of modern submarine canyons have been limited to individual canyon morphometric parameters and to consideration of specific environmental controls, with the datasets being limited in terms of their geographic coverage prior to the advent of a global inventory of modern submarine canyons – comprising 5,849 canyons – compiled by Harris and Whiteway (2011).

Source-to-sink (S2S) research investigates sediment budget dynamics and process-response relationships in both ancient and modern sedimentary systems. Scaling relationships between sedimentary systems and attributes of segments of the S2S profile are commonly established. These relationships can aid in the reconstruction and prediction of characteristics of sedimentary systems and their associated S2S system, chiefly their geometry and scale (e.g. Sømme et al., 2009; Martinsen et al., 2010; Nyberg et al., 2018). The focus of such studies has been primarily on fluvial systems and submarine fans (e.g. Sømme et al., 2009; Nyberg et al., 2018), whereas submarine canyons remain relatively understudied.

From this, the following issues arise:

(i) Relationships between different canyon morphometric parameters have not yet been fully investigated over a global dataset; whether such relationships are universal or limited to specific environmental settings remains unknown.

(ii) The extent to which, and manner in which, individual canyon morphometric parameters are affected by external and environmental factors is unclear.

This study addresses these knowledge gaps. A fundamental knowledge of these factors (i) will aid in the development and validation of both conceptual and numerical models of submarine canyons, deep-water systems, and their superordinate S2S systems, (ii) will

support the reconstruction and interpretation of Quaternary and ancient canyon systems, and (iii) could assist in the prediction of how modern submarine canyons may evolve.

3 Dataset and methodology

A database was collated that stores data describing the geomorphology of submarine canyons, their environmental context and geological controlling factors. Data have been sourced from 282 globally distributed modern submarine canyons and have been grouped into 96 separate case studies, with each case study corresponding to the study of one or several submarine canyons by a particular group of researchers (Fig 1. and Tab. 1). The database comprises literature-derived, high-resolution bathymetric surveys of the seabed and high-resolution seismic datasets of the shallow subsurface, derived from 135 publications (Tab. 1) and open-source worldwide bathymetry data sets (GEBCO 2019 NOAA NCEI Visualization; Google Earth).

A.

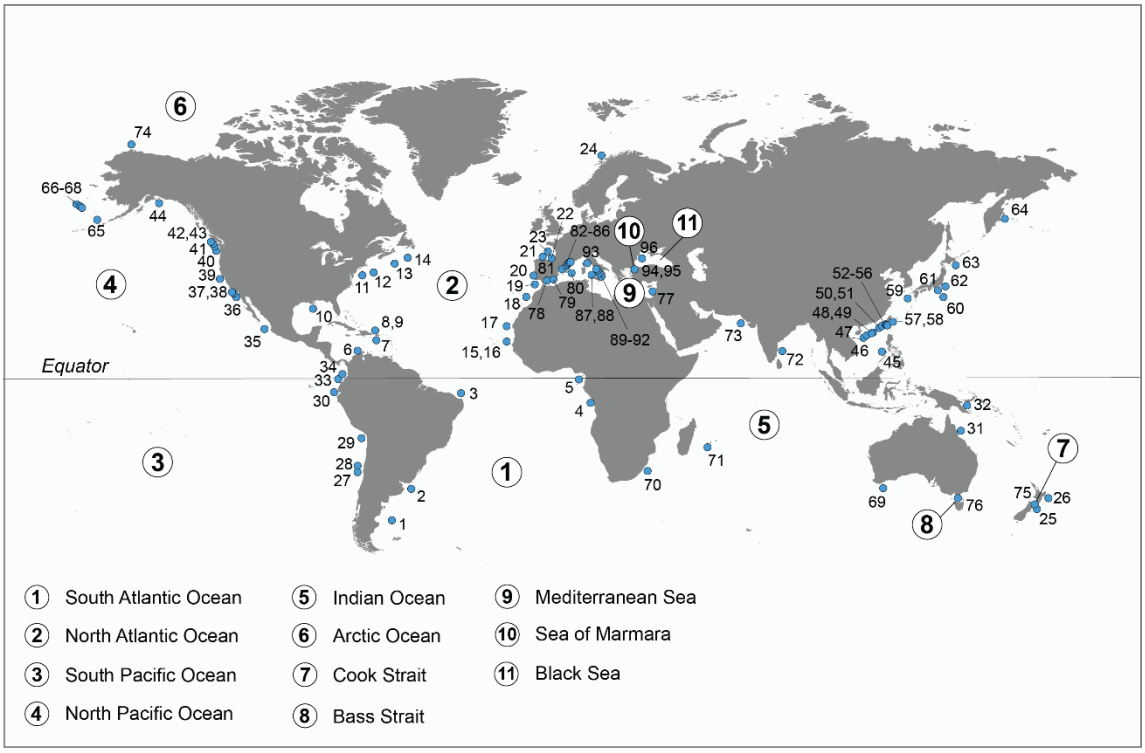

B.

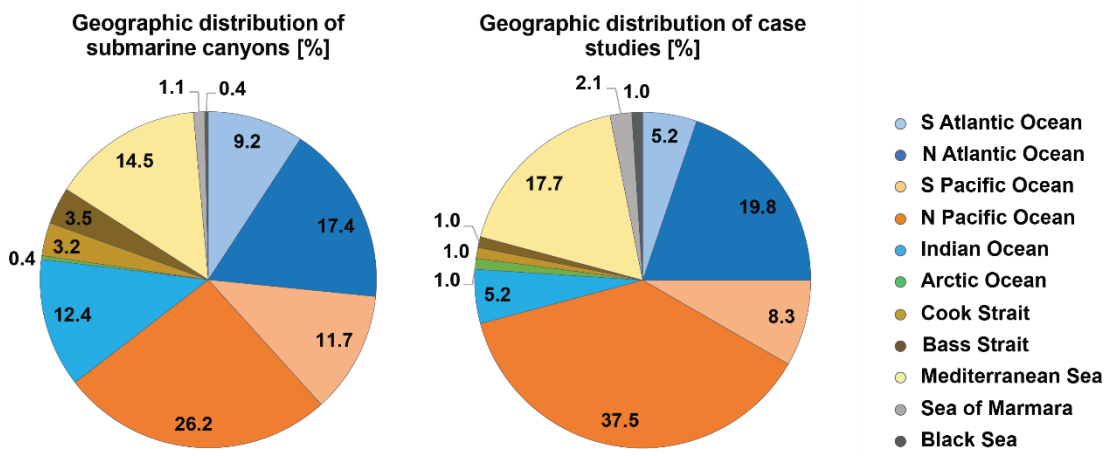

Figure 1: A. Overview map of distribution of the 96 case studies. B. Geographic distribution of the 96 case studies and 282 studied submarine canyons (World map from freevectormaps.com).

ID	Case study	No. of canyons	Oceanic region	Reference(s)
1	Patagonia canyons, SE Argentina	8	South Atlantic Ocean	*Lastras et al., 2011a*

2	Mar del Plata Canyon, E Argentina	1	South Atlantic Ocean	*Krastel et al., 2011; Warratz et al., 2019*
3	Potiguar Basin canyons, NE Brazil	14	South Atlantic Ocean	*de Almeida et al., 2015*
4	Congo Canyon, W Democratic Republic of Congo	1	South Atlantic Ocean	*Babonneau et al., 2002; Ferry et al., 2004*
5	Avon and Mahin canyons, SW Nigeria	2	South Atlantic Ocean	*Jimoh et al., 2018*
6	Aguja Canyon, N Colombia	1	North Atlantic Ocean (Caribbean Sea)	*Restrepo-Correa and Ojeda, 2010*
7	Guayanilla canyon system, S Puerto Rico	4	North Atlantic Ocean (Caribbean Sea)	*Trumbull and Garrison, 1973*
8	Arecibo and Quebradillas canyons, NW Puerto Rico	2	North Atlantic Ocean	*Gardner et al., 1980*
9	Mona Canyon, NW Puerto Rico	1	North Atlantic Ocean	*Mondziel et al., 2010*
10	Mississippi Canyon, S USA	1	North Atlantic Ocean (Gulf of Mexico)	*Coleman et al., 1982*
11	Hudson Canyon, NE USA	1	North Atlantic Ocean	*Rona et al., 2015*
12	Lydonia and Oceanographer canyons, NE USA	2	North Atlantic Ocean	*Valentine et al., 1980*
13	Logan Canyon, SE Canada	1	North Atlantic Ocean	*Li et al., 2019*
14	SW Grand Banks Slope canyons, SE Canada	3	North Atlantic Ocean	*Armitage et al., 2010*
15	Dakar Canyon, W Senegal	1	North Atlantic Ocean	*Pierau et al., 2010, 2011*
16	Cayar Canyon, W Senegal	1	North Atlantic Ocean	*Dietz et al., 1968*
17	Timiris Canyon, NW Mauritania	1	North Atlantic Ocean	*Krastel et al., 2004; Antobreh and Krastel, 2006*
18	Agadir Canyon	1	North Atlantic Ocean	*Ercilla et al., 1998; Wynn et al., 2002*
19	Faro and Portimao canyons, SW Portugal	2	North Atlantic Ocean (Gulf of Cadiz)	*Mulder et al., 2006*
20	Nazaré, Cascais and Setubal-Lisbon canyons, W Portugal	4	North Atlantic Ocean	*Arzola et al., 2008; Lastras et al., 2009; Allin et al., 2016*
21	Aviles Canyon system and Navia canyon, N Spain	5	North Atlantic Ocean (Bay of Biscay)	*Goméz-Ballesteros et al., 2014*
22	Capbreton Canyon, SW France	1	North Atlantic Ocean (Bay of Biscay)	*Mazières et al., 2014*
23	Audierne and Blackmud canyons, SW France	2	North Atlantic Ocean (Bay of Biscay)	*Mulder et al., 2012*
24	Lofoten-Vesterålen canyons (incl. Andøya Canyon), NW Norway	15	North Atlantic Ocean	*Rise et al., 2013*
25	Kaikoura Canyon, E New Zealand	1	South Pacific Ocean	*Lewis and Barnes, 1999*
26	Lachlan Canyon, NE New Zealand	1	South Pacific Ocean	*Walsh et al., 2007*
27	Biobío Canyon system, SW Chile	2	South Pacific Ocean	*Bernhardt et al., 2015*
28	San Antonio Canyon, NW Chile	1	South Pacific Ocean	*Hagen et al., 1996; Laursen and Normark, 2002*
29	E Arequipa Basin canyons, NW Chile	3	South Pacific Ocean	*Hagen et al., 1994*
30	Guayaquil and Santa Elena canyons, NW Equador	2	South Pacific Ocean	*Michaud et al., 2015*
31	N Great Barrier Reef canyons, NE Australia	15	South Pacific Ocean (Coral Sea)	*Puga-Bernabeu et al., 2011*
32	Solomon Sea canyons, E and SE Papua New Guinea	8	South Pacific Ocean (Solomon Sea)	*Davies et al., 1987; Galewsky and Silver, 1997*
33	Esmeraldas Canyon, NW Ecuador	1	North Pacific Ocean	*Michaud et al., 2015*
34	Mira and Patia canyons, SW Colombia	2	North Pacific Ocean	*Ratzov et al., 2012*

35	Ipala Canyon, W Mexico	1	North Pacific Ocean (South China Sea)	*Urías Espinosa et al., 2016*
36	La Jolla and Scripps canyons, SW USA	2	North Pacific Ocean	*Le Dantec et al., 2010; Paull et al., 2013*
37	Redondo, Santa Monica and Dume canyons, SW USA	3	North Pacific Ocean	*Gardner et al., 2003; Tubau et al., 2015*
38	Mugu and Hueneme canyons, SW USA	2	North Pacific Ocean	*Piper et al., 1999;*
39	Monterey and Soquel canyons, SW USA	2	North Pacific Ocean	*Greene et al., 2002; Xu and Noble, 2009*
40	Astoria Canyon, NW USA	1	North Pacific Ocean	*Hickey, 1997; Bosley et al., 2004*
41	Quinault Canyon, NW USA	1	North Pacific Ocean	*Baker and Hickey, 1986; Carson et al., 1986*
42	Juan de Fuca Canyon, NW USA	1	North Pacific Ocean (heads in the Juan de Fuca Strait)	*Alford and MacCready, 2014*
43	Barkley Canyon, SW Canada	1	North Pacific Ocean	*Allen et al., 2001*
44	Tarr Canyon, NW USA	1	North Pacific Ocean (Gulf of Alaska)	*Carlson et al., 1990*
45	North Palawan Canyon, S China	1	North Pacific Ocean (South China Sea)	*Yin et al., 2018*
46	Modern Central Canyon, S China	1	North Pacific Ocean (South China Sea)	*Su et al., 2015*
47	3 canyons and 4 gullies, S China	3 (4)	North Pacific Ocean (South China Sea)	*Chen et al., 2017*
48	Pearl River Mouth Basin canyons, S China	17	North Pacific Ocean (South China Sea)	*Han et al., 2010; Su et al., 2020*
49	Zhujiang/Pearl River Canyon, S China	1	North Pacific Ocean (South China Sea)	*Han et al., 2010; Ding et al., 2013*
50	Dongsha Canyon	1	North Pacific Ocean (South China Sea)	*Yin et al., 2015*
51	Taiwan Canyon, SW Taiwan	1	North Pacific Ocean (South China Sea)	*Xu et al., 2014*
52	Hongtsai Canyon, SW Taiwan	1	North Pacific Ocean (South China Sea)	*Yu and Chiang, 1995*
53	Fangliao Canyon, SW Taiwan	1	North Pacific Ocean (South China Sea)	*Yu and Lu, 1995; Chiang et al., 2012*
54	Gaoping/Kaoping Canyon, SW Taiwan	1	North Pacific Ocean (South China Sea)	*Chiang and Yu, 2006; Liu et al., 2016*
55	Kaohsiung Canyon, SW Taiwan	1	North Pacific Ocean (South China Sea)	*Yu et al., 1992*
56	Penghu Canyon, SW Taiwan	1	North Pacific Ocean (South China Sea)	*Yu and Chang, 2002; Hsiung and Yu, 2011; Su et al., 2015*
57	Taitung Canyon, SE Taiwan	1	North Pacific Ocean (Philippine Sea)	*Schnuerle et al., 1998*
58	Hualien Canyon, SE Taiwan	1	North Pacific Ocean (Philippine Sea)	*Hsiung et al., 2017*
59	Goto Canyon, SW Japan	1	North Pacific Ocean (East China Sea)	*Oiwane et al., 2011*
60	Aoga Shima Canyon, SE Japan	1	North Pacific Ocean (Philippine Sea)	*Klaus and Taylor, 1991*
61	Tenryu Canyon, SE Japan	1	North Pacific Ocean	*Soh and Tokuyama, 2002*
62	Boso Canyon, SE Japan	1	North Pacific Ocean	*Soh et al., 1990*
63	Kushiro Canyon, NE Japan	1	North Pacific Ocean	*Noda et al., 2008; Noda and Tuzino, 2010; Tuzino and Noda, 2010*
64	Submarine canyons of Kamchatka, NE Russia	7	North Pacific Ocean	*Gnibidenko and Svarichevskaya, 1984*
65	Bering Canyon, Bering Sea	1	North Pacific Ocean (Bering Sea)	*Carlson and Karl, 1988; Harris and Whiteway, 2011*
66	Zhemchug, Pervenets and Navarin canyons, Bering Sea	3	North Pacific Ocean (Bering Sea)	*Carlson and Karl, 1988*
67	Middle canyon system, Bering Sea	2	North Pacific Ocean (Bering Sea)	*Carlson and Karl, 1984, 1988*
68	St. Matthew canyon system, Bering Sea	2	North Pacific Ocean (Bering Sea)	*Carlson and Karl, 1984, 1988*
69	Albany canyons, SW Australia	11	Indian Ocean	*Exon et al., 2005*
70	Tugela Canyon, E South Africa	1	Indian Ocean	*Wiles et al., 2013*

71	Saint-Etienne and Pierrefonds canyons, SW La Reunion	2	Indian Ocean	*Babonneau et al., 2013*
72	Palar Basin canyons, E India	20	Indian Ocean	*Susanth et al., 2021*
73	Indus Canyon, SE Pakistan	1	Indian Ocean (Arabian Sea)	*Von Rad and Tahir, 1997; Salmanidou et al., 2019*
74	Barrow Canyon, NW USA	1	Arctic Ocean	*Eittreim et al., 1982; Pisareva et al , 2019*
75	Cook Strait canyons, E New Zealand	9	Cook Strait	*Mountjoy et al., 2009, 2014; Micallef et al., 2014*
76	Bass canyon system, SE Australia	10	Bass Strait	*Mitchell et al., 2007*
77	Akhviz and Sour canyons, NW Israel	2	Mediterranean Sea	*Mart, 1989; Almagor, 1993*
78	Almeria, Western, Eastern and Guadiaro canyons, S Spain	4	Mediterranean Sea	*Alonso and Ercilla, 2003; Palanques et al., 2005*
79	Alías-Almanzora canyon system, SE Spain	4	Mediterranean Sea	*Puig et al., 2017*
80	Menorca Canyon, SW Menorca, Balearic Islands	1	Mediterranean Sea	*Acosta et al., 2002*
81	Orpesa Canyon, NE Spain	1	Mediterranean Sea	*Amblas et al., 2012*
82	Foix Canyon system, NE Spain	3	Mediterranean Sea	*Puig et al., 2000; Tubau et al., 2013*
83	Blanes Canyon, SE France	1	Mediterranean Sea	*Lastras et al., 2011b*
84	Palamós/La Fonera Canyon, NE Spain	1	Mediterranean Sea	*Martin et al., 2006; Palanques et al., 2006; Lastras et al., 2011b*
85	Cap de Creus Canyon	1	Mediterranean Sea	*Baztan et al., 2005; Lastras et al., 2007; 2011b*
86	Bourcart Canyon, SE France	1	Mediterranean Sea	*Mauffrey et al., 2015*
87	Gulf of Palermo canyons, NW Sicily, Italy	7	Mediterranean Sea	*Lo Iacono et al., 2011; 2014*
88	Gulf of Castellammare canyons, NW Sicily, Italy	2	Mediterranean Sea	*Lo Iacono et al., 2014*
89	Messina Canyon, NE Sicily, Italy	1	Mediterranean Sea	*Ridente et al., 2014*
90	Petrace, Gioia and Mesima canyons, SW Italy	3	Mediterranean Sea	*Pierdomenico et al., 2016, Casalbore et al., 2018*
91	Luna and Infreschi canyons, SW Italy	2	Mediterranean Sea	*Budillon et al., 2011*
92	Dohrn Canyon, SW Italy	1	Mediterranean Sea	*Milia, 2000*
93	Golo system canyons, NE Corsica, France	4 (2)	Mediterranean Sea	*Gervais et al., 2004; 2006*
94	North İmralı Canyon, NW Turkey	1	Sea of Marmara	*Vardar, 2019*
95	Sarköy and Izmit canyons, NW Turkey	2	Sea of Marmara	*Çağatay et al., 2015*
96	Danube/Viteaz Canyon, SE Romania	1	Black Sea	*Popescu et al., 2004*

Table 1: The 96 case studies of the present study. Numbers in brackets refer to channel forms termed as submarine ‘gullies’ by the authors. See Figure 1 for locations.

Submarine canyon definition

In this study, a submarine canyon is defined as a single dominantly erosional channel form incised into a continental slope. The chosen definition of submarine canyon does not consider criteria relating to bathymetric setting, minimum canyon dimensions (cf. Harris and Whiteway, 2011), genetic origin, or canyon cross-sectional shape, and is therefore inclusive of what other authors commonly refer to as 'gullies' (e.g. Field et al., 1999; Gales et al., 2013; Chen et al., 2017), ‘gulleys’ (e.g. Gulliksen, 1978; Normark et al., 2009) or ‘potential submarine canyons’ (e.g. Almeida et al., 2015). A general definition was adopted for the following reasons: (i) submarine gullies have been considered to constitute forms at the early stage of canyon formation (e.g. Amblas et al., 2017); (ii) canyon geomorphologic attributes such as canyon size can be inherently limited by their physiographic setting; and (iii) both terms are variably used for smaller-scale erosional channel-forms on the slope.

The canyon apex is defined as the point of the shallowest bathymetry and canyon mouth as the most distal point, along a canyon axis. The term “canyon apex” has been used herein in preference to “canyon head”, the latter being a common but loosely defined term in the literature referring to the proximal part of a submarine canyon. Therefore “canyon apex” is used *sensu stricto* and “canyon head” *sensu lato.* In networks of connected channel forms, each channel-form is treated as an individual submarine canyon, whereas the network itself is termed a ‘canyon system’ (e.g. Mitchell et al., 2007; Mountjoy et al., 2009).

3.1 Study parameters

Data on submarine canyons, environmental setting and external controlling factors have been coded in the form of attributes recorded in the Deep-Marine Architecture Knowledge Store (DMAKS; Cullis et al., 2019). DMAKS is a relational database that allows the systematic and standardized collation of data on deep-water sedimentary systems, as originally obtained using different methods (e.g. outcrop, core, seismic, bathymetric, sonar imaging). DMAKS stores data on the architectural, geomorphological and facies characteristics of deep-water depositional systems, as well as on their external controls and depositional context (Cullis et al., 2019). Several additional bespoke attributes have been

added to DMAKS to enable the present study. The full set of variables employed in the analyses undertaken in this study is summarised in Tab. 2.

3.1.1 Canyon morphometric parameters

Canyon geomorphology has been characterized by the following six morphometric parameters: (i) canyon length, (ii) canyon width (maximum and streamwise average), (iii) canyon bankfull depth (maximum and streamwise average), (iv) overall canyon sinuosity, (v) average canyon thalweg gradient, and (vi) maximum canyon sidewall steepness (Fig. 2a). Definitions of these variables are reported in Tab. 2. Values reported by authors have only been included for studies based on surveys that include bathymetric coverage of the entire canyon area.

3.1.2 Environmental parameters and external controls

For the investigation of relationships between submarine canyon geomorphology and the environmental context of the submarine canyons, attributes have been defined to record (i) canyon physiographic setting, (ii) the configuration of the canyon terrestrial catchment, continental shelf and slope, and (iii) external controls operating at the location of the canyon (Tab. 2 & Fig. 3).

3.1.2.1 Physiographic setting

The bathymetry of the canyon is characterized by the seafloor depth at its apex and mouth (Tab. 1). The canyons are also classified in relation to the position of their apices relative to the shelf-break as either (i) shelf-incising, where the canyon extends into the continental shelf, or (ii) slope-confined, where the apex of the canyon is situated below the shelf break (cf. Jobe et al., 2011; Huang et al., 2014).

3.1.2.2 Source-to-sink-system parameters

Relationships between the geomorphology of submarine canyons and attributes of their terrestrial catchment have been investigated for canyons with sediment connectivity to a

fluvial system at present or in the past. For these canyons, descriptors of fluvial system length, mean annual fluvial discharge, catchment area and maximum catchment area elevation (Tab. 1), have been recorded. Sediment connectivity of a submarine canyon with a fluvial source is defined based on the following three criteria:

(i) *The submarine canyon displays a present connection with a fluvial system*. This includes canyons fronting a river mouth, canyons for which across-shelf sediment transport from a fluvial outlet has been inferred by authors, e.g. from sedimentary structures on the seafloor as sediment waves (e.g. Puig et al., 2017), and canyons connected to up-dip subenvironments, such as shelf channels and tributary canyons, which are physically connected with a fluvial system.

(ii) *The submarine canyon was connected to a river in the past.* This includes canyons that might not currently be connected to a fluvial system, e.g. due to present-day sea-level highstand conditions or to river-mouth shift of natural or anthropogenic cause, but that are known to have been connected in the past to a river (e.g. Sweet et al., 2020).

(iii) *The canyon apex is located within 5 km of a fluvial outlet*. This criterion has been considered in view of the typical length-scale over which sand tends to be distributed to submarine canyons by rivers that lack a bathymetric connection to the canyons (see Sweet and Blum, 2016).

For canyons linked with several rivers, their cumulative length, mean annual fluvial discharge and catchment area have been recorded, to enable comparison with canyons fed by single fluvial systems. For investigation of relationships between canyon geomorphology and maximum elevation of the terrestrial catchment, the elevation above mean sea level of the highest point in the combined catchment has been recorded.

The continental shelf and slope hosting the canyons have been described in terms of width, average gradient and depth.

3.1.2.3 Continental-margin type

The source-to-sink system has been classified as being associated with either a passive or a tectonically active continental margin, the latter comprising canyons along both convergent and transform plate boundaries, following the continental-margin classification of Harris et al. (2014; see their Fig. 2).

3.1.2.4 Source-to-sink setting

The source-to-sink setting associated with the studied canyons has been classified on whether the terrestrial catchment, shelf and slope are associated with continental landmasses (continental setting) or an island (insular setting). Canyons which could not unambiguously assigned a setting have not been included.

3.1.2.5 Oceanographic environment

To investigate the possible controls exerted by hydrodynamic processes that vary with scale and confinement of seas, and potential relationships between canyon morphometric parameters and the scale and degree of confinement of the seas where they occur, canyons are classified with respect to their oceanographic environment. To this end, two groups have been distinguished: (i) open seas, which comprise the World's oceans and experience hydrodynamic interactions with adjacent seas; and which may be characterized by the occurrence of oceanic gyres; (ii) semi-enclosed and enclosed seas, which are largely bounded by landmasses and are therefore characterized by a limited hydrodynamic interaction with the oceans or seas with which they are connected; this second class includes seas, gulfs and straits.

3.1.2.6 Latitude

The latitudinal positions of canyon heads are recorded as absolute values for both hemispheres. For scopes of analysis, latitude values have been binned in a manner that relates to major climate belts, i.e., into tropical (corresponding to latitudes between 0° and 23.5°), temperate (between 23.5° and 66.5°), and polar zones (corresponding to latitudes

higher than 66.5°). This simplified approach to the investigation of latitude-related climatic influences has been implemented for the following reasons: (i) existing climate classification schemes are commonly based on parameters of the terrestrial catchment and would therefore have limited applicability to canyons that do not receive significant fluvial discharge or none at all; moreover, climatic conditions in the marine environment are commonly not considered in these schemes; (ii) climate histories, including temperature and precipitation, would have to be reconstructed for both the present and the past to permit a consistent analysis of their impact on canyon evolution; this becomes particularly challenging for submarine canyons associated with large source-to-sink systems; (iii) the age of inception of the majority of the canyons in the present study is poorly constrained, so that climate histories cannot be matched closely to canyon age.

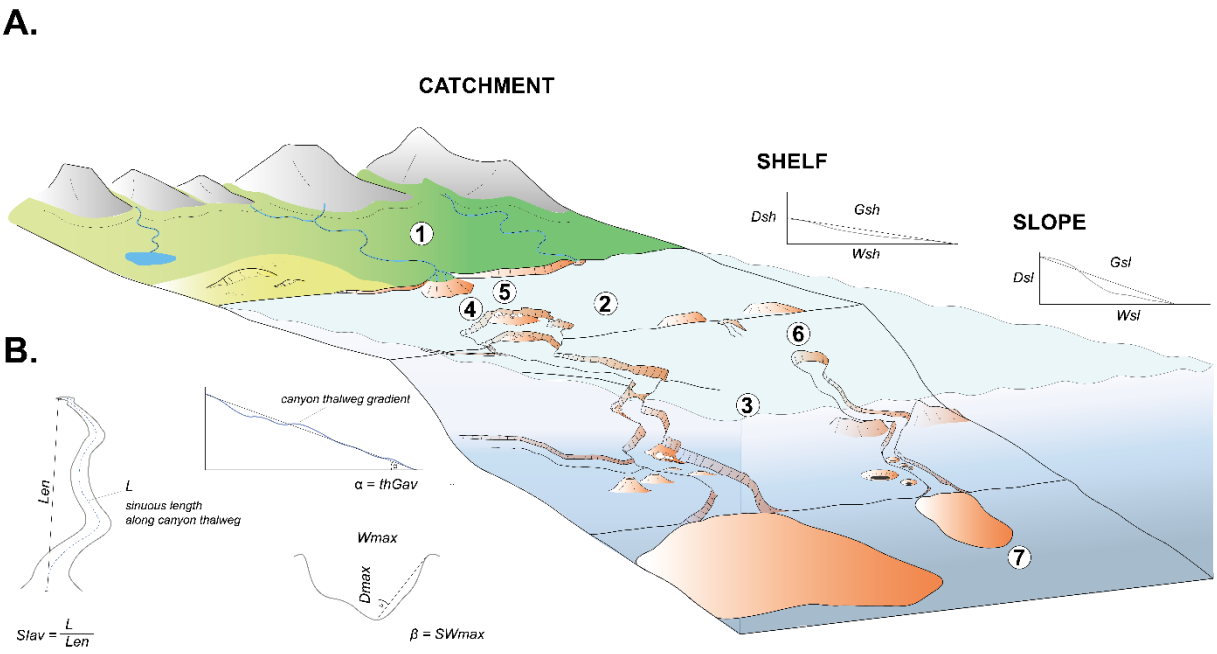

Figure 2: A. Attributes of the source-to-sink system and physiographic setting investigated in the study: 1. Terrestrial catchment: fluvial system length, average annual fluvial discharge, catchment size, maximum elevation. 2. Shelf configuration: width, depth, average gradient. 3. Slope configuration: width, depth, average gradient. 4. Canyon-apex location relative to the shelf-break. 5. Minimum distance to shoreline. 6. Seafloor depth at the top of the canyon. 7. Seafloor depth at the canyon mouth. B. Key canyon morphometric parameters considered in the study: L= canyon length along thalweg L_{en} = canyon length along endpoints; W_{max} = maximum canyon width; D_{max} = maximum canyon depth; SI_{av} = average canyon sinuosity index; thG_{av} = average canyon thalweg gradient; SW_{max} = maximum canyon sidewall steepness.

Study parameter	**Definition**
Canyon morphometrics	
L [m]**	streamwise length of the canyon between canyon apex and canyon mouth as measured along the canyon thalweg
W_{max} [m]**	maximum width of the canyon orthogonal to the canyon length
W_{av} [m]*	average canyon width over the length of the entire canyon
D_{max} [m]*	maximum depth of the canyon, i.e. depth of the canyon thalweg relative to the elevation of the canyon margins
D_{av} [m]*	average canyon thalweg depth over the length of the entire canyon
SI_{av}**[-]	average canyon sinuosity index, i.e. ratio between the sinuous canyon length measured along its thalweg and the straight distance between canyon apex and canyon mouth
thG_{av} [°]**	average canyon thalweg gradient, evaluated between canyon apex and canyon mouth
SW_{max} [°]*	maximum canyon-sidewall steepness, representing the maximum value of gradient between canyon rim and canyon bottom, evaluated along the entire length of the canyon
Physiographic setting	

canyon apex location	the location of the canyon apex relative to the shelf break, classified as ‘shelf-incising’ or ’slope-confined’
Dis_{min} *[m]***	minimum distance between the canyon and the shoreline
SD_{min} [m]**	seafloor depth at the top of the canyon
SD_{max} [m]**	seafloor depth at the mouth of the canyon
Canyon terrestrial catchment	
L_{fls} [km]**	length of the river with a present-day or previous connection with the canyon, from headwater to river mouth; for canyons connected with several rivers the cumulative length has been considered
Q_{fls} [km^3/yr]*	mean annual discharge of the fluvial system; for canyons connected with several rivers the cumulative mean annual discharge has been considered
A_{flsc} [km^2]*	size of the catchment associated with the fluvial system; for canyons connected with several rivers the maximum elevation of the combined catchment has been considered
H_{flsc} [m]**	maximum elevation of the catchment area relative to sea level; for canyons connected with several rivers the elevation of the highest peak in the combined catchment has been considered
Continental shelf	
W_{sh} [km]**	width of the shelf at the canyon location
G_{sh} [°]**	average shelf gradient at the canyon location
D_{sh} [m]**	shelf-break depth at the canyon; for shelf edges with variable bathymetry, the deepest point is considered
Continental slope	
W_{sl} [km]**	width of the slope at the canyon location
G_{sl} [°]**	average slope gradient between the shelf break and the slope break
D_{sl} [m]**	slope-break depth at the canyon
Other parameters	
Lat_{abs} [°]**	absolute value of the latitude of the canyon apex
source-to-sink setting	physiography of the source-to-sink system the canyon is associated with, classified as: (i) continental setting; (ii) insular setting; canyons situated in trenches between islands and continents have not been included
continental-margin type	for canyons located along continental margins, including canyons associated with

	islands: (i) active margin (including both convergent and transform settings); (ii) passive margin
oceanographic environment	(i) open sea: canyons located in an oceanic environment with open hydrodynamic interaction with adjacent seas; exposed to oceanic gyres; (ii) semi-enclosed and enclosed sea: canyons located in a sea which is largely bounded by landmasses and therefore has no or limited hydrodynamic interaction and connection with oceans; the definition includes seas, gulfs and straits

Table 2: Overview and definition of the study parameters that have been considered in this work. Three asterisks (***) denote values that have been calculated. Two asterisks (**) denote values that have been obtained either from the literature, as reported by the original authors, measured or calculated. A single asterisk (*) denotes values that have been retrieved from the literature, as stated by the original authors.

3.2 Statistical analysis

Relationships between canyon morphometric parameters and descriptors of physiographic setting and external controlling factors have been investigated by statistical analyses.

(i) Descriptive statistics of frequency distributions of canyon morphometric parameters are evaluated for classes of: canyon-apex location relative to the shelf-break, continental-margin type, source-to-sink setting, oceanographic environment, and latitudinal position of the canyon apex or head. Comparisons between distributions of values in canyon groups are undertaken.

(ii) Hypothesis testing has been used to evaluate whether differences in mean values of canyon morphometrics between groups of canyons are statistically significant. For assessment across two groups, two-sample t-tests have been conducted, whereas differences in mean values between more than two canyon groups have been assessed by means of one-way analysis of variance (ANOVA). To test

datasets with heteroscedastic distributions, Welch's t-test and Welch's ANOVA have been used throughout. Test statistics, degrees of freedom (DF) and P-values are presented for all tests. Results with p-values ≤0.01 are reported as statistically significant.

(iii) Correlation analysis has been applied to investigate pairwise relationships between the studied parameters. The strength and sign of correlation between two parameters is quantified by Pearson's correlation coefficient (r), to reveal linear relationships, and by Spearman's rank correlation coefficient (r_s), to reveal monotonic relationships. A correlation is considered statistically significant for p-values ≤0.01.

Although statistical analyses have been performed for any number of readings (N), the results are commonly presented and discussed when N≥15; it is explicitly stated when N<15.

All statistical analyses have been undertaken in Minitab 19.

3.3 Limitations of the study

Some of the key limitations of this study can be summarized as follows.

(i) In studies of submarine canyons there exists some geographic bias, as recognized by Matos et al. (2018), and some of that bias may have been inherited by this work. Nonetheless, an effort has been made to compile a globally representative dataset (see Fig. 1); the study also incorporates 12 canyon studies published after 2016, which were not considered by Matos et al. (2018) in their analysis.

(ii) As in any metastudy, erroneous data reported in the primary data sources may have been inadvertently included in the database. However, all reasonable measures have been taken to ensure data accuracy.

(iii) Although this study considers many environmental factors that may act as controls on canyon geomorphology, some relationships might arise from covariance of said factors with one or several parameters that have not been included in our analyses.

(iv) Shelf-break and slope-break depths of continental margins lacking distinct morphological breaks at the shelf-slope transition and/or in the base-of-slope region are difficult to determine precisely. As such, these attributes may have not been reported in the literature, and have not been included in the current dataset.

(v) Although the study of modern sedimentary systems provides good control on the physiographic setting, external factors and process-response relationships, observations only represent snapshots of the temporal evolution of the studied forms.

(vi) The continental-margin type, source-to-sink setting, and oceanographic environment constitute factors that apply to the entire extent of the studied canyons, and thus allow consistent grouping. In contrast, along their length, some submarine canyons might stretch across two latitudinal zones. The position of the canyon apex relative to the shelf break can be variable over time, but incision of the shelf by the canyon does not per se represent a more mature evolutionary stage of the canyon. Some canyons that are presently slope-confined might have had a physical connection to the shelf in the past: their canyon heads and proximal parts may have been backfilled (Pratson et al., 2007) or may have prograded basinwards (Mauffrey et al., 2015). This must be considered in analyses of frequency distributions of canyon morphometrics across slope-confined and shelf-incising forms.

4 Scaling relationships between canyon morphometrics

4.1 Observations

Statistically significant correlations are seen between canyon morphometric parameters, but only some of these are strong in magnitude (Figs. 3 & 4a-o).

Maximum dimensions of the studied canyons are moderately correlated with each other (Fig. 4a-c). Strong relationships that are statistically significant exist for average canyon width with maximum width (Fig. 3), length (Fig. 4a) and maximum depth (Fig. 4c), and for the latter with average depth (Fig. 3). In addition, modest significant scaling is demonstrated for maximum width and average depth (Fig. 4c). In contrast, correlations of average canyon depth with canyon length (Fig. 4b) and average canyon width (Fig. 4c) are weak and not significant.

Average canyon sinuosity shows significant, respectively modest and moderate, positive correlations with canyon length (Fig. 4d) and average canyon depth (Fig. 4f), and modest correlations with maximum canyon width (Fig. 4e). The negative correlation between sinuosity and average canyon thalweg gradient is significant but rather weak (Fig. 4m), whereas no correlation is seen between sinuosity and maximum canyon sidewall steepness (Fig. 4n).

The average canyon thalweg gradient demonstrates moderate negative correlation with canyon length (Fig. 4g) and weak negative correlation with maximum canyon width (Fig. 4h), both of which are statistically significant. The positive moderate correlation between thalweg gradient and average canyon depth is not statistically significant (N = 12; Fig. 4i). No correlation exists between thalweg gradient and either average width (Fig. 4h) and maximum sidewall steepness (Fig. 4o).

Positive, modest and significant relationships are seen between maximum canyon sidewall steepness and both maximum canyon width (Fig. 4k) and depth (Fig. 4l); the maximum canyon sidewall steepness is more weakly correlated with canyon length (Fig. 4j).

4.2 Interpretations

Statistically significant correlations between pairs of canyon morphometric parameters indicate that these canyon characteristics may be affected by the same process or controlling factors. Lack or weakness in correlation may instead reflect how sedimentary and hydrodynamic processes, structural controls and biogenic processes (sections 4.2.1 to 4.2.4) may control individual canyon morphologic parameters in ways that vary in magnitude and direction.

In some cases, correlations may arise – either in part or fully – due to covariance with other parameters, and this may be inherent in the definition of the parameters themselves. For example, more sinuous canyons tend to have longer streamwise canyon length for a given slope extent, whereas deeper channel forms are expected to have steeper margins.

In addition, some canyon morphometrics appear to be more strongly related to certain environmental controls; this is discussed in sections 5, 6 and 7.

4.2.1 Sedimentary processes

Because the effects of sedimentary processes on canyon evolution depend primarily on the sediment volumes they mobilise, their erosive strength and their areal extent, sedimentary processes can affect canyon morphometrics in different ways, at different locations along a canyon and even during the same event (e.g. Su et al., 2020). The ability of sediment gravity flows and slope failures to trigger one another (e.g. Pratson and Coakley, 1996; Bernhardt et al., 2015) and the common transition of the latter into the former (e.g. Puig et al., 2014) makes it difficult to differentiate between the relative importance of these processes in shaping canyon geomorphology. As a consequence, it may not be possible to establish causal links between intra-canyon-scaling relationships and sediment-transport mechanisms. Nevertheless, observed scaling between some canyon morphometric parameters suggests that the influence of one or several controlling factors tends to be prevalent, giving rise to

canyon geomorphologic characteristics that are recognizable on a global scale despite specific regional or local conditions.

Canyon enlargement can be driven by active erosive processes, such as primary erosion by sediment gravity flows passing through the canyon (e.g. Li et al., 2021) or by slope failure within the canyon and on the adjacent slope (e.g. Post et al., 2022), but also by accretion of the adjacent slope or of ridges between canyons, which may be caused by along-slope currents (e.g. Rona 1970), by background sedimentation or spillover of sediment gravity flows passing through canyons (e.g. Straub and Mohrig, 2009; Armitage et al., 2010), or due to primary carbonate production (e.g. Shepard, 1972; Tournadour et al., 2017). By contrast, intra-canyon aggradation, e.g. by backfilling (Cronin et al., 2005), sediment accumulation in canyon heads (e.g. Walsh et al., 2007) and hemipelagic sedimentation (e.g. Jobe et al., 2011) weaken the effect of erosive processes on positive scaling relationships in canyon morphometry, for example by shortening canyons and decreasing their depths.

The fact that these processes can variably modify individual canyon morphometric parameters is likely reflected in the observed scaling between maximum and average canyon dimensions. The rather strong scaling of canyon length with average canyon width may be linked to the ability of down-canyon flows to maintain their erosive behaviour beyond the canyon mouth. The moderate scaling of canyon length with maximum width might be related to the fact that lateral slope failures lead to local widening of the canyon over the excavated area, but may only increase canyon length where the mobilised sediment volume – which might also comprise intra-canyon sediment sources – is sufficient to extend the canyon beyond its present mouth. This may arise, for example, by breaching of intra-slope structural highs or by facilitating the progradation of the continental rise. Retrograde slope failures act as a primary cause of canyon lengthening (e.g. Orange et al., 1994; Pratson and Coakley, 1996; Pratson et al., 2007) and might cause the local widening of canyons in their proximal parts in correspondence of slump scars, where these are intercepted (e.g. Mulder et al., 2012). Relatively strong scaling of maximum depth with maximum and average width in the

sampled canyons may in part reflect simultaneous canyon-margin aggradation and intra-canyon erosion. The positive scaling between maximum width and maximum canyon sidewall steepness can in part be explained by lateral canyon-slope failures causing a local increase in canyon width and canyon sidewall steepness, and by thalweg erosion.

4.2.2 Hydrodynamic processes

Marine hydrodynamic processes on the shelf and slope can variably influence canyon geomorphology: intra-canyon erosion, remobilisation and transport of sediment might be caused by focussing of waves within a canyon (e.g. Smith et al., 2018) and from tidal (e.g. Liu and Yin, 2004), and unidirectional oceanic currents (e.g. Itoh et al., 2015) passing through it. Sediment can be distributed to a canyon by recurrent processes like tides (e.g. Mountjoy et al., 2014), long-lived longshore drifts (e.g. Normark et al., 2009) and slope currents (e.g. Wang et al., 2018), by high-energetic waves like solitary waves (e.g. Yin et al., 2019) and storm waves (e.g. Sequeiros et al., 2019), and through dense shelf-water cascading (e.g. Canals et al., 2006). Oceanic currents can transport sediment discharged by rivers along continental margins to submarine canyons located down current (e.g. Normark et al., 2009), with littoral cells being able to transport sediment over distances >100 km to canyons (e.g. Romans et al., 2009). The interception of sediment discharge from fluvial systems by along-shelf and slope currents can decrease the sediment volume supplied to a canyon from within the shelf and slope, or can even shut down supply from fluvial sediment sources.

Hence, the influence of marine hydrodynamic processes on canyon geomorphology is complex and might both amplify or weaken relationships between aspects of canyon morphometry caused by sedimentary processes. For example, canyons hosted on continental margins with strong oceanic currents might experience less frequent canyon-margin failures and reduced aggradation, due to the ability of such currents to inhibit sedimentation along canyon margins (e.g. Green, 2011). As a result, the impact of axial sediment gravity flows on scaling in canyons might be, to a lesser degree, overprinted by

lateral failure in these canyons. On the contrary, currents that can lead to sediment accumulation along canyon margins may strengthen the scaling between canyon depth, width and margin slopes (see section 4.2.1).

4.2.3 Structural controls

Structural controls might affect canyon geomorphology by their influence on pre-existing and developing seafloor topography, which might have contributed to the weakening of some of the relationships between canyon morphometric attributes. For example, where fault and diapiric structures form part of the canyon walls or are in vicinity of the canyon margin, they can steepen the canyon sidewalls (e.g. Yu and Chang, 2002; Bernhardt et al., 2015), and might overprint the effect of concurrent intra-canyon erosion by down-canyon sediment flows and canyon sidewall failure on canyon width, depth and sidewall steepness and the strength of their scaling with each other. In addition, emerging topography, generated for example by coral reef growth (e.g. Puga-Bernabéu et al., 2011) or diapiric uplift (e.g. Chiang et al., 2012), might cause flow deceleration, flow deflection, flow stripping and/or grain size segregation, which in turn might weaken the erosional effect of a flow further down-canyon. Similarly, substrate heterogeneity arising from pre-existing structural features or buried canyons might cause spatial variations in substrate erodibility, which in turn might counteract or enhance the erodibility of canyon floors or walls over the affected area.

4.2.4 Biogenic processes

The effect of the colonization of canyon walls and margins by marine fauna on canyon-wall stability has received limited attention in the literature (e.g. Shepard, 1981; Eittreim et al., 1982; Carlson and Karl, 1984; and references therein). Depending on factors such as nature of substrate, degree of bioturbation, filling and cementation, the canyon sidewall stability might be increased or decreased by bioturbation. Similarly, vegetation cover in proximal parts of canyons, specifically by marine flora in the photic zone, might reduce the erodibility of canyon slopes. The resulting variability in the erodibility of canyon walls and apices might

weaken the scaling relationships between canyon length, width and sidewall steepness. Thus, biogenic processes might constitute a controlling factor on scaling in canyon morphology.

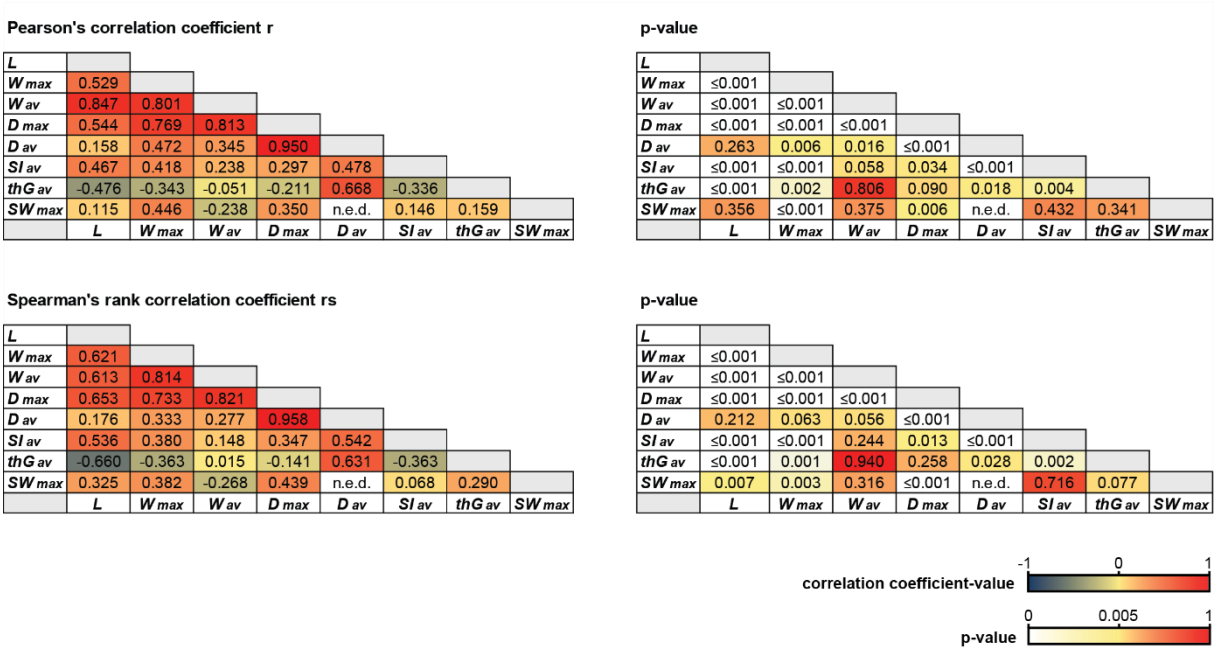

Pearson's correlation coefficient r								
L								
W max	0.529							
W av	0.847	0.801						
D max	0.544	0.769	0.813					
D av	0.158	0.472	0.345	0.950				
SI av	0.467	0.418	0.238	0.297	0.478			
thG av	-0.476	-0.343	-0.051	-0.211	0.668	-0.336		
SW max	0.115	0.446	-0.238	0.350	n.e.d.	0.146	0.159	
	L	W max	W av	D max	D av	SI av	thG av	SW max

p-value								
L								
W max	≤0.001							
W av	≤0.001	≤0.001						
D max	≤0.001	≤0.001	≤0.001					
D av	0.263	0.006	0.016	≤0.001				
SI av	≤0.001	≤0.001	0.058	0.034	≤0.001			
thG av	≤0.001	0.002	0.806	0.090	0.018	0.004		
SW max	0.356	≤0.001	0.375	0.006	n.e.d.	0.432	0.341	
	L	W max	W av	D max	D av	SI av	thG av	SW max

Spearman's rank correlation coefficient rs								
L								
W max	0.621							
W av	0.613	0.814						
D max	0.653	0.733	0.821					
D av	0.176	0.333	0.277	0.958				
SI av	0.536	0.380	0.148	0.347	0.542			
thG av	-0.660	-0.363	0.015	-0.141	0.631	-0.363		
SW max	0.325	0.382	-0.268	0.439	n.e.d.	0.068	0.290	
	L	W max	W av	D max	D av	SI av	thG av	SW max

p-value								
L								
W max	≤0.001							
W av	≤0.001	≤0.001						
D max	≤0.001	≤0.001	≤0.001					
D av	0.212	0.063	0.056	≤0.001				
SI av	≤0.001	≤0.001	0.244	0.013	≤0.001			
thG av	≤0.001	0.001	0.940	0.258	0.028	0.002		
SW max	0.007	0.003	0.316	≤0.001	n.e.d.	0.716	0.077	
	L	W max	W av	D max	D av	SI av	thG av	SW max

Figure 3: Heat maps of correlations of canyon morphometric parameters with each other for canyons of the study displaying values of Pearson's correlation coefficient r and Spearman's rank correlation coefficient rs, and their respective p-values. *L* = canyon length; W_{max} = maximum canyon width; W_{av} = average canyon width; D_{max} = maximum canyon depth; D_{av} = average canyon depth; SI_{av} = average canyon sinuosity index; thG_{av} = average canyon thalweg gradient; SW_{max} = maximum canyon sidewall steepness. n.e.d. = not enough data to facilitate statistical analyses.

A.

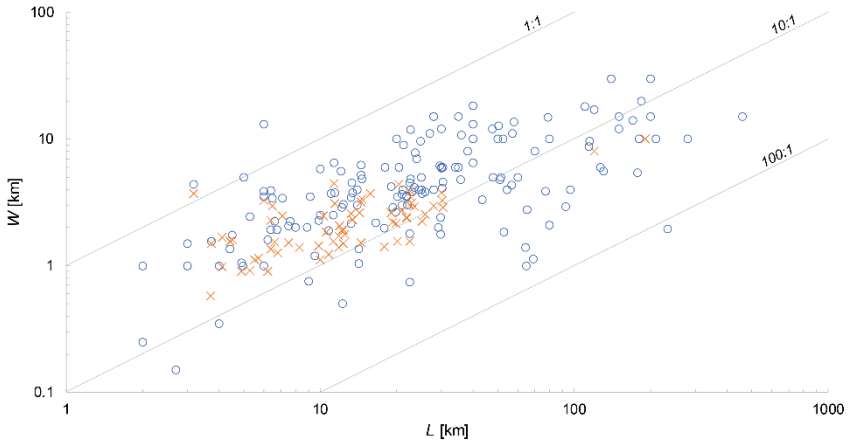

○ ***L vs Wmax:*** **N=156**	r=0.529	p≤0.001	× ***L vs Wav:*** **N=66**	r=0.847	p≤0.001
	r_s=0.621	p≤0.001		r_s=0.613	p≤0.001

B.

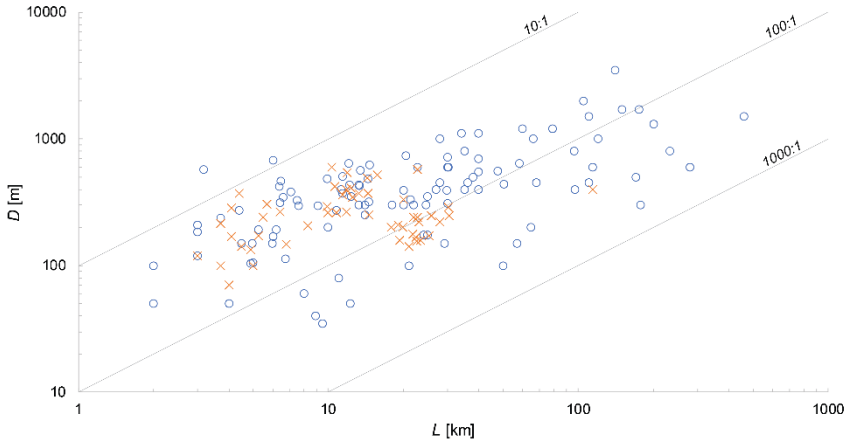

○ ***L vs Dmax:*** **N=107**	r=0.544	p≤0.001	× ***L vs Dav:*** **N=52**	r=0.158	p=0.263
	r_s=0.653	p≤0.001		r_s=0.176	p=0.212

C.

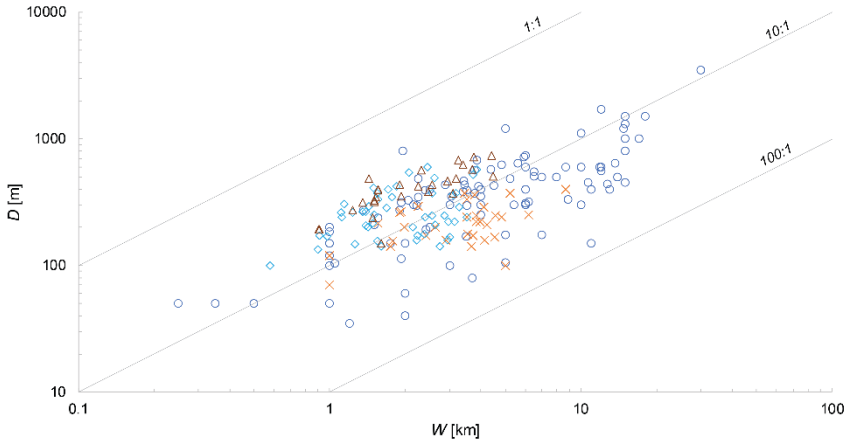

○ ***Wmax vs Dmax:*** **N=100**	r=0.769	p≤0.001	△ ***Wav vs Dmax:*** **N=27**	r=0.813	p≤0.001
	r_s=0.733	p≤0.001		r_s=0.821	p≤0.001
× ***Wmax vs Dav:*** **N=32**	r=0.472	p=0.006	◇ ***Wav vs Dav:*** **N=48**	r=0.345	p=0.016
	r_s=0.333	p=0.063		r_s=0.277	p=0.056

D.

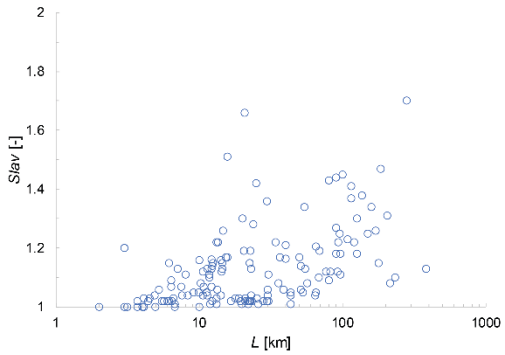

○	***L vs Slav:***	r=0.467	p≤0.001
	N=148	rs=0.536	p≤0.001

E.

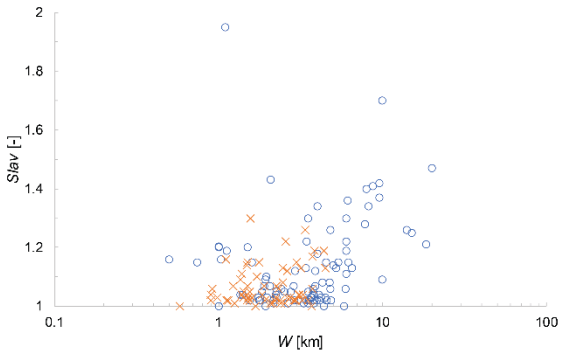

○	***Wmax vs Slav:***	r=0.418	p≤0.001
	N=96	rs=0.380	p≤0.001
×	***Wav vs Slav:***	r=0.238	p=0.058
	N=64	rs=0.148	p=0.244

F.

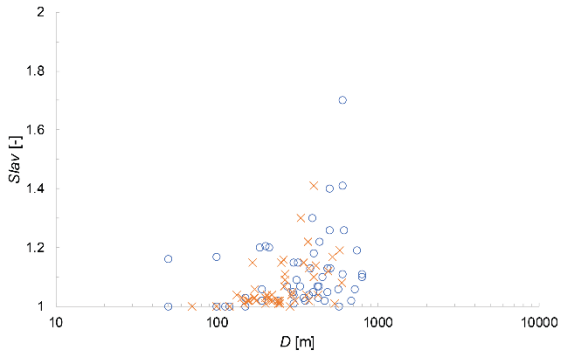

○	***Dmax vs Slav:***	r=0.297	p=0.034
	N=51	rs=0.347	p=0.013
×	***Dav vs Slav:***	r=0.478	p≤0.001
	N=51	rs=0.542	p≤0.001

G.

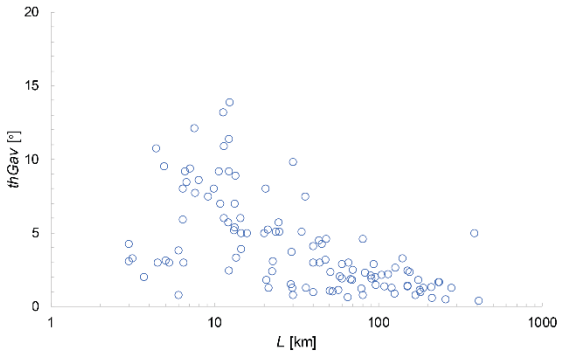

○	***L vs thGav:***	r=-0.476	p≤0.001
	N=112	rs=-0.660	p≤0.001

H.

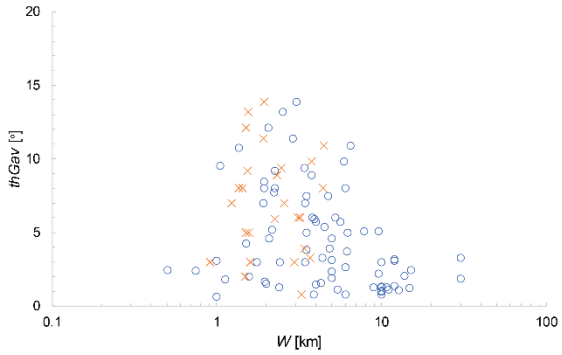

○	***Wmax vs thGav:***	r=-0.343	p=0.002
	N=78	rs=-0.363	p=0.001
×	***Wav vs thGav:***	r=-0.051	p=0.806
	N=26	rs=0.015	p=0.940

I.

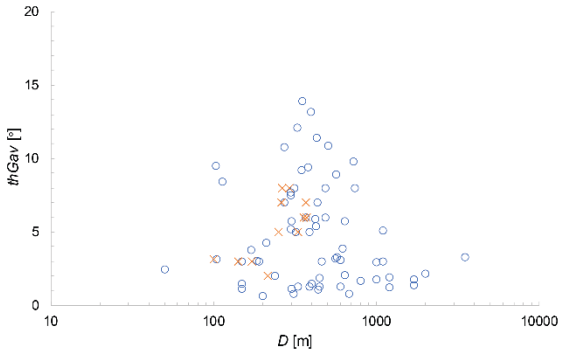

○	***Dmax vs thGav:***	r=-0.211	p=0.090
	N=66	rs=-0.141	p=0.258
×	***Dav vs thGav:***	r=0.668	p=0.018
	N=12	rs=0.631	p=0.028

Figure 4a-o (continued).

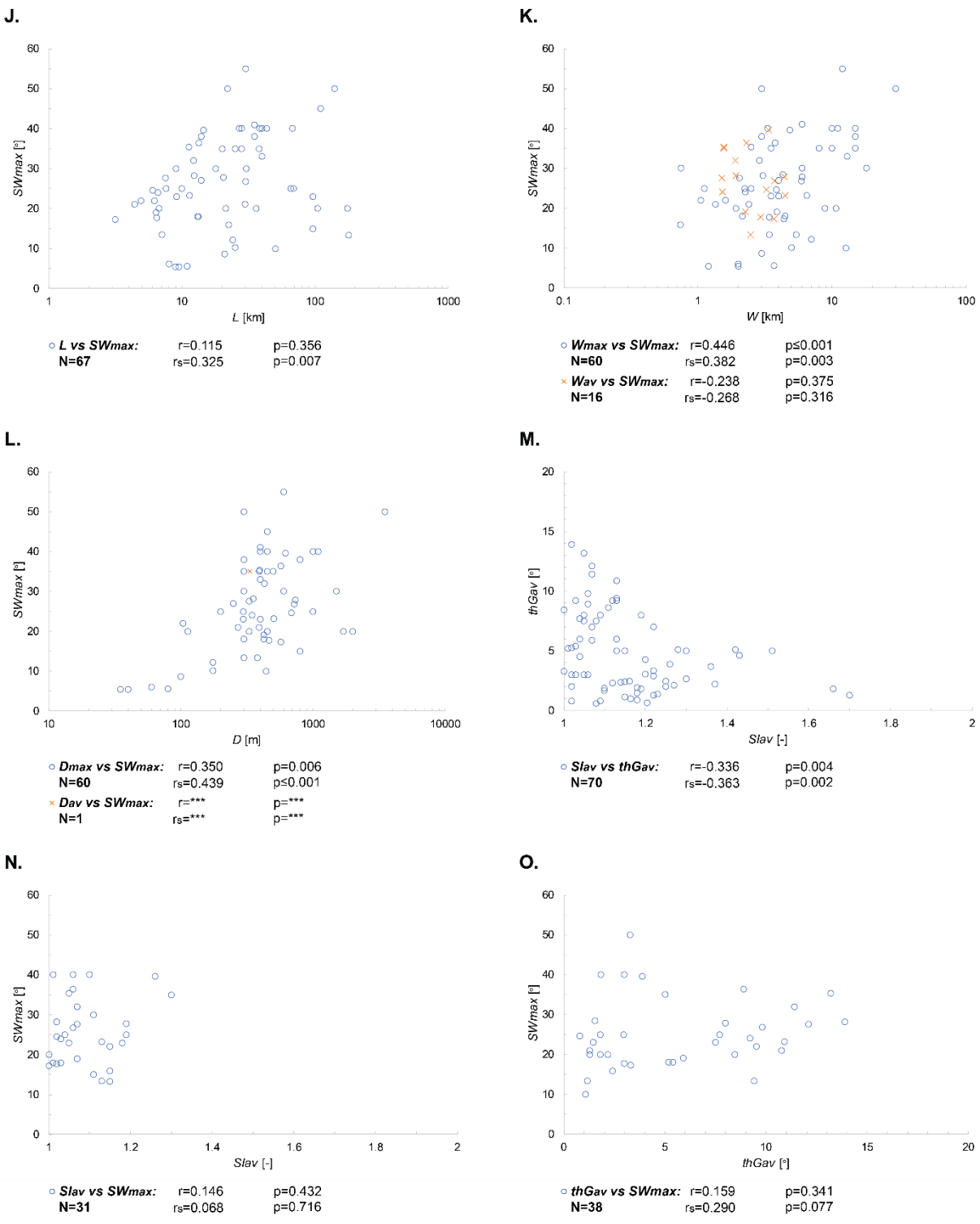

Fig. 4a-o: Scatterplots of canyon morphometric parameters for studied canyons. N = number of observations; r = Pearson's correlation coefficient; r_s = Spearman's rank correlation coefficient.

5 Relationships between canyon morphometric parameters and parameters of the physiographic setting

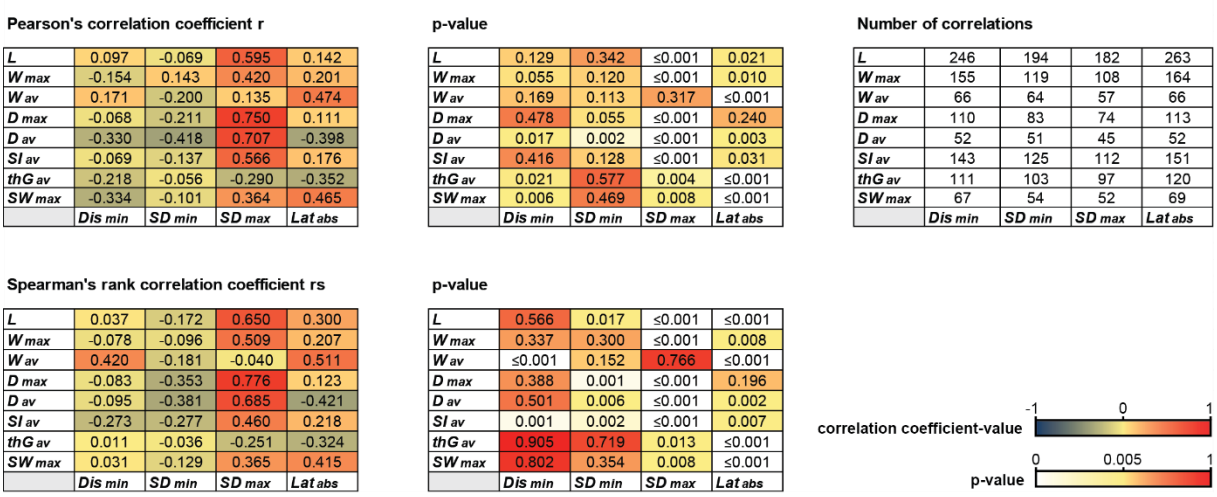

Figure 5: Heat maps for correlations of canyon morphometrics with the physiographic setting displaying values of Pearson's correlation coefficient r and Spearman's rank correlation coefficient rs, and their respective p-values. *L* = canyon length; W_{max} = maximum canyon width; W_{av} = average canyon width; D_{max} = maximum canyon depth; *Dav* = average canyon depth; SI_{av} = average canyon sinuosity index; thG_{av} = average canyon thalweg gradient; SW_{max} = maximum canyon sidewall steepness; Dis_{min} = minimum distance between the canyon and shoreline; SD_{min} = minimum seafloor depth at the canyon; SD_{max} = maximum seafloor depth at the canyon; Lat_{abs} = absolute value of the latitude of the canyon apex.

5.1 Distance between canyon and shoreline

5.1.1 Observations

The minimum distance between the canyon apex and the shoreline is not correlated to any of the canyon morphometric parameters except for the average canyon width (Figs. 5 & 6a-f), for which modest but statistically significant positive correlation is seen (Fig. 6b). However, in the assessment of a relationship with average canyon width, the average widths of canyons with a distance to a continent or island of ≤ 25 kilometres could not be evaluated.

5.1.2 Interpretations

Although the distance of the canyon to the shoreline plays a role in sediment distribution from fluvial sources across shelves and slopes (section 6.1), the results show that relationships between the distance of the canyon to the shoreline and overall canyon geomorphology are weak. It can thus be inferred that the distance to the shoreline itself is not a major factor, relative to others.

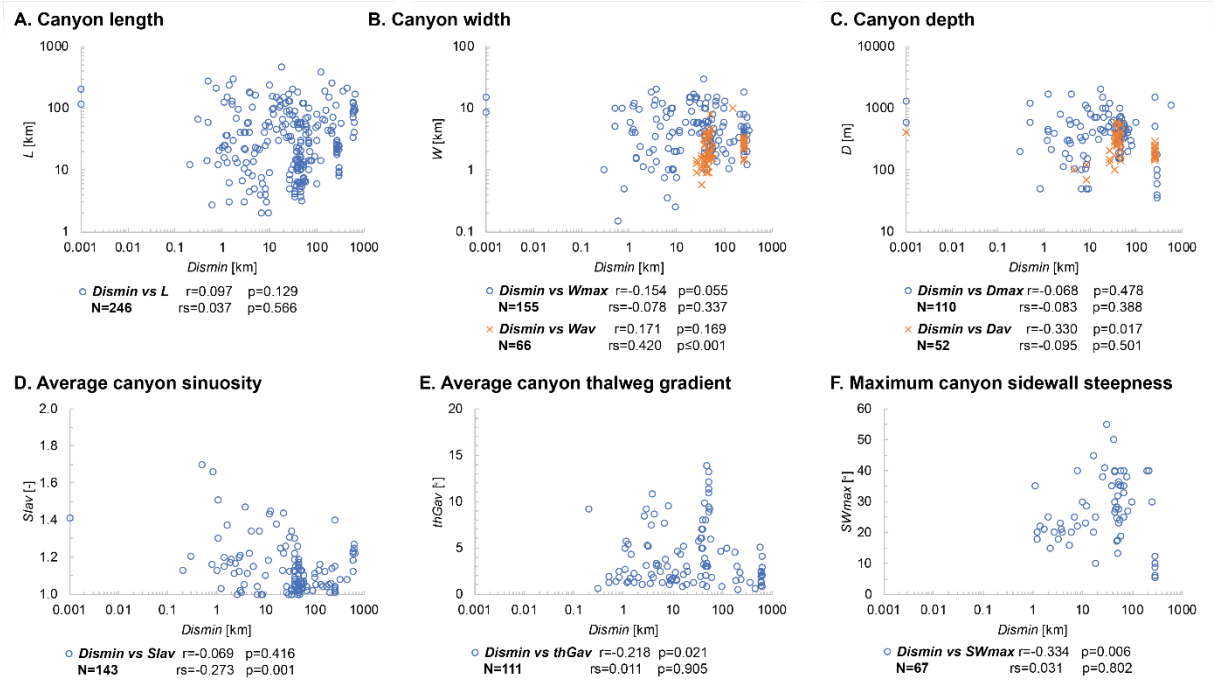

Fig. 6a-f: Scatterplots of minimum canyon-shoreline distance and canyon morphometric parameters. N = number of correlations; r = Pearson's correlation coefficient; r_s = Spearman's rank correlation coefficient.

5.2 Canyon bathymetry

5.2.1 Observations

5.2.1.1 Seafloor depth at the canyon apex

Most canyon morphometrics correlate poorly with seafloor depth at the canyon apex (Figs. 5 & 7a-f). Negative modest correlations are seen with average canyon depth, and a weak negative relationship with maximum canyon depth, both of which are statistically significant (Fig. 7c). A weak but significant negative correlation is also displayed with average canyon sinuosity (Fig. 7d).

5.2.1.2 Seafloor depth at the canyon mouth

The seafloor depth at the canyon mouth tends to correlate significantly with all investigated canyon morphometric parameters except for average canyon width (Figs. 5 & 8a-f). Moderate positive correlations are seen with canyon length (Fig. 8a), maximum canyon width (Fig. 8b), both maximum and average canyon depth (Fig. 8c), and with average canyon sinuosity (Fig. 8d), whereas correlations with maximum canyon sidewall steepness are weaker (Fig. 8f). In contrast, a weak negative correlation is seen with the average canyon thalweg gradient (Fig. 8e).

5.2.2 Interpretations

5.2.2.1 Seafloor depth at the canyon apex

No clear relationships are seen between canyon geomorphology and the seafloor depth at the apex of the canyon, except for canyon depth. Data on maximum and average canyon dimensions demonstrate that large canyons can develop regardless of the seafloor depth at the canyon apex. The results indicate that the absolute canyon-apex depth does not necessarily relate to controlling factors influencing canyon geomorphology, such as a connection to sediment sources (section 6.1), the hydrodynamic regime (section 4.2) or structural controls (section 4.3). Although the canyon length increases with retrograde

erosion at the canyon head, which leads to progressive shallowing of the canyon apex, the bathymetry of the basin ultimately determines the canyon length (section 6.3). The tendency of canyons to be deeper when their apex is shallower might reflect how canyon deepening may be facilitated by erosive sediment gravity flows linked to the progressive retrogradation of the canyon, which can enhance sediment delivery from terrestrial and intrashelf sources and from sediment remobilisation within the canyon.

5.2.2.2 Seafloor depth at the canyon mouth

The results suggest that canyons reaching greater depths tend to have greater maximum dimensions and average depths, but not average widths. The observed increase in maximum canyon width and depth with increasing seafloor depth at the canyon mouth may be linked to the widening and deepening of canyons by turbidity currents in the region of the canyon mouth as a response to a decrease in slope gradient (e.g. Brunt et al., 2013). In addition, results of physical experiments suggest that in long canyons the upwelling of along-slope currents via the canyon mouth creates cyclonic eddies in the mouth region (Waterhouse et al., 2009). This mechanism might cause lateral erosion at the canyon margins and might promote intra-canyon erosion in the canyon-mouth area.

Our results also indicate that canyons reaching into deeper waters tend to be more sinuous, which might reflect an increased impact of seafloor relief on canyon geomorphology with progressive extension of the canyon across the continental slope. For example, canyons might become more sinuous and longer where their pathways are deflected and redirected by topographic highs (e.g. Micallef et al., 2014) and intraslope depressions (e.g. Bourget et al., 2010). The effect of seafloor topographic variability might also in part explain the positive scaling of maximum width with seafloor depth, in view of how longer canyons are more likely to have a larger number of “swells” in planform, for example where intraslope depressions are incorporated in the canyon.

For maximum canyon sidewall steepness, the positive scaling with seafloor depth at the canyon mouth might in part reflect how the studied canyons located in open seas tend to

have steeper canyon margins than those in semi-enclosed and enclosed seas (section 7.4), and continental slopes in open oceanic settings reaching greater depths.

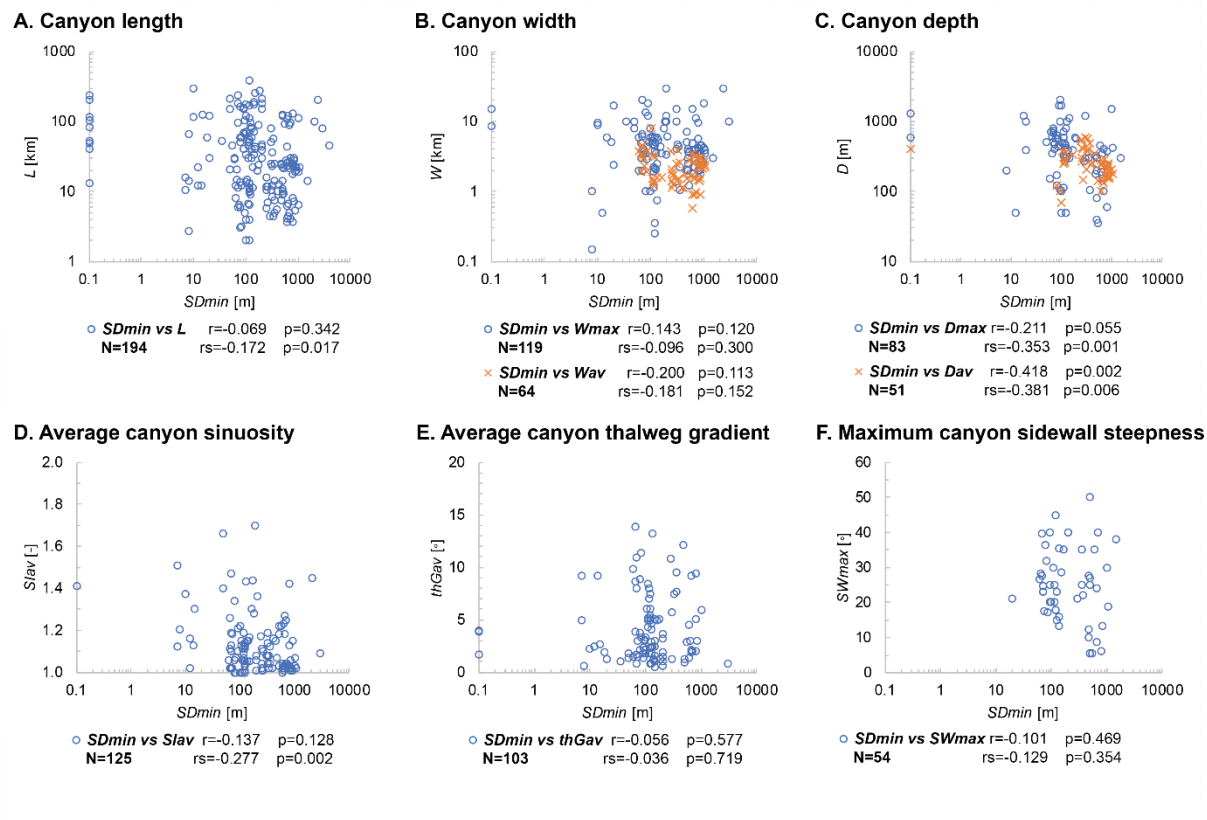

Fig. 7a-f: Scatterplots of seafloor depth at the top of the canyon and canyon morphometric parameters. N = number of correlations; r = Pearson's correlation coefficient; r_s = Spearman's rank correlation coefficient.

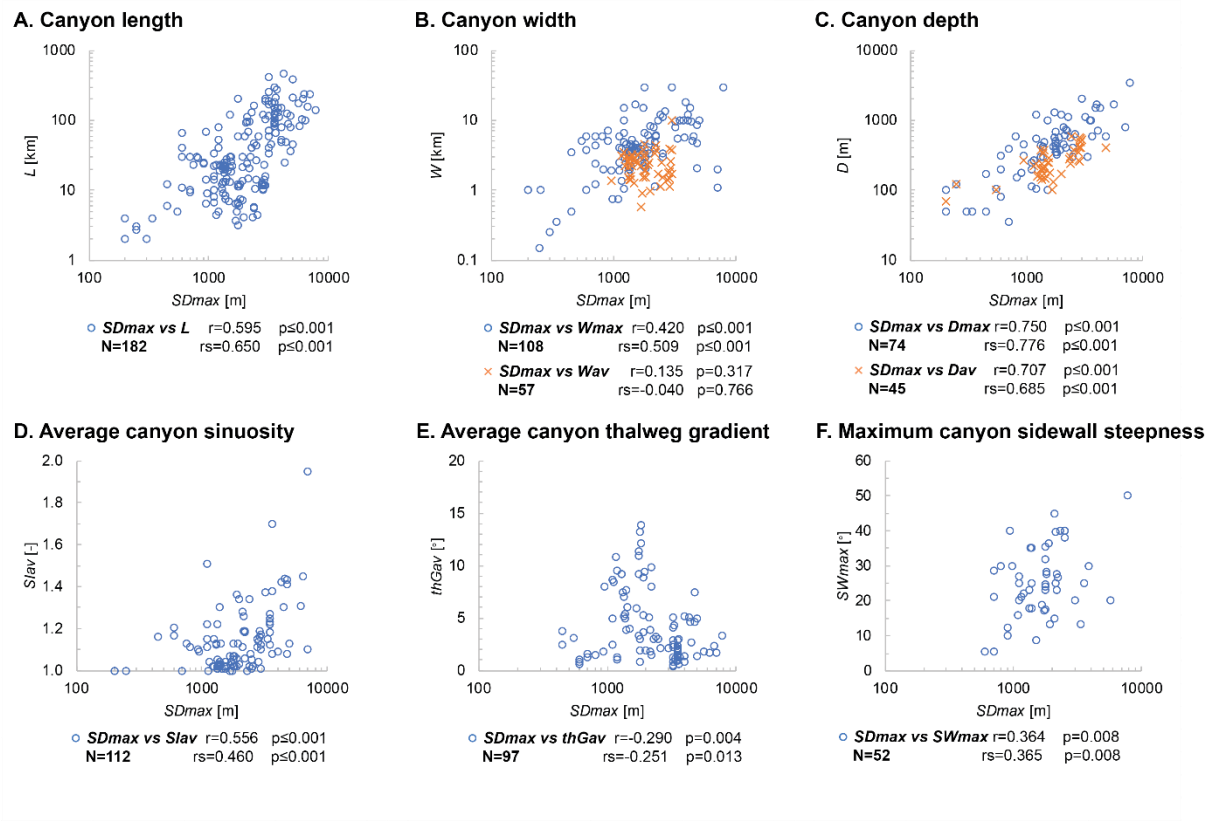

Fig. 8a-f: Scatterplots of seafloor depth at the canyon mouth and canyon morphometric parameters. N = number of correlations; r = Pearson's correlation coefficient; r_s = Spearman's rank correlation coefficient.

5.3 Latitudinal position of the canyon apex

5.3.1 Observations

For absolute values of latitude of the canyon apex and canyon morphometric parameters, correlations are weak to moderate in strength (Figs. 5 & 9a-f). Moderate positive correlation exists between latitude and average canyon width (Fig. 9b), and modest negative correlations between latitude and both average depth (Fig. 9c) and maximum canyon sidewall steepness (Fig. 9f). Weaker but statistically significant correlations are seen for canyon length (Fig. 9a), average canyon sinuosity (Fig. 9d) and the average canyon thalweg gradient (Fig. 9e), which are negative for the latter and positive for the former two parameters.

The informative value of the results is limited by the small number of high-latitude submarine canyons considered in this study.

5.3.2 Interpretations

The results suggest that processes that tend to vary with latitude do not leave any particular signature in the maximum dimensions, overall sinuosity and average canyon thalweg gradient of submarine canyons. The influence of factors related to latitude on canyon geomorphology appears to be modest, in particular on average width and maximum sidewall steepness.

The limited correlation between latitude and canyon morphometric parameters is interpreted to arise from the complex ways in which climate can influence canyon evolution and size. Climate can variously influence sediment fluxes to submarine canyons, for example by exerting control on precipitation and subaerial erosion. Fluvial sediment discharge to the sea has been shown to vary with latitude (see Milliman and Farnsworth, 2011), and certain mechanisms that might impact canyon geomorphology are prevalent in – or even exclusive to – certain latitudinal belts. These include, for example, typhoon-driven hyperpycnal flows and turbidity currents at low latitudes (e.g. Zhang et al., 2018; Porcile et al., 2020) and glacial processes at high latitudes (e.g. Armitage et al., 2010). In high-latitude settings, sediment connection of canyons to terrestrial catchments might also be affected by glacial isostatic adjustment subsequent to glacial intervals leading to river diversions (e.g. Pico et al., 2018).

One factor that might contribute to steeper margins and greater average widths in canyons in higher latitudes is the glaciation of continental margins. The prevalence of line sources in glacial margin settings as opposed to point sources in low-latitudinal settings has been suggested (e.g. Martinsen, 2005; Armitage et al., 2010): sediment can be discharged rapidly from glaciers and ice streams, and distributed sediment dispersal across the continental slope (Martinsen, 2005) can promote the aggradation of canyon margins and inter-canyon ridges due to background sedimentation and overspill from channelised flows in canyons, which in turn increase their proneness to slope failure (Armitage et al., 2010). In addition,

sediment can efficiently be supplied to slope environments where ice sheets have prograded across continental shelves (Gales et al., 2013). Also, the progradation of ice sheets onto shelf margins during glacial maxima and sea-level lowstands has been proposed as a trigger to mass failures on continental slopes by the effect of ice loading (Mulder and Moran, 1995). This mechanism might contribute to intra-canyon erosion by slope failures triggering, or evolving into, sediment gravity flows; ice loading can also cause intra-canyon mass failures where canyons have reached or retrograded into the shelf and are overlain by an ice sheet.

Although the data for investigation of relationships between latitude and sinuosity only include submarine canyons at latitudes up to 45°, the lack of any relationships is in agreement with findings by Harris and Whiteway (2011) for shelf-incising canyons. The influence of latitude-related processes on submarine-channel sinuosity is debated. An inverse relationship between channel sinuosity and latitude, linked to influence of the Coriolis force and variations in sediment type and flow type within different latitudinal zones, has been proposed (e.g. Peakall et al., 2012), but its robustness has been subsequently challenged (e.g. Sylvester and Pirmez, 2017). The results indicate that mechanisms invoked as latitudinal controls on sinuosity for submarine channels may not be applicable to submarine canyons. This needs further investigation.

Nevertheless, the results must be viewed with reservation due to the limited size of the datasets for arctic and tropical examples, and because of geographic bias. For example, canyons offshore NW Norway are accommodated on a passive margin in an open-sea setting, two environmental conditions that appear to promote steepening of canyon sidewalls; the former by promoting slope failure within canyons (section 7.2) and the latter by favouring canyon margin aggradation related to oceanic currents in open-sea settings (section 7.4). In contrast, several of the canyons in tropical and temperate latitudes are associated with active margins in semi-enclosed seas, particularly from the eastern part of the South China Sea and the Mediterranean Sea.

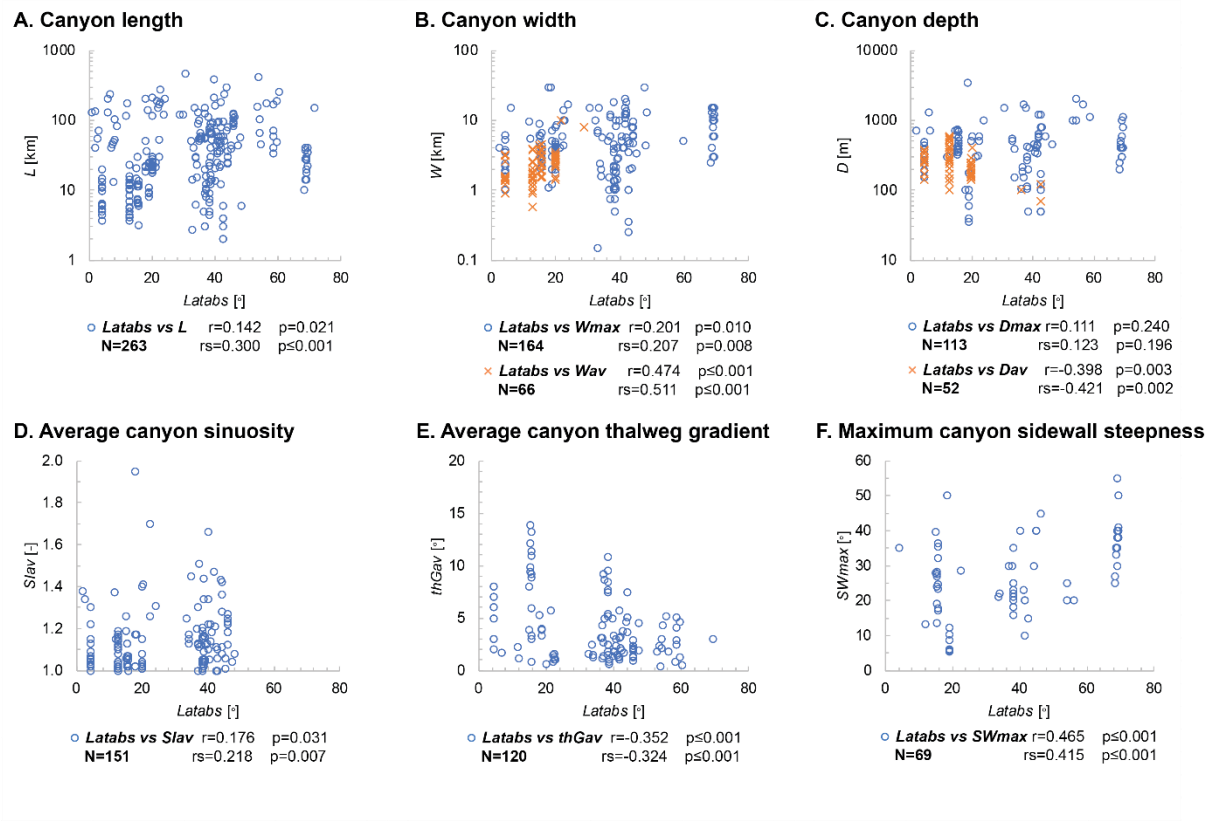

Fig. 9a-f: Scatterplots of absolute values of latitude of the canyon apex and canyon morphometric parameters. N = number of correlations; r = Pearson's correlation coefficient; r_s = Spearman's rank correlation coefficient.

6 Scaling relationships between canyon morphometric parameters and source-to-sink system parameters

Scaling relationships between canyon morphometric parameters and attributes of related terrestrial catchments, continental shelves and slopes have been evaluated. For 69 submarine canyons, which represent 24% of the studied canyons, scaling relationships between canyon and terrestrial-catchment parameters have been investigated, except for maximum canyon sidewall steepness, average canyon width and depth, due to data paucity. The same applies for correlations of average canyon width and depth with slope characteristics.

An overview of the results is presented in form of heatmaps of correlation (Fig. 10a-c). Furthermore, relationships between attributes of canyon-associated S2S systems (Fig. 11) have been investigated. This has been undertaken to aid in the interpretation of controls on canyon morphometry by identifying where relationships might in part reflect covariance with one or several other factors. Correlations of canyon morphometrics with attributes of the catchment, shelf and slope are presented as scatterplots in sections 6.1 to 6.3 (Figs. 12-15), in which the findings for the individual S2S segments are discussed. In addition, canyon morphometry has been quantitatively assessed for canyons grouped based on shelf-break thresholds of 120 m and 130 m below present-day sea level at the site of the canyon (Fig. 14a-f).

A. Terrestrial catchment

Pearson's correlation coefficient r

L	0.184	0.244	0.210	0.387
W max	0.358	0.306	0.452	0.633
D max	0.414	***	0.372	***
SI av	-0.075	0.057	-0.089	0.586
thG av	-0.345	***	-0.273	-0.193
SW max	***	***	***	***
	L fls	*Q fls*	*A flsc*	*H flsc*

p-value

L	0.130	0.091	0.091	0.003
W max	0.056	0.232	0.014	0.001
D max	0.098	***	0.117	***
SI av	0.601	0.743	0.539	≤0.001
thG av	0.067	***	0.138	0.402
SW max	***	***	***	***
	L fls	*Q fls*	*A flsc*	*H flsc*

Spearman's rank correlation coefficient rs

L	0.107	0.666	0.137	0.636
W max	0.424	0.123	0.633	0.588
D max	0.736	***	0.737	***
SI av	-0.165	0.510	-0.127	0.602
thG av	-0.171	***	-0.106	-0.286
SW max	***	***	***	***
	L fls	*Q fls*	*A flsc*	*H flsc*

p-value

L	0.381	≤0.001	0.274	≤0.001
W max	0.022	0.639	≤0.001	0.002
D max	0.001	***	≤0.001	***
SI av	0.248	0.002	0.378	≤0.001
thG av	0.375	***	0.572	0.208
SW max	***	***	***	***
	L fls	*Q fls*	*A flsc*	*H flsc*

B. Continental shelf

Pearson's correlation coefficient r

L	0.223	0.382	-0.162
W max	0.071	0.362	-0.133
W av	0.189	0.496	0.692
D max	0.213	0.362	-0.208
D av	-0.346	***	-0.384
SI av	-0.042	0.387	0.249
thG av	-0.244	-0.348	-0.095
SW max	0.552	-0.152	-0.395
	W sh	*D sh*	*G sh*

p-value

L	0.002	≤0.001	0.082
W max	0.440	0.002	0.280
W av	0.128	0.009	≤0.001
D max	0.061	0.004	0.110
D av	0.012	***	0.157
SI av	0.620	0.001	0.035
thG av	0.012	0.002	0.404
SW max	≤0.001	0.439	0.038
	W sh	*D sh*	*G sh*

Spearman's rank correlation coefficient rs

L	0.238	0.537	-0.188
W max	0.164	0.270	-0.028
W av	0.398	0.555	0.592
D max	0.411	0.217	-0.239
D av	-0.227	***	-0.353
SI av	-0.252	0.437	0.150
thG av	-0.155	-0.334	0.005
SW max	0.457	-0.051	-0.408
	W sh	*D sh*	*G sh*

p-value

L	0.001	≤0.001	0.043
W max	0.076	0.025	0.823
W av	0.001	0.003	0.001
D max	≤0.001	0.096	0.066
D av	0.105	***	0.197
SI av	0.002	≤0.001	0.207
thG av	0.116	0.003	0.962
SW max	0.003	0.797	0.031
	W sh	*D sh*	*G sh*

C. Continental slope

Pearson's correlation coefficient r

L	0.439	0.207	-0.099
W max	0.407	0.145	-0.125
W av	***	***	***
D max	0.442	0.601	-0.023
D av	***	***	***
SI av	0.121	0.231	-0.316
thG av	-0.416	-0.002	0.493
SW max	-0.427	-0.150	0.758
	W sl	*D sl*	*G sl*

p-value

L	0.001	0.014	0.370
W max	0.008	0.179	0.340
W av	***	***	***
D max	0.003	≤0.001	0.868
D av	***	***	***
SI av	0.655	0.076	0.053
thG av	0.020	0.983	≤0.001
SW max	0.060	0.367	≤0.001
	W sl	*D sl*	*G sl*

Spearman's rank correlation coefficient rs

L	0.875	0.371	-0.246
W max	0.700	0.032	-0.141
W av	***	***	***
D max	0.637	0.462	0.112
D av	***	***	***
SI av	-0.234	0.208	-0.383
thG av	-0.504	0.062	0.461
SW max	-0.286	-0.628	0.744
	W sl	*D sl*	*G sl*

p-value

L	≤0.001	≤0.001	0.023
W max	≤0.001	0.772	0.284
W av	***	***	***
D max	≤0.001	≤0.001	0.417
D av	***	***	***
SI av	0.383	0.111	0.018
thG av	0.004	0.597	≤0.001
SW max	0.221	≤0.001	≤0.001
	W sl	*D sl*	*G sl*

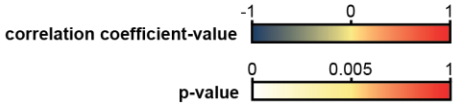

Fig. 10a-c: Heat maps for correlations of canyon morphometrics with parameters of the associated source-to-sink system displaying values of Pearson's correlation coefficient r and Spearman's rank correlation coefficient rs, and their respective p-values. A. Terrestrial catchment. B. Continental shelf. C. Continental slope. L = canyon length; W_{max} = maximum canyon width; W_{av} = average canyon width; D_{max} = maximum canyon depth; D_{av} = average canyon depth; SI_{av} = average canyon sinuosity index; thG_{av} = average canyon thalweg gradient; SW_{max} = maximum canyon sidewall steepness; L_{fls} = fluvial system length; $Qfls$ = average annual fluvial discharge; A_{flsc} = size of the catchment; H_{flsc} = maximum elevation in the catchment area; W_{sh} = shelf width; D_{sh} = shelf-break depth; G_{sh} = average shelf gradient; W_{sl} = slope width; D_{sl} = slope-break depth; G_{sl} = average slope gradient; *** indicates scarcity of data (N<15).

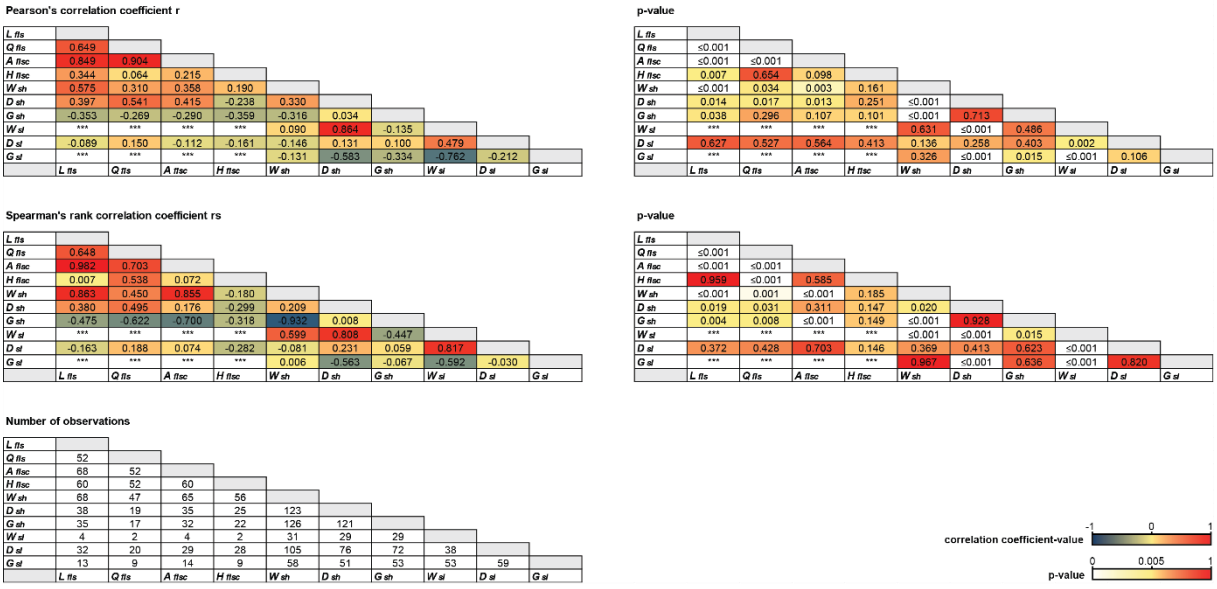

Fig. 11: Heat maps for correlations of parameters of the source-to-sink system specific to studied canyons displaying values of Pearson's correlation coefficient r and Spearman's rank correlation coefficient rs, and their respective p-values. L_{fls} = fluvial system length; *Qfls* = average annual fluvial discharge; A_{flsc} = size of the catchment; H_{flsc} = maximum elevation in the catchment area; W_{sh} = shelf width; D_{sh} = shelf-break depth; G_{sh} = average shelf gradient; W_{sl} = slope width; D_{sl} = slope-break depth; G_{sl} = average slope gradient; *** indicates scarcity of data (N<15).

6.1 Terrestrial catchment

6.1.1 Observations

Fluvial system length displays moderate and statistically significant positive correlation with maximum canyon depth (Fig. 12i), and modest and not significant positive correlation with maximum canyon width (Fig. 12e).

Similarly, moderate significant positive correlations between catchment size and canyon maximum depth and width are seen (Figs. 12 g & k).

Average annual fluvial discharge has moderate direct correlations with canyon length (Fig. 12b) and average canyon sinuosity (Fig. 12n); both relationships are statistically significant.

Moderate statistically significant positive correlations exist between maximum catchment elevation and canyon length (Fig .12d), maximum width (Fig. 12h) and average sinuosity (Fig. 12p).

6.1.2 Interpretations

The observed relationships between canyon length, maximum canyon depth and average canyon sinuosity with attributes of the terrestrial catchment likely reflect how fluvial sediment discharge can promote intra-canyon erosion by down-canyon flows, e.g. the upslope

lengthening of canyons at their apices (e.g. Piper & Normark, 2009), their deepening in the region of canyon mouths, and how the streamwise length of more sinuous canyons is inherently longer (see section 5.2.2.2).

The extent to which the morphology of a submarine canyon is affected by fluvial sediment discharge depends on its erosional versus depositional impact on individual canyon morphometrics, which is determined by many factors and their interplay. The bedrock lithology of terrestrial source areas has been invoked as a control on canyon formation in view of how it can influence the runout distance and erosive strength of submarine flows, e.g. by affecting sediment density, composition and transport mechanisms (Smith et al., 2017). In addition, characteristics of the seafloor substrate can impact its erodibility, which also has an effect on the magnitude of intra-canyon erosion by the flows; for example carbonate cementation can decrease erodibility and stabilise the substrate and canyon walls (e.g. Oiwane et al., 2011), thereby reducing the potential of mass failure on slopes (e.g. Chang et al., 2021) and within canyons. With increasing distance between the river mouth and the submarine canyon head, the sediment transport efficiency decreases as a function of distance and grain size. A global study on sediment delivery to submarine canyons from fluvial systems (Sweet and Blum, 2016) indicates that canyons tend to intercept gravel-sized sediment when their head is within ca. 500 m of a fluvial source, sand-sized sediment when it is within 1 to 5 km, and silt and clay-sized sediment when it is within ca. 40 km. The segregation of grain sizes in shelf-crossing submarine flows can impact canyon evolution; findings from studies of the Monterey Canyon suggest that the presence of unconsolidated sands within a canyon might be a prerequisite for intra-canyon turbidity current generation (Paull et al., 2018), whereas surficial mud deposits on the canyon floor might promote self-acceleration of these flows (Hereema et al., 2020).

The variability of these factors across S2S systems can explain the weakness with which canyon morphometric parameters are scaled with attributes of the terrestrial catchments. Weakness in correlation may also be due to other controls overprinting the effect of fluvial discharge on canyon geomorphology; these controls may include, for example, intra-canyon

sedimentary processes (see section 4.2.1), hydrodynamic processes (section 4.2.2), structural controls (4.2.3) and biogenic processes (4.2.4), as well as sediment remobilisation within the shelf and slope.

A. **Fluvial system length vs length**

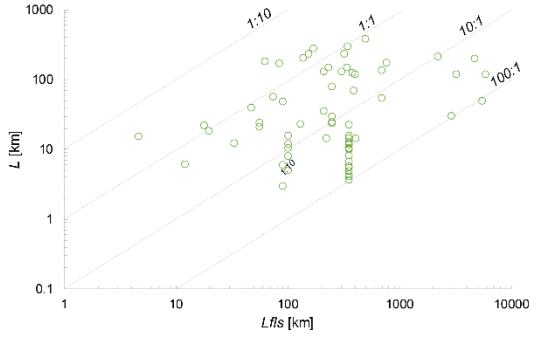

○ ***Lfls vs L:*** r=0.184 p=0.130
N=69 rs=0.107 p=0.381

B. **Av. annual fluvial discharge vs length**

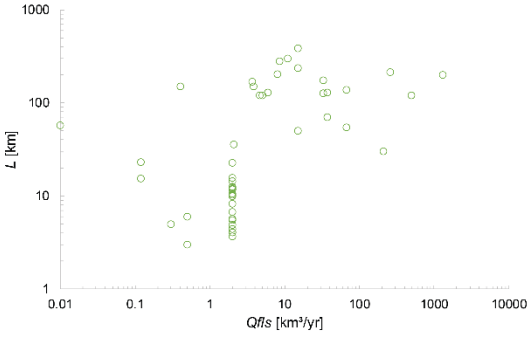

○ ***Qfls vs L:*** r=0.244 p=0.091
N=49 rs=0.666 p≤0.001

C. **Catchment size vs length**

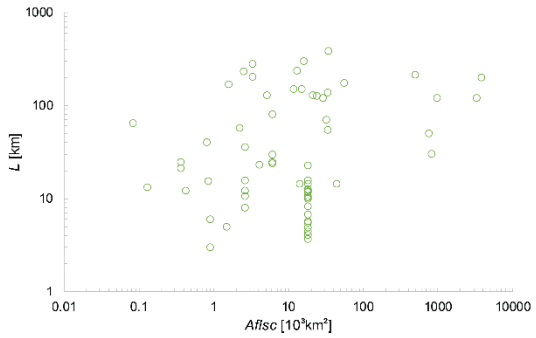

○ ***Aflsc vs L:*** r=0.210 p=0.091
N=66 rs=0.137 p=0.274

D. **Max. catchment elevation vs length**

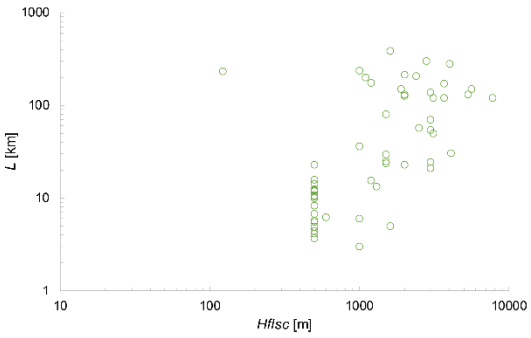

○ ***Hflsc vs L:*** r=0.387 p=0.003
N=58 rs=0.636 p≤0.001

E. **Fluvial system length vs width**

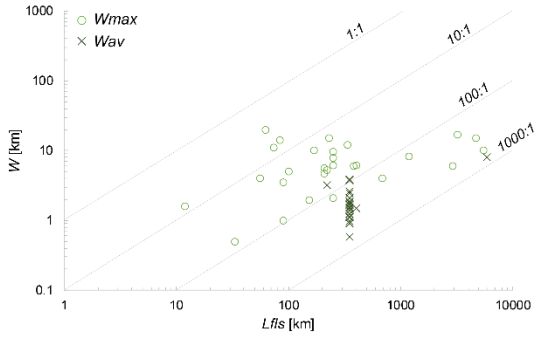

○ ***Lfls vs Wmax:*** r=0.358 p=0.056
N=29 rs=0.424 p=0.022

F. **Av. annual fluvial discharge vs width**

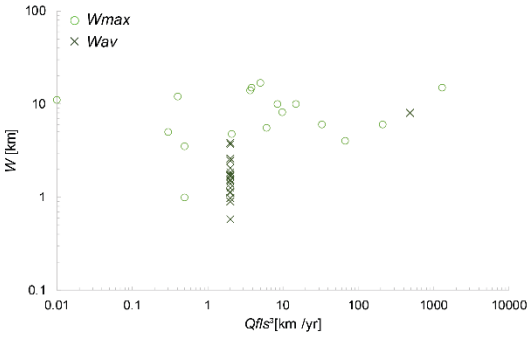

○ ***Qfls vs Wmax:*** r=0.306 p=0.232
N=17 rs=0.123 p=0.639

G. **Catchment size vs width**

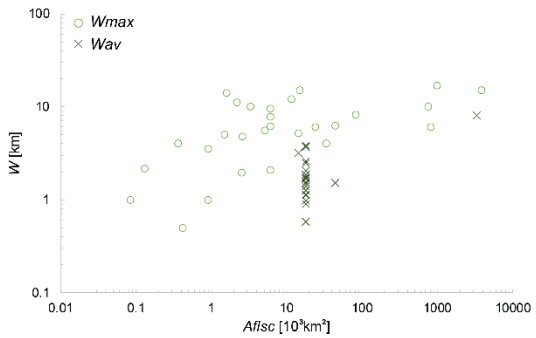

○ ***Aflsc vs Wmax:*** r=0.452 p=0.014
N=29 rs=0.633 p≤0.001

H. **Max. catchment elevation vs width**

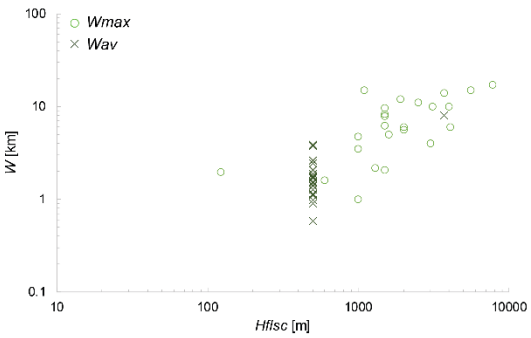

○ ***Hflsc vs Wmax:*** r=0.633 p=0.001
N=26 rs=0.588 p=0.002

I. **Fluvial system length vs depth**

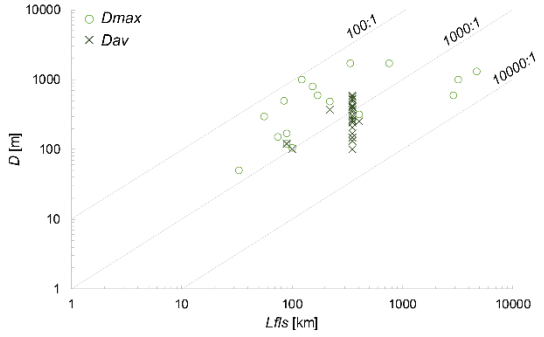

○ ***Lfls vs Dmax:*** r=0.414 p=0.098
N=17 rs=0.736 p=0.001

J. **Av. annual fluvial discharge vs depth**

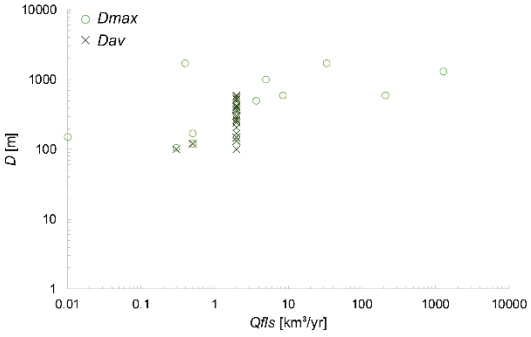

○ ***Qfls vs Dmax:*** r=0.316 p=0.343
N=11 rs=0.586 p=0.058

K. **Catchment size vs depth**

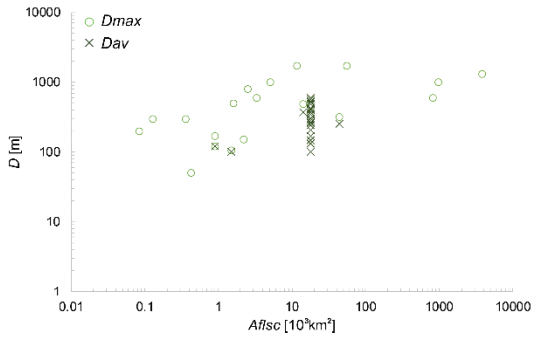

○ ***Aflsc vs Dmax:*** r=0.372 p=0.117
N=19 rs=0.737 p≤0.001

L. **Max. catchment elevation vs depth**

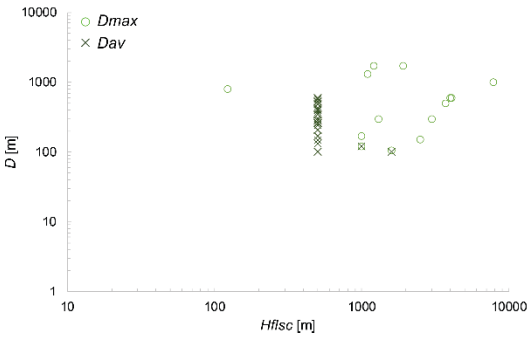

○ ***Hflsc vs Dmax:*** r=0.036 p=0.902
N=14 rs=0.126 p=0.669

M. **Fluvial system length vs average sinuosity**

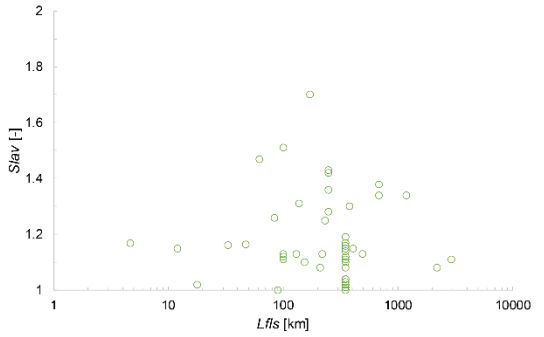

○ ***Lfls vs Slav:*** r=-0.075 p=0.601
N=51 rs=-0.165 p=0.248

N. **Av. annual fluvial discharge vs average sinuosity**

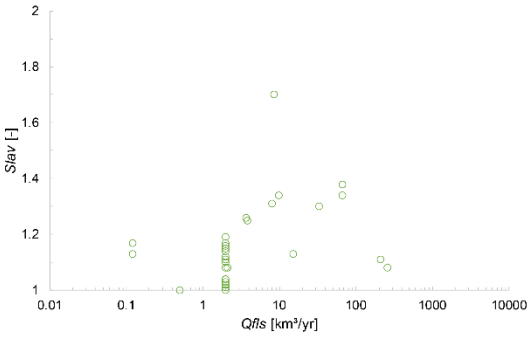

○ ***Qfls vs Slav:*** r=0.057 p=0.743
N=35 rs=0.510 p=0.002

O. **Catchment size vs average sinuosity**

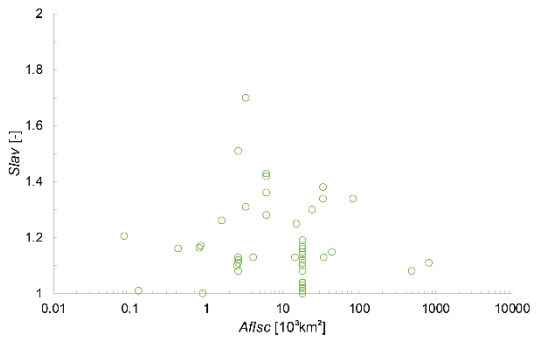

○ ***Aflsc vs Slav:*** r=-0.089 p=0.539
N=50 rs=-0.127 p=0.378

P. **Max. catchment elevation vs average sinuosity**

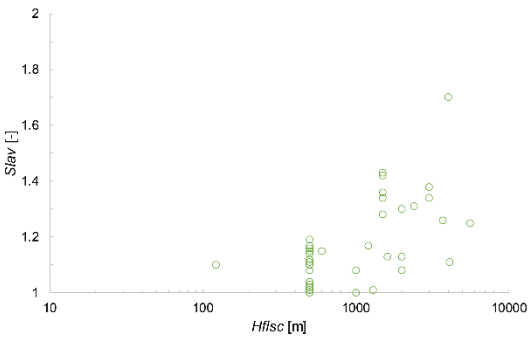

○ ***Hflsc vs Slav:*** r=0.586 p≤0.001
N=26 rs=0.602 p≤0.001

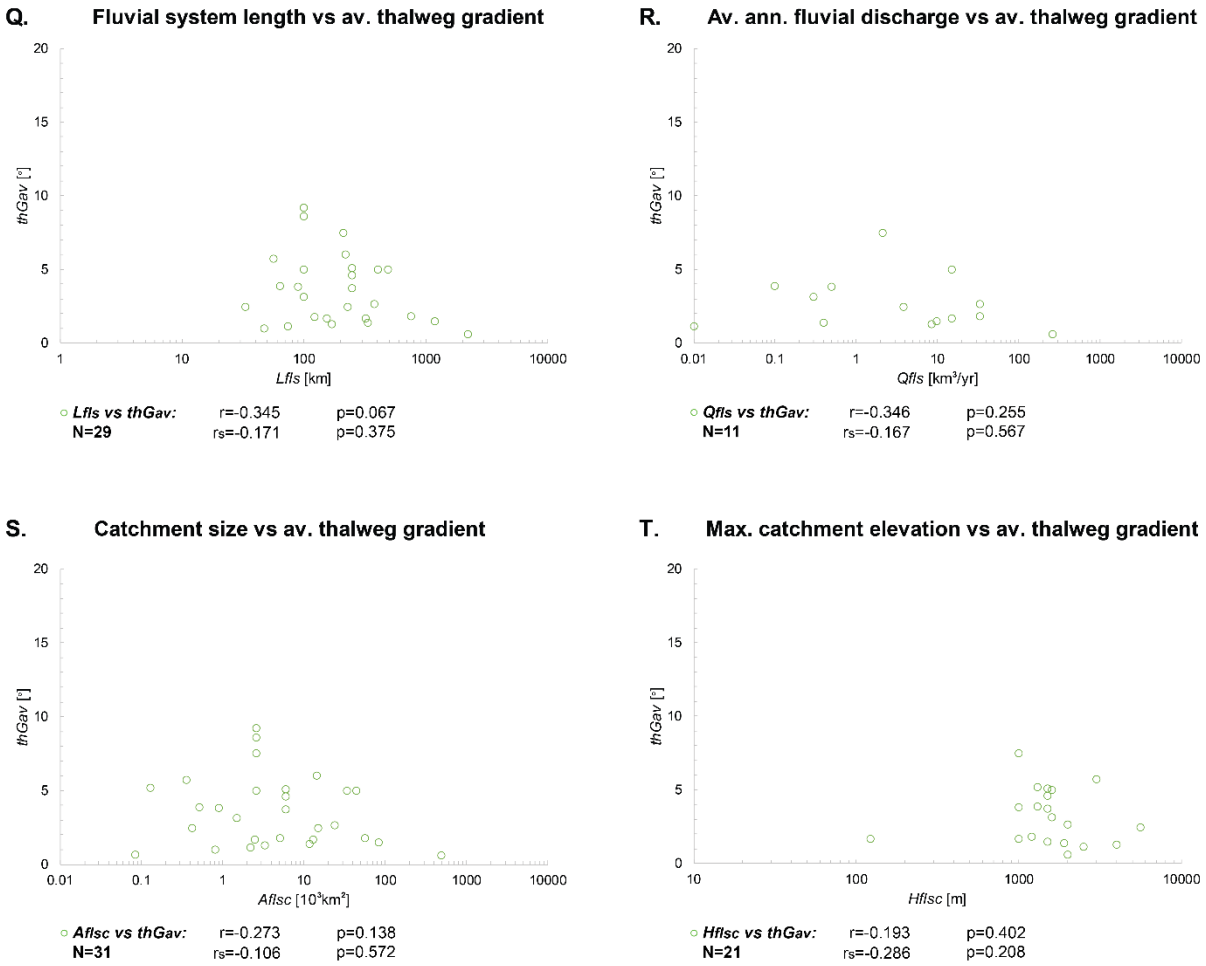

Fig. 12a-t: Scatterplots between attributes of terrestrial catchments and canyon morphometric parameters. N = number of correlations; r = Pearson's correlation coefficient; r_s = Spearman's rank correlation coefficient.

6.2 Continental shelf

6.2.1 Observations

The shelf width is moderately directly correlated with the maximum canyon sidewall steepness (Fig. 13p), and only modestly with average canyon width (Fig. 13d) and maximum canyon depth (Fig. 13g). The shelf width is directly correlated with the canyon length (Fig. 13a) and inversely with the average canyon sinuosity (Fig. 13j), but these relationships are weak.

The shelf-break depth correlates significantly with all investigated canyon morphometric parameters except for the maximum canyon sidewall steepness (Fig. 13q), exhibiting moderate positive correlation with the canyon length (Fig. 13b) and modest correlation with the average canyon sinuosity (Fig. 13k); correlations with maximum width (Fig. 13e) and depth (Fig. 13h) are weaker. In contrast, the average canyon thalweg gradient shows weak but significant inverse scaling with the shelf-break depth (Fig. 13n). Moderate scaling exists between the shelf-break depth and the average canyon width, but the data stem from two geographic regions only: offshore NE Australia and NE Brazil, both associated with shallow (70-85 m) shelves (Fig. 13e).

Correlations of canyon morphometric parameters with the average shelf gradient are mostly weak and not significant (Fig. 13a-r). Moderate and significant correlation is observed between shelf gradient and average canyon width (Fig. 13f), but these results are based on data from two geographic regions only. Modest inverse correlation is seen between shelf gradient and maximum canyon sidewall steepness, which is not statistically significant (Fig. 13r).

Submarine canyons with present-day shelf break deeper than 120 m bsl are on average longer and have greater maximum widths and depths, higher average canyon sinuosities and steeper average canyon thalweg gradients than canyons with a shelf-break lower than 120 m bsl. The same trends are seen for groups of canyons distinguished based on a threshold of shelf-break depth of 130 m (Fig. 14a-f). Although a greater range in maximum canyon sidewall steepness is seen in canyons associated with shelf breaks deeper than 120 m, average values between both canyon groups are very similar. Data on maximum canyon depth and maximum canyon sidewall steepness that can be employed in this analysis are limited, whereas data on average width and depth are only available for canyons installed on slopes with shelf breaks shallower than 120 m.

6.2.2 Interpretations

The width of the shelf plays a role in across-shelf sediment distribution from fluvial outlets to the shelf edge (e.g. Sweet et al., 2020). Narrower shelves are characterized by shorter distances to fluvial outlets that can deliver sediment to canyon heads, and may allow sediment connection of canyons with rivers and littoral cells to be maintained during sea-level highstands (e.g. Covault et al., 2007; Normark et al., 2009; Jipa and Panin, 2020). Steeper shelf gradients might also inhibit deposition by hyperpycnal flows and promote bedload transport of coarse sediment from rivers across shelves (e.g. Jipa & Panin, 2020).

By contrast, the effect of hydroisostasy on continental levering and the ensuing steepening of continental shelves is thought to be stronger for wider shelves, probably by a factor ≤0.3 since the Last Glacial Maximum (LGM), relative to narrower shelves (Hutton et al., 2013). Nevertheless, despite being more prone to hydroisostatic flexure, wider shelves tend to have gentler gradients than narrower shelves.

Wider shelves also tend to have resulted from greater shelf-edge progradation, which can occur in response to greater rates of sediment supply to the outer shelf and upper slope from terrestrial catchments and from shelf-internal sources (e.g. Mougenot et al., 1983; Carvajal et al., 2009; Blum et al., 2013), as well as from the up-building of slope sediment prisms from drifts (e.g. Fulthorpe and Carter, 1991). However, although a wider shelf indicates a more sustained sediment supply to a shelf margin, sediment transport across wide shelves into submarine canyons is most effective for canyons that have significantly retrograded the shelf and/or are connected with a river, either directly or via shelf channels or shelf-edge deltas. With increasing shelf width, the effectiveness of across-shelf sediment transport from fluvial outlets decreases for coarser grained sediment, leading to variations in grain-size distribution of sediment discharged from rivers across the shelf. Hence, the importance of erosion by submarine flows linked to rivers on canyon morphology becomes likely less significant on shelves wider than 5 km, given the expected paucity of sand grain-size fractions reaching beyond this boundary (section 6.1). In addition, the frequency and magnitude of hyperpycnal

flows can be affected by factors other than the shelf width, such as salinity of the water body, climate and relative sea-level change (e.g. Mulder et al., 2003; Dadson et al., 2005).

The effectiveness of across-shelf sediment transport is also affected by hydrodynamic processes associated with tidal currents, along-shelf currents and waves (Nittrouer and Wright, 1994; Wang et al., 2010). The ability of waves to remobilise sediment is greater at shallower depths (Peters and Loss, 2012); this sediment transport mechanism might have a greater areal effect on wide and shallow shelves with lower gradients.

Moreover, the shelf topography can variably affect across-shelf sediment dispersal into submarine canyons: shelf uplift and deformation by tectonic activity (e.g. Johnson et al., 2017) can create seafloor topography and modify shelf gradients, which in turn can force sediment transport pathways and pathways of shelf valleys and submarine canyons incising the shelf. Currents, waves and flows carrying sediment might also be deflected away from canyons by intrashelf highs of variable origin.

The subaerial exposure of continental shelves at lowstand can lead to the amalgamation of river catchment areas as confluences are established; this might significantly enhance sediment supply to individual fluvial outlets, and in turn to canyons with sediment connectivity to these systems, especially for large fluvial systems that can arise as wide shelves are exposed (Blum et al., 2013). Additional sediment might be conveyed to canyons from the local erosion of shelf substrate when rivers traverse the exposed shelf (e.g. Sweet et al., 2020).

Some of the scaling relationships between shelf configuration and canyon morphometrics may also be due to covariance with other related parameters. For example, scaling of canyon length with shelf-break depth might in part reflect how deeper shelves are associated with wider slopes, and how shelf-break depths tend to increase for terrestrial catchments associated with larger fluvial systems or multiple fluvial sources, greater average annual discharge and catchment size. However, scaling relationships between shelf-break depth and attributes of the terrestrial catchment are not significant.

During episodes of sea-level lowstand, such as during the LGM, canyons with their heads in vicinity of the shelf-edge could be fed by fluvial systems that had prograded onto the shelves (e.g. Sweet et al., 2020).

In sequence stratigraphic models, routing of significant volumes of sand-sized sediment across continental slopes to basin floors and the development of submarine fans is perceived to be most effective during relative sea-level lowstands (e.g. Posamentier et al., 1991), which would suggest that canyon evolution by down-canyon sediment gravity flows might also be enhanced during these intervals. Reconstructions and estimates for the eustatic fall during the LGM have been variably placed between ca. 120 m to 135 m bsl (e.g. Clark and Mix, 2002; Simms et al., 2019, and references therein), so that most shelves with shelf breaks shallower than 120 m bsl have likely been subaerially exposed during the LGM. Despite this, our findings are that canyons hosted on shelves with shelf breaks deeper than 120 m bsl tend to be larger, to be more sinuous, and to have steeper canyon thalweg gradients than those with shelf breaks at 120 m or less. This indicates that sediment connection of canyons to rivers and littoral cells during phases of sea-level lowstands is not as important a control on canyon geomorphology compared to other controls. The findings might also indicate how deeper shelves tend to be associated with larger terrestrial catchments (Fig. 15; Wang et al., 2019).

The complex role of shelf physiography and across-shelf sediment transport, together with covariance in shelf and canyon characteristics in response to common controls on sediment dispersal, explain the limited value of shelf configuration as a predictor of canyon geomorphology.

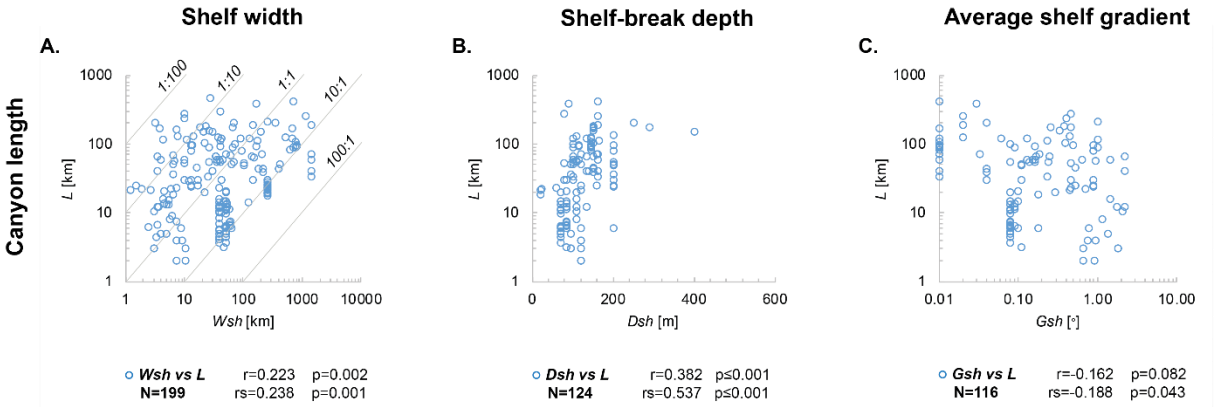
Shelf width
Shelf-break depth
Average shelf gradient
Canyon length
A.
B.
C.
L [km]
Wsh [km]
Dsh [m]
Gsh [°]
1:100
1:10
1:1
10:1
100:1
Wsh vs L r=0.223 p=0.002
N=199 rs=0.238 p=0.001
Dsh vs L r=0.382 p≤0.001
N=124 rs=0.537 p≤0.001
Gsh vs L r=-0.162 p=0.082
N=116 rs=-0.188 p=0.043

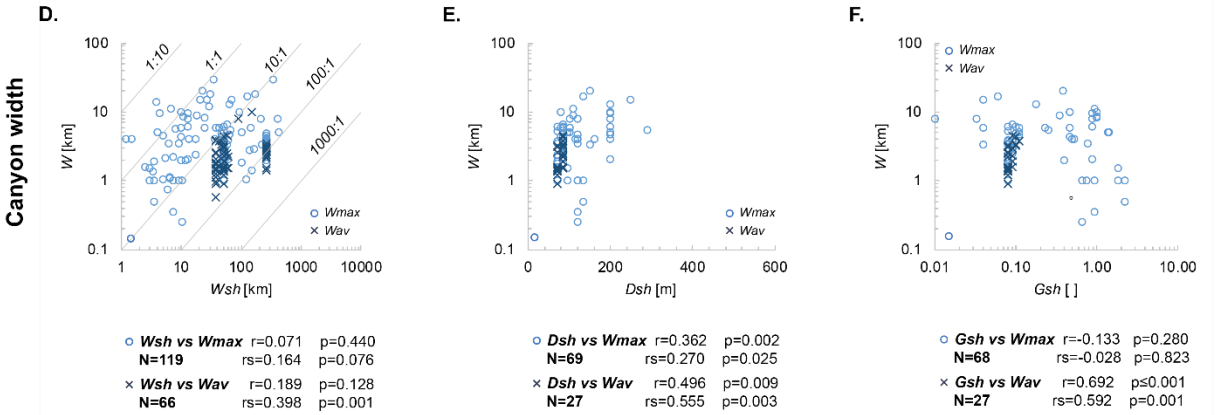
Canyon width
D.
E.
F.
W [km]
Wsh [km]
Dsh [m]
Gsh [ ]
1:10
1:1
10:1
100:1
1000:1
Wmax
Wav
Wsh vs Wmax r=0.071 p=0.440
N=119 rs=0.164 p=0.076
Wsh vs Wav r=0.189 p=0.128
N=66 rs=0.398 p=0.001
Dsh vs Wmax r=0.362 p=0.002
N=69 rs=0.270 p=0.025
Dsh vs Wav r=0.496 p=0.009
N=27 rs=0.555 p=0.003
Gsh vs Wmax r=-0.133 p=0.280
N=68 rs=-0.028 p=0.823
Gsh vs Wav r=0.692 p≤0.001
N=27 rs=0.592 p=0.001

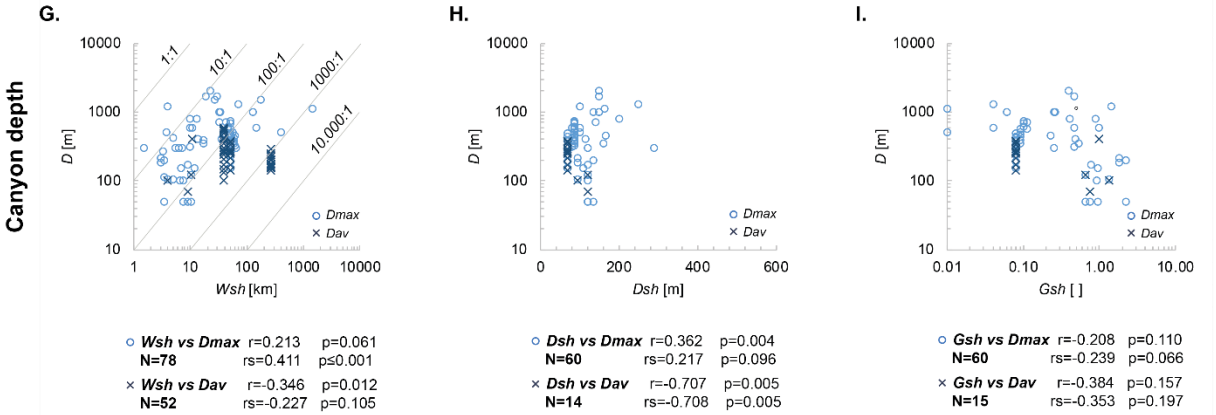
Canyon depth
G.
H.
I.
D [m]
Wsh [km]
Dsh [m]
Gsh [ ]
1:1
10:1
100:1
1000:1
10,000:1
Dmax
Dav
Wsh vs Dmax r=0.213 p=0.061
N=78 rs=0.411 p≤0.001
Wsh vs Dav r=-0.346 p=0.012
N=52 rs=-0.227 p=0.105
Dsh vs Dmax r=0.362 p=0.004
N=60 rs=0.217 p=0.096
Dsh vs Dav r=-0.707 p=0.005
N=14 rs=-0.708 p=0.005
Gsh vs Dmax r=-0.208 p=0.110
N=60 rs=-0.239 p=0.066
Gsh vs Dav r=-0.384 p=0.157
N=15 rs=-0.353 p=0.197

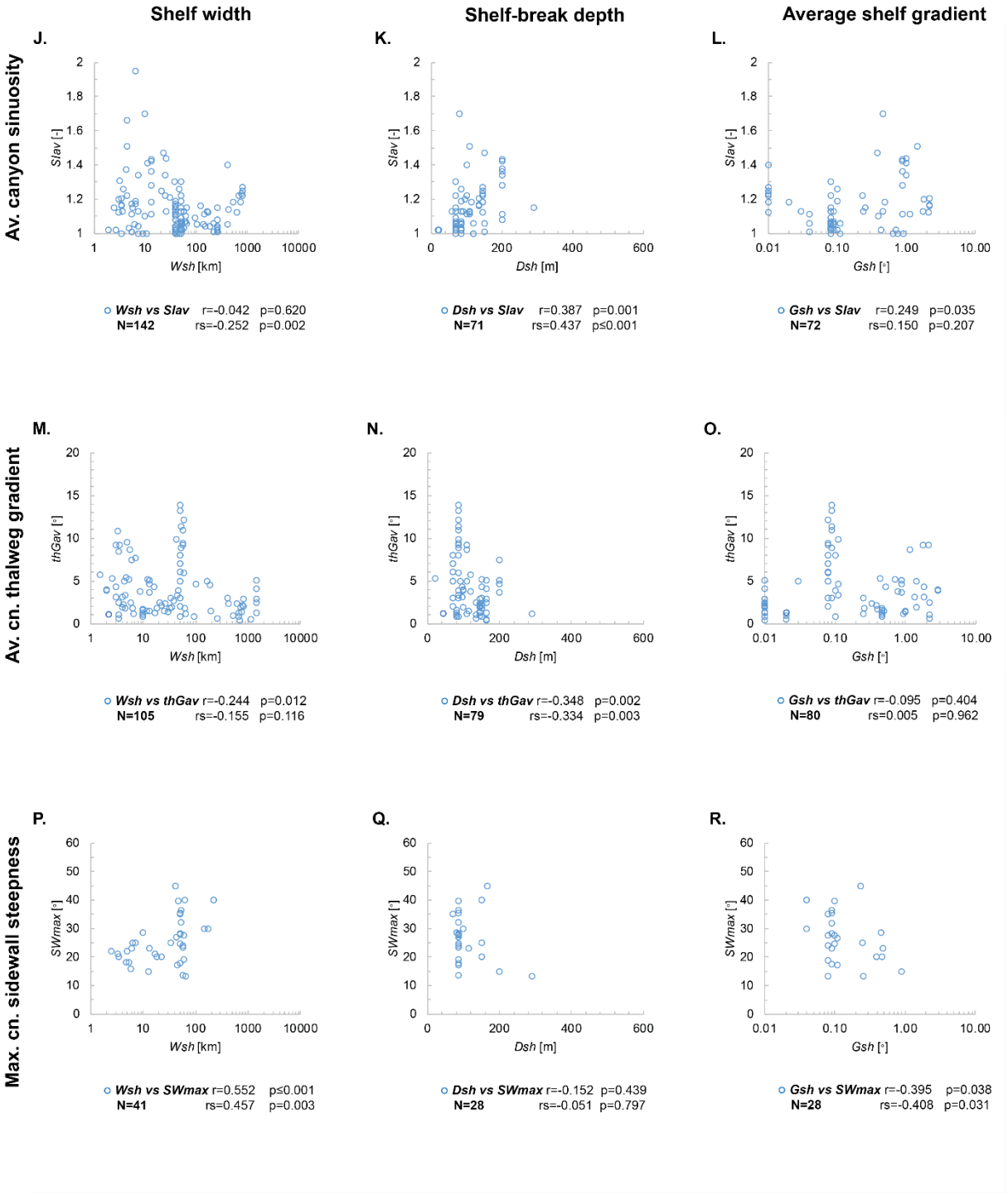

Fig. 13a-r: Scatterplots between attributes of the continental shelf and canyon morphometric parameters. N = number of correlations; r = Pearson's correlation coefficient; r_s = Spearman's rank correlation coefficient.

A. Length

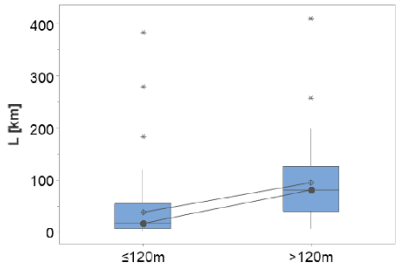

	N	min	mean	StDev	median	max
≤120	**78**	2.00	38.14	58.60	17.02	384.05
>120	**46**	6.00	95.50	74.00	81.30	411.00
T-Value =-4.49 DF = 80 P-Value ≤ 0.001						
≤130	**78**	2.00	37.45	57.15	17.02	384.05
>130	**46**	6.00	96.60	75.00	81.30	411.00
T-Value =-4.62 DF = 75 P-Value ≤ 0.001						

B. Maximum width

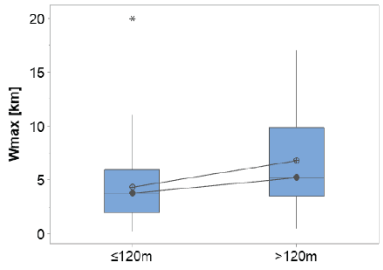

	N	min	mean	StDev	median	max
≤120	**53**	0.25	4.33	3.37	3.78	20.00
>120	**16**	0.50	6.79	4.91	5.20	17.00
T-Value =-1.87 DF = 19 P-Value = 0.077						
≤130	**52**	0.25	4.03	2.58	3.78	11.00
>130	**17**	0.50	7.56	5.73	5.40	20.00
T-Value =-2.46 DF = 18 P-Value = 0.024						

C. Maximum depth

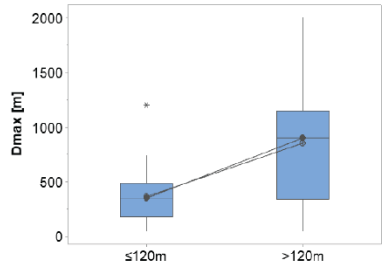

	N	min	mean	StDev	median	max
≤120	**46**	50.00	364.50	225.50	350.00	1200.00
>120	**14**	50.00	854.00	567.00	900.00	2000.00
T-Value =-3.15 DF = 14 P-Value = 0.007						
≤130	**46**	50.00	364.50	225.50	350.00	1200.00
>130	**14**	50.00	854.00	567.00	900.00	2000.00
T-Value =-3.15 DF = 14 P-Value = 0.007						

D. Average canyon sinuosity

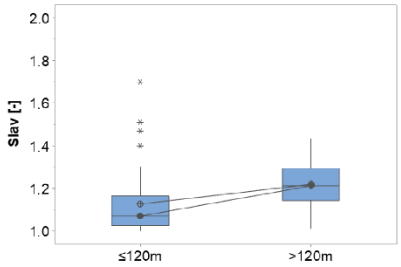

	N	min	mean	StDev	median	max
≤120	**49**	1.00	1.1265	0.14	1.07	1.70
>120	**22**	1.01	1.22	0.12	1.21	1.43
T-Value =-2.90 DF = 49 P-Value = 0.006						
≤130	**48**	1.00	1.12	0.14	1.07	1.70
>130	**23**	1.01	1.23	0.12	1.22	1.47
T-Value =-3.41 DF = 47 P-Value = 0.001						

E. Average canyon thalweg gradient

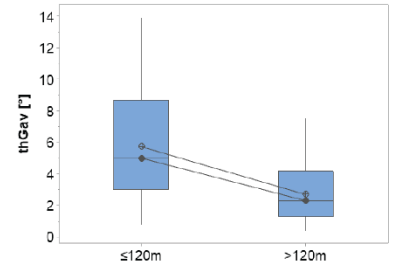

	N	min	mean	StDev	median	max
≤120	**46**	0.78	5.72	3.53	5.00	13.90
>120	**33**	0.40	2.69	1.72	2.30	7.50
T-Value = 5.04 DF = 69 P-Value ≤ 0.001						
≤130	**46**	0.78	5.72	3.53	5.00	13.90
>130	**33**	0.40	2.69	1.72	2.30	7.50
T-Value = 5.04 DF = 69 P-Value ≤ 0.001						

F. Maximum canyon sidewall steepness

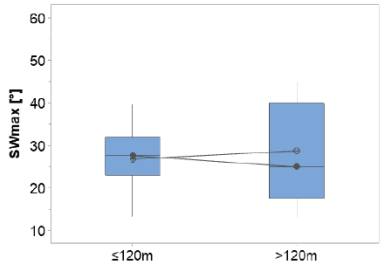

	N	min	mean	StDev	median	max
≤120	**19**	13.40	26.82	7.05	27.60	39.60
>120	**9**	13.30	28.70	12.40	35.00	45.00
T-Value =-0.42 DF = 10 P-Value = 0.681						
≤130	**19**	13.40	26.82	7.05	27.60	39.60
>130	**9**	13.30	28.70	12.40	35.00	45.00
T-Value =-0.42 DF = 10 P-Value = 0.681						

Fig. 14a-f: Boxplots of frequency distributions of canyon morphometric parameters for studied canyons distinguished based on shelf-break depth thresholds of 120 m at the canyon. Tabulated statistics refer to canyon grouped based on shelf-break thresholds of 120 m and 130 mbsl, respectively. N = number of readings; min = minimum value; mean = mean value; StDev = standard deviation; median = median value; max = maximum value.

6.3 Continental slope

6.3.1 Observations

The slope width exhibits strong and significant correlation with canyon length (Fig. 15a), and moderate significant correlations with maximum width (Fig. 15d), maximum depth (Fig. 15g) and the average canyon thalweg gradient (Fig. 15m).

The slope-break depth shows moderate scaling with maximum canyon depth (Fig. 15h) and maximum canyon sidewall steepness (Fig. 15q), and rather weak but statistically significant correlation with canyon length (Fig. 15b).

For the average slope gradient, moderate correlations are demonstrated with maximum canyon sidewall steepness (Fig. 15r) and average canyon thalweg gradient (Fig. 15o), whereas correlations with other parameters are weak and not significant (Fig. 15a-r).

6.3.2 Interpretations

The canyon length is the only canyon morphometric parameter that is related to the slope width, as reflected in the strong scaling between these two variables and, to smaller extent, in the relationship between canyon length and slope-break depth.

Positive relationships are seen for slope width with maximum canyon width and depth, and for the latter with slope-break depth; these relationships reflect how intra-canyon erosion is promoted at the canyon mouth (see section 5.1.1.2).

The positive relationship between slope-break depth and maximum canyon depth might also reflect how canyons in open seas tend to be deeper compared to canyons in semi-enclosed and enclosed seas (see section 7.4).

The results show that average canyon sinuosity is not correlated to the slope-break depth or to slope steepness. Additional data are needed to evaluate potential correlation between slope width and average canyon sinuosity.

The modest, positive correlation between the overall slope gradient and average canyon thalweg gradient relates to how the average canyon thalweg gradient is constrained by the average gradient of the continental slope; yet important variability is observed. In this study, as in previous ones (e.g. Harris and Whiteway, 2011), the overall canyon thalweg gradient is determined in part by the position of both canyon apex and mouth, which are themselves related to local seafloor relief. The observed moderate negative relationship between slope width and average canyon thalweg gradient reflects how wider slopes tend to display gentler gradients (Fig. 11; cf. Sømme et al., 2009).

The moderate, positive scaling seen between maximum canyon sidewall steepness and the average slope gradient may reflect how slopes that are steeper on average may be associated with increased erosion in submarine canyons, in relation to steeper slopes promoting processes of mass failure (e.g. McGregor, 1983; Susanth et al., 2021), and potentially driving retrograde slope failure (Lo Iacono et al., 2014), as well as vertical canyon incision (e.g. Susanth et al., 2021). Following this line of interpretation, the negative correlation of slope width with maximum canyon sidewall steepness might be a record of the covariance between average slope gradient and slope width. An inverse moderate relationship is seen between slope-break depth and maximum canyon sidewall steepness, but the dataset does not include slope-break depths between 4,000 and 6,000 m bsl and dominantly includes canyons associated with continental-slope breaks that are 2,000 to 4,000 m bsl. More data are needed to confirm this relationship.

The lack of correlation between the average slope gradient and maximum canyon dimensions indicate that the slope gradient has no significant influence on canyon size, in spite of how the slope steepness might affect the magnitude of retrograde erosion and the erosive strength of down-canyon sediment gravity flows. Also, the average slope gradient does not capture local relief along the slope profiles, which can control sediment bypass (e.g. Soutter et al., 2021); further investigation of the role of slope relief and slope profile types as controls on canyon geomorphology is required.

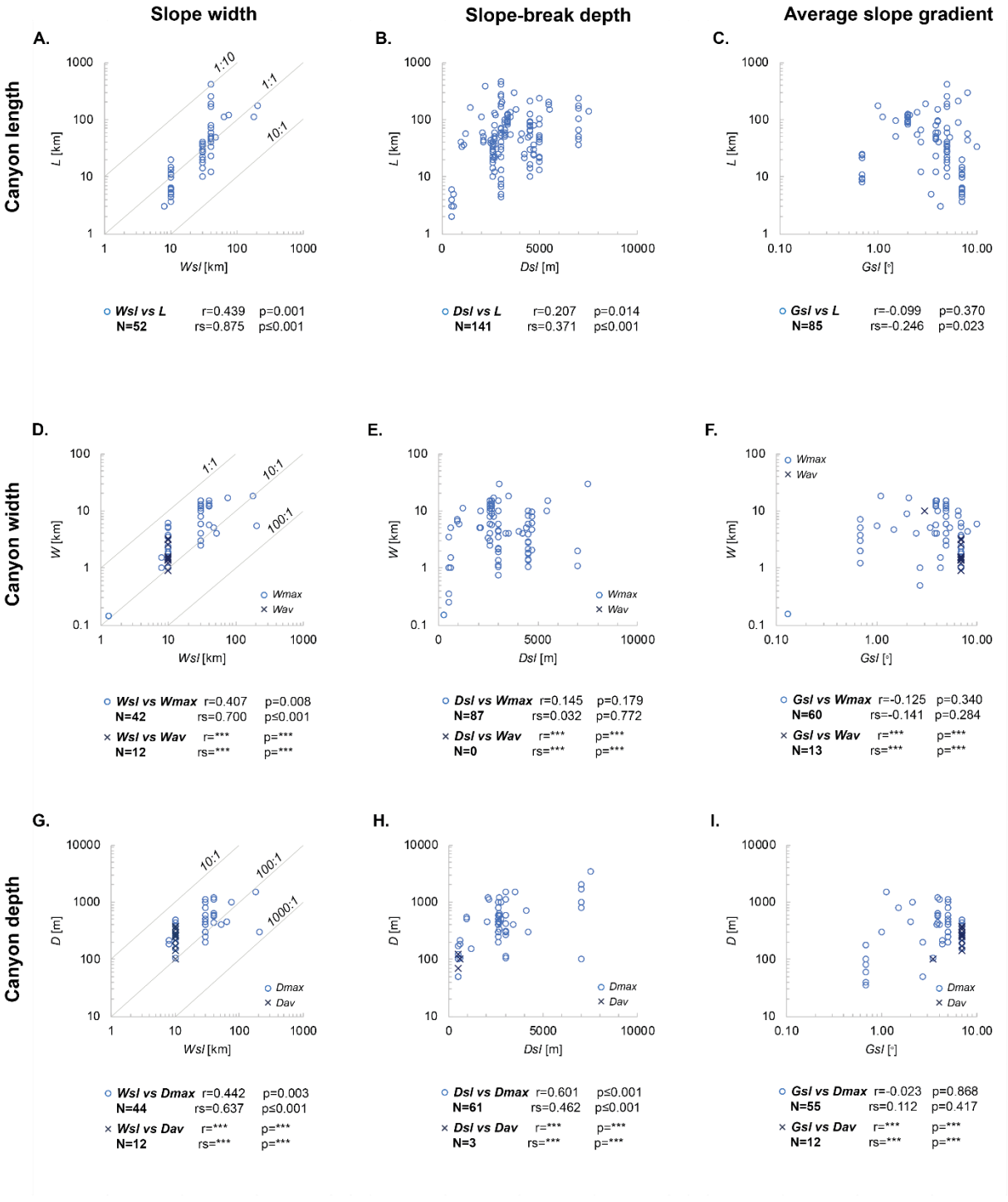
Slope width
Slope-break depth
Average slope gradient
Canyon length
Canyon width
Canyon depth
A.
B.
C.
D.
E.
F.
G.
H.
I.
L [km]
W [km]
D [m]
Wsl [km]
Dsl [m]
Gsl [°]
1:10
1:1
10:1
100:1
1000:1
Wmax
Wav
Dmax
Dav
Wsl vs L r=0.439 p=0.001 N=52 rs=0.875 p≤0.001
Dsl vs L r=0.207 p=0.014 N=141 rs=0.371 p≤0.001
Gsl vs L r=-0.099 p=0.370 N=85 rs=-0.246 p=0.023
Wsl vs Wmax r=0.407 p=0.008 N=42 rs=0.700 p≤0.001
Wsl vs Wav r=*** p=*** N=12 rs=*** p=***
Dsl vs Wmax r=0.145 p=0.179 N=87 rs=0.032 p=0.772
Dsl vs Wav r=*** p=*** N=0 rs=*** p=***
Gsl vs Wmax r=-0.125 p=0.340 N=60 rs=-0.141 p=0.284
Gsl vs Wav r=*** p=*** N=13 rs=*** p=***
Wsl vs Dmax r=0.442 p=0.003 N=44 rs=0.637 p≤0.001
Wsl vs Dav r=*** p=*** N=12 rs=*** p=***
Dsl vs Dmax r=0.601 p≤0.001 N=61 rs=0.462 p≤0.001
Dsl vs Dav r=*** p=*** N=3 rs=*** p=***
Gsl vs Dmax r=-0.023 p=0.868 N=55 rs=0.112 p=0.417
Gsl vs Dav r=*** p=*** N=12 rs=*** p=***

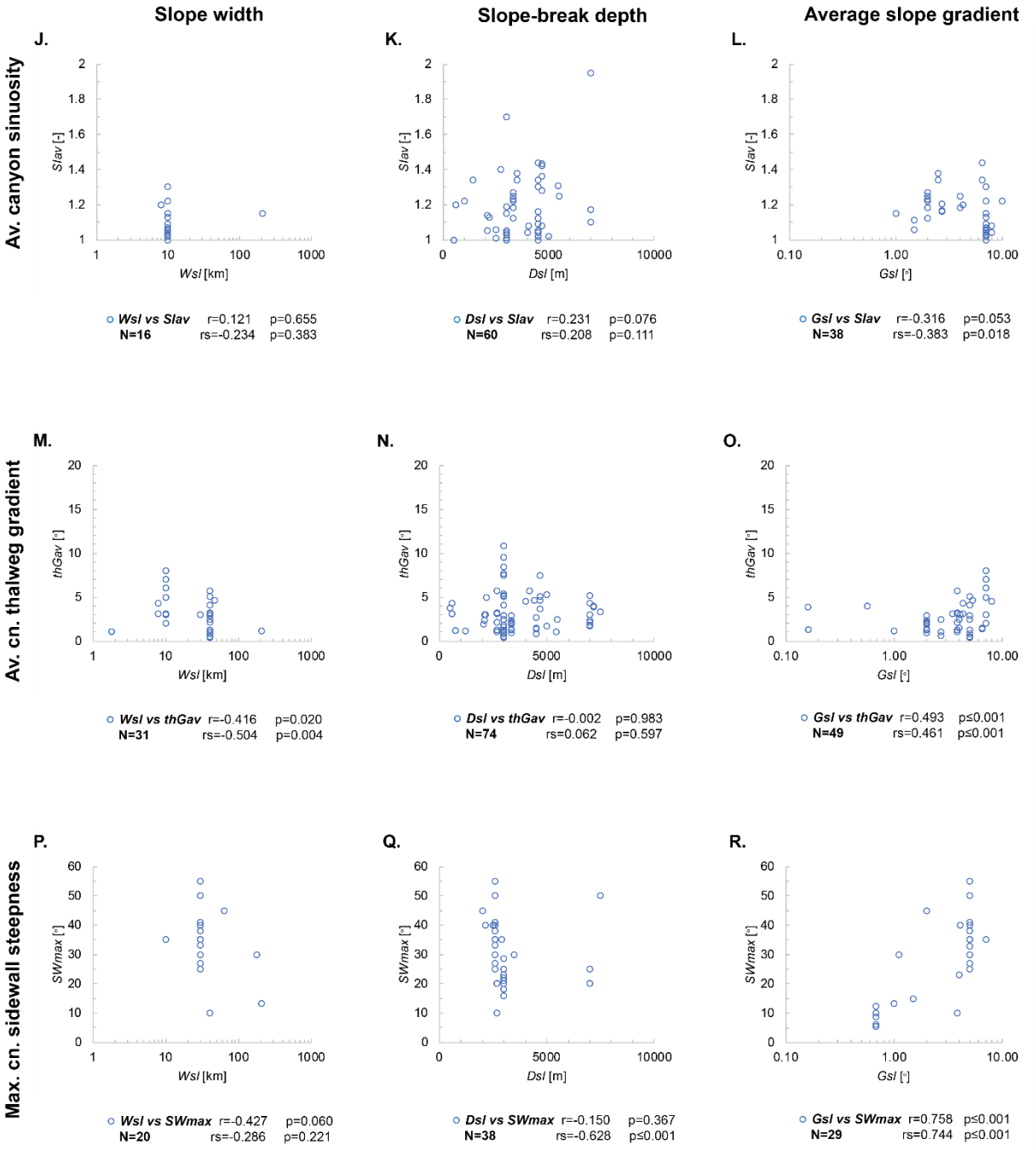

Fig. 15a-r: Scatterplots between attributes of the slope vs canyon morphometrics. N = number of correlations; r = Pearson's correlation coefficient; rs = Spearman's rank correlation coefficient.

7 Variations in canyon morphometric parameters across classes of environments

A. Length

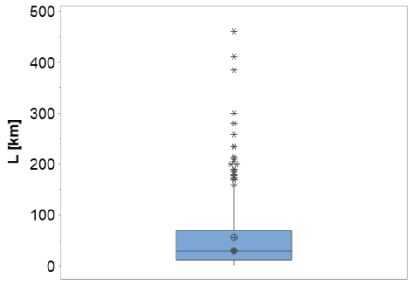

	N	min	mean	StDev	median	max
L	**263**	2.00	56.52	69.15	29.79	460.00

B. Width

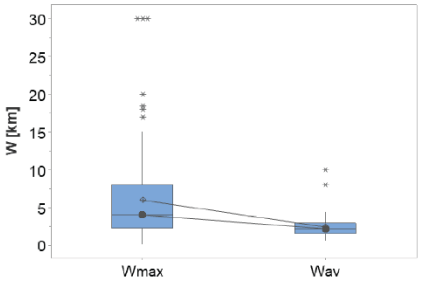

	N	min	mean	StDev	median	max
Wmax	**164**	0.15	5.97	5.43	4.00	30.00
Wav	**66**	0.58	2.41	1.50	2.18	10.00

C. Depth

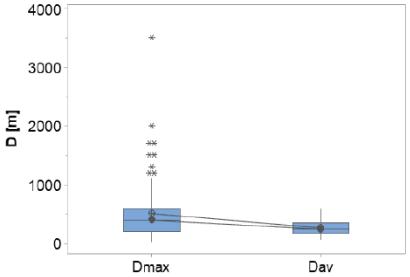

	N	min	mean	StDev	median	max
Dmax	**113**	35.00	508.00	475.10	400.00	3500.00
Dav	**52**	70.00	268.10	126.30	244.00	594.00

D. Average canyon sinuosity

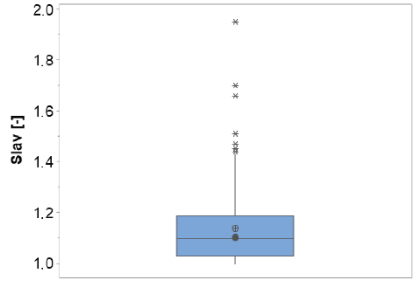

	N	min	mean	StDev	median	max
Slav	**151**	1.00	1.14	0.15	1.1	1.95

E. Average canyon thalweg gradient

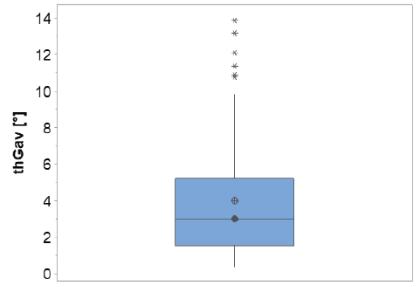

	N	min	mean	StDev	median	max
thGav	**120**	0.40	3.98	3.09	3.00	13.90

F. Maximum canyon sidewall steepness

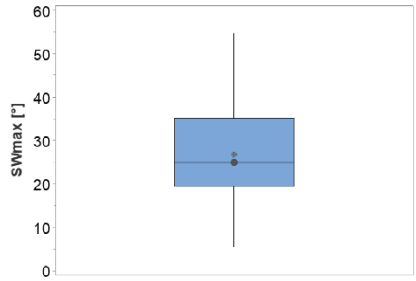

	N	min	mean	StDev	median	max
SWmax	**69**	5.40	26.80	11.48	25.00	55.00

Figure 16a-f: Boxplots of frequency distributions of the investigated canyon morphometric parameters. L = canyon length; W_{max} = maximum canyon width; W_{av} = average canyon width; D_{max} = maximum canyon depth; D_{av} = average canyon depth; SI_{av} = average canyon sinuosity index; thG_{av} = average canyon thalweg gradient; SW_{max} = maximum canyon sidewall steepness. N = number of readings; min = minimum value; mean = mean value; StDev = standard deviation; median = median value; max = maximum value.

Descriptive statistics of frequency distributions of canyon morphometric parameters have been evaluated for the entire dataset (Fig. 16a-f), as well as for separate groups of canyons reflecting categories of canyon-apex location relative to the shelf-break, continental-margin type, source-to-sink setting, oceanographic environment, and latitudinal zones (sections 7.1 to 7.5). This was done to investigate whether and how factors associated with the environmental setting may control canyon geomorphology. Meaningful comparisons of average canyon width and depth as a function of S2S system setting and latitudinal zone, and for average canyon depth relative to canyon-head location, were not possible due to limited data availability.

In addition, ratios of maximum width to maximum depth across the different environmental settings have been assessed (section 7.6).

The distributions of each canyon morphometric parameter are graphically presented in form of boxplots and are discussed in sections 7.1 to 7.6 below.

7.1 Canyon-apex location relative to the shelf break

7.1.1 Observations

The studied shelf-incising canyons tend to be longer than slope-confined canyons, on average by a factor of 2.25 (Fig. 17a), and to be more sinuous (Fig. 17f); across these two groups, these are the only two morphometric parameters whose mean values differ significantly. Canyons incising the shelf display on average slightly greater maximum and overall widths, but slope-confined canyons reach the same values of maximum widths, and

the largest value of average width is seen in a slope-confined canyon (Fig. 17c). Although greater maximum depths (Fig. 17d), and lower overall thalweg gradients (Fig. 17g) are seen in canyons incising the shelf, differences in their average values are not statistically significant. The data on average canyon depth are limited, but the results show very similar ranges in values across the two groups (Fig. 17e). On average, the maximum sidewall steepness is similar between groups of canyons classified on the location of the canyon apex relative to the shelf break, but slope-confined canyons display a greater range (Fig. 17h).

7.1.2 Interpretations

The greater lengths of shelf-incising canyons may reflect how retrograde incision of the shelf and the promotion of canyon progradation by sediment gravity flows originating on the shelf and in the terrestrial catchment constitute primary controls on the length of submarine canyons. Sediment is supplied to the canyons via coupling with fluvial outlets or littoral cells and locally from within the shelf (sections 5.1 & 5.2). In addition, canyon heads placed above the storm wave-base can intercept sediment mobilised and transported during storm events (e.g. Sequeiros et al., 2019) (section 4.2.2).

In contrast, characteristics like the maximum and average canyon width, maximum depth, average canyon thalweg gradient and maximum canyon sidewall steepness are not related to whether canyons are incised into the shelf. This in turn suggests that the relative position of the canyon apex to the shelf break does not constitute a dominant control on overall canyon morphology.

The evolution of slope-confined canyons is not necessarily driven by intra-canyon slope failures alone. Slope-confined canyons can be fed by sands overpassing the shelf edge if their heads are in the range of the run-out distance of turbidity currents linked to fluvial discharge or littoral cells (e.g. Cronin et al., 2005; Yin et al., 2019). Sediment remobilised within the slope can also be distributed to a slope-confined canyon by contour currents, if the canyon is coupled with a contourite system (e.g. Warratz et al., 2019).

Despite the role of sediment gravity flows in canyon growth and sinuosity increase, mean values of average canyon sinuosity are very similar across the two groups. This indicates that the importance of connections of the canyon to the shelf as a control on its sinuosity might be limited, in contrast with current understanding. Specifically, the process of canyon shelf-breaching, by enabling linkages with shelf and terrestrial sediment sources, has been suggested to lead to distinctively higher sinuosities in shelf-incising canyons compared to slope-confined ones (e.g. Farre et al., 1983; Orange et al., 1994; Wiles et al., 2019). On this basis, the sinuosity of canyons has been utilised to deduct canyon head location relative to the shelf-break on a regional scale in absence of sufficient bathymetric data coverage of proximal parts of canyons (see Wiles et al., 2019). Based on our analyses, it appears that the overall canyon sinuosity is not a suitable predictor of the position of the canyon apex relative to the shelf break.

More generally, considering the findings of this work in light of those of earlier studies (Harris and Whiteway, 2011; Huang et al. 2014), it is concluded that whether a canyon is incised in the shelf is not a reliable predictor of canyon size and geomorphology.

A. Length

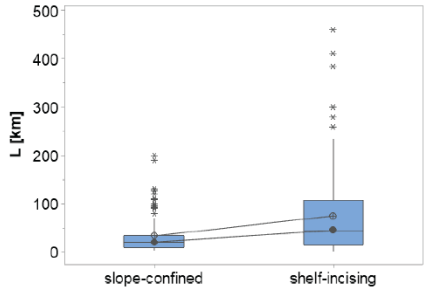

	N	min	mean	StDev	median	max
slope	**98**	3.70	33.37	39.32	21.00	200.00
shelf	**137**	2.00	75.13	84.69	45.00	460.00
T-Value =-5.06 DF = 204 P-Value ≤ 0.001						

B. Maximum width

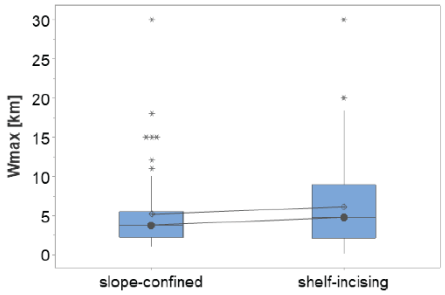

	N	min	mean	StDev	median	max
slope	**64**	1.00	5.12	4.96	3.74	30.00
shelf	**87**	0.15	6.14	5.32	4.79	30.00
T-Value =-1.21 DF = 140 P-Value = 0.230						

C. Average width

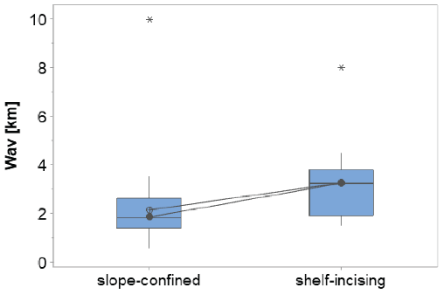

	N	min	mean	StDev	median	max
slope	**45**	0.58	2.15	1.41	1.85	10.00
shelf	**17**	1.51	3.26	1.58	3.25	8.00
T-Value =-2.56 DF = 26 P-Value = 0.017						

D. Maximum depth

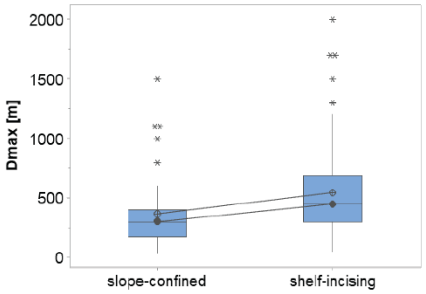

	N	min	mean	StDev	median	max
slope	**39**	35.00	367.30	322.10	300.00	1500.00
shelf	**65**	50.00	545.10	410.10	450.00	2000.00
T-Value =-2.46 DF = 94 P-Value = 0.016						

E. Average depth

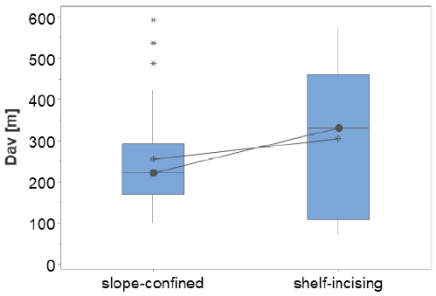

	N	min	mean	StDev	median	max
slope	**39**	100.00	255.30	115.70	222.00	594.00
shelf	**9**	70.00	304.90	183.40	331.00	576.00
T-Value =-0.78 DF = 9 P-Value = 0.457						

F. Average canyon sinuosity

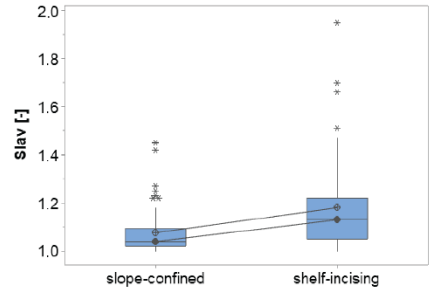

	N	min	mean	StDev	median	max
slope	**61**	1.00	1.08	0.09	1.04	1.45
shelf	**79**	1.00	1.18	0.17	1.13	1.95
T-Value =-4.50 DF = 125 P-Value ≤ 0.001						

G. Average canyon thalweg gradient

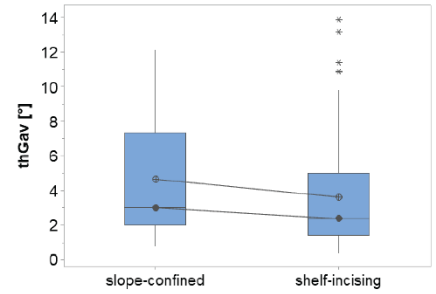

	N	min	mean	StDev	median	max
slope	**29**	0.78	4.65	3.29	3.00	12.10
shelf	**77**	0.40	3.62	3.14	2.37	13.90
T-Value = 1.46 DF = 48 P-Value = 0.151						

H. Maximum canyon sidewall steepness

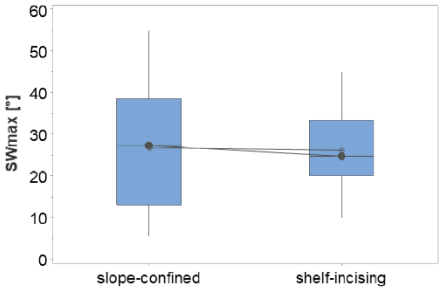

	N	min	mean	StDev	median	max
slope	**30**	5.40	26.82	13.92	27.30	55.00
shelf	**38**	10.00	26.18	8.68	24.80	45.00
T-Value = 0.22 DF = 46 P-Value = 0.825						

Fig. 17a-h: Boxplots of frequency distributions of canyon morphometric parameters for studied canyons classified on the location of the canyon apex relative to the shelf break. *L* = canyon length; W_{max} = maximum canyon width; W_{av} = average canyon width; D_{max} = maximum canyon depth; D_{av} = average canyon depth; SI_{av} = average canyon sinuosity index; thG_{av} = average canyon thalweg gradient; SW_{max} = maximum canyon sidewall steepness. N = number of readings; min = minimum value; mean = mean value; StDev = standard deviation; median = median value; max = maximum value. Results of Two-Sample T-test: DF = degrees of freedom.

7.2 Continental-margin type

7.2.1 Observations

Submarine canyons located along passive margins tend to be overall deeper (Fig. 18e), and have steeper thalwegs (Fig. 18g) and greater maximum sidewall steepness (Fig. 18h), with statistically significant differences in mean values. Groups of canyons associated with active and passive margins exhibit frequency distributions of maximum canyon dimensions (Figs. 18a, b & d) and average canyon sinuosity (Fig. 18f) that are rather similar. Studied active-margin canyons are on average longer (Fig. 18a). Average values for maximum canyon width (Fig. 18b) and depth (Fig. 18d) are almost identical across continental-margin types, but canyons from active margins display greater ranges in both morphometric parameters.

On average, continental slopes associated with studied canyons along passive margins tend to be significantly steeper than those along active margins (~3.22° vs. ~5.16°, respectively; Two-sample t-test: T-Value: -4.64 DF= 88 P-Value ≤0.001; N_{active}= 44; $N_{passive}$= 47).

7.2.2 Interpretations

The results suggest that margin type is not a primary predictor of maximum canyon dimensions, average canyon width, or sinuosity. Canyons along passive margins, however,

tend to display larger average depths and steeper canyon thalweg gradients compared to their active-margin counterparts. These findings can be explained by various reasons, as follows.

The seafloor relief, which influences sediment transport pathways, hydrodynamic processes and canyon geomorphology, can be sculpted by different processes, which are not limited to one particular continental-margin setting: faulting, although prominent in active-margin environments can also occur along passive margins (e.g. Osmundsen and Redfield, 2011); diapirism can be variably linked to processes acting in both margin types, such as mud and salt movements.

Another aspect to consider is that the physiography of continental margins can vary significantly in both tectonic settings. Although continental shelves along passive margins tend to be wider and with gentler lower-shelf gradients compared to those of active margins (e.g. Inman and Nordstrom, 1971; Blum and Hattier-Womack, 2009; Harris et al., 2014; Harris and Macmillan-Lawler, 2016; Nyberg et al., 2018), other shelf morphotypes exist. For example, shelves associated with passive margins can be as narrow as those associated with active margins (e.g. Harris and Macmillan-Lawler, 2016). The continental slopes of active margins are, on average, 1.28 times narrower (36 km) than those of passive margins (46 km); maximum widths are 368 km and 254 km, respectively (Harris et al., 2014). Given the strong relationship between slope width and canyon length (see section 6.3), similarity in the ranges and mean values of canyon length for the two margin types may be partly related to the limited difference in slope width between active and passive margins. By contrast, the steeper average thalweg gradients of passive-margin canyons likely reflect how the average canyon thalweg gradient is influenced by the overall slope gradient (cf. section 6.3), and that overall gradients of continental slopes associated with studied canyons along passive margins tend to be higher compared to those along active ones. Considering the observed variability in relationships between aspects of catchment, shelf and slope configuration and

canyon morphometric parameters (sections 6.2 & 6.3), contrasting characteristics in margin physiography are unlikely to lead to particular geomorphologic characteristics in canyons.

The tendency of canyons from passive margins to have greater maximum sidewall steepness compared to canyons in active-margin settings might be explained by the effect of recurrent seismic activity on the stabilisation of seafloor substrate: although active margins are characterized by recurrent and high-magnitude seismic activity, the occurrence of submarine mass-transport processes can be subdued (e.g. Strozyk et al., 2010). The influence of background seismic activity on slope stability and mass-transport processes is variable and complex: seismic strengthening by recurrent earthquakes has been proposed as an effective mechanism leading to slope stabilization and a decrease in both scale and occurrence of slope-failure processes (e.g. Strozyk et al., 2010; Nelson et al., 2011; Molenaar et al., 2019). Recurrent seismic activity can decrease the potential oversteepening of slopes by inducing a steady remobilization and redistribution of slope deposits (Strozyk et al., 2010). However, at the same time the magnitude of earthquakes controls mass-failure processes, whereby higher-magnitude earthquakes tend to trigger larger-scale slope failures (e.g. Strozyk et al., 2010; Molenaar et al., 2019). Thus, slope failure may play a less important role in controlling canyon morphology on active margins compared to passive margins. Furthermore, earthquakes of small to high magnitudes do occur on passive margins (e.g. Stein et al., 1989; Wolin et al., 2012; Katz and Hamiel, 2018) and might act as a trigger of sediment remobilisation (e.g. Katz and Hamiel, 2018).

Our findings support the view that submarine canyon geomorphology does not vary greatly between active and passive margins.

A. Length

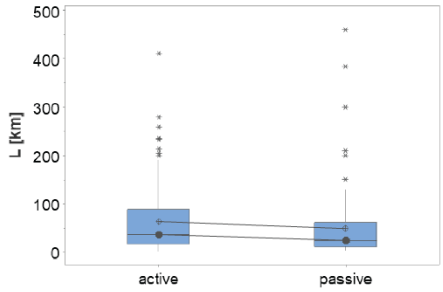

	N	min	mean	StDev	median	max
active	**141**	2.00	62.90	69.85	36.00	411.00
pass.	**122**	3.16	49.15	67.87	24.71	460.00
T-Value = 1.62 DF = 257 P-Value = 0.107						

B. Maximum width

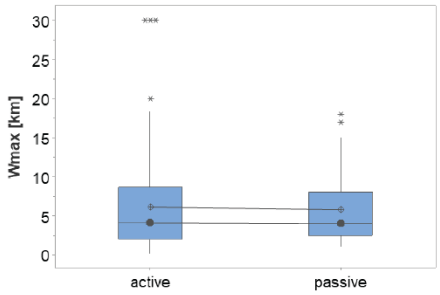

	N	min	mean	StDev	median	max
active	**91**	0.15	6.11	6.19	4.10	30.00
pass.	**73**	1.00	5.79	4.33	4.00	18.00
T-Value = 0.39 DF = 159 P-Value = 0.700						

C. Average width

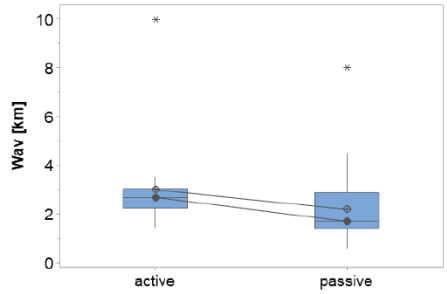

	N	min	mean	StDev	median	max
active	**18**	1.42	3.00	1.83	2.69	10.00
pass.	**48**	0.58	2.19	1.31	1.70	8.00
T-Value = 1.72 DF = 23 P-Value = 0.098						

D. Maximum depth

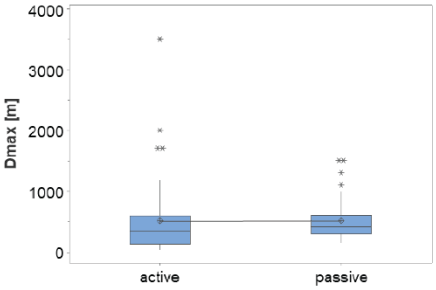

	N	min	mean	StDev	median	max
active	**60**	35.00	505.40	584.40	340.00	3500.00
pass.	**53**	150.00	511.00	314.10	422.60	1500.00
T-Value =-0.06 DF = 92 P-Value = 0.948						

E. Average depth

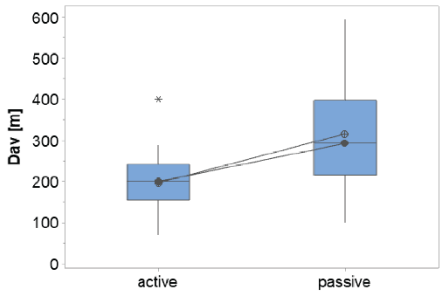

	N	min	mean	StDev	median	max
active	**21**	70.00	196.70	71.10	200.00	400.00
pass.	**31**	100.00	316.40	133.20	293.00	594.00
T-Value =-4.20 DF = 47 P-Value ≤ 0.001						

F. Average canyon sinuosity

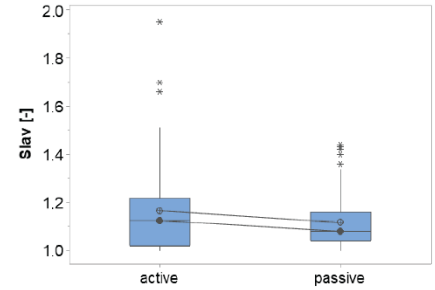

	N	min	mean	StDev	median	max
active	**68**	1.00	1.17	0.19	1.13	1.95
pass.	**83**	1.00	1.12	0.11	1.08	1.44
T-Value = 1.90 DF = 103 P-Value = 0.061						

G. Average canyon thalweg gradient

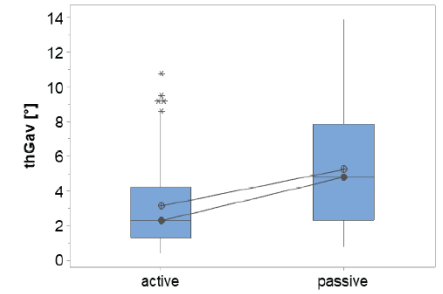

	N	min	mean	StDev	median	max
active	**72**	0.40	3.13	2.47	2.28	10.773
pass.	**48**	0.80	5.24	5.24	4.80	13.90
T-Value =-3.62 DF = 77 P-Value = 0.001						

H. Maximum canyon sidewall steepness

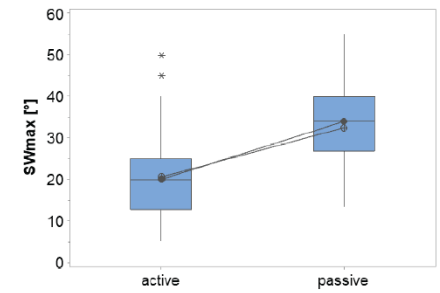

	N	min	mean	StDev	median	max
active	**33**	5.40	20.60	10.80	20.00	50.00
pass.	**36**	13.40	32.50	8.95	34.00	55.00
T-Value =-4.97 DF = 62 P-Value ≤ 0.001						

Fig. 18a-h: Boxplots of frequency distributions of canyon morphometric parameters for studied canyons classified based on the continental-margin type (classification after Harris et al., 2014). See Fig. 17 for legend.

7.3 Source-to-sink system setting

7.3.1 Observations

Submarine canyons in continental and insular settings display similar frequency distributions of canyon morphometric parameters. Between the two groups, mean values only differ by a factor 1.08 or lower, except for the average canyon thalweg gradient, which is on average 1.17 times greater in continental-setting canyons. Frequency distributions of average canyon width and depth could not be evaluated due to lack of data for insular canyons (Fig. 19a-h).

For studied canyons with a sediment connection to one or several fluvial systems, the size of associated terrestrial catchments tends to be markedly greater in continental settings – on average by a factor of ~100 (341.842 km^2 compared to 3071 km^2; Two-sample t-test: T-Value= 2.10 DF= 30 P-Value=0.044; $N_{continental}$= 31 and $N_{insular}$= 10). Whereas more data is needed to corroborate this finding, the results demonstrate that continental catchments display a great variability in size; studied catchments display a range from 84 km^2 to 3,800,000 km^2. Insular shelves tend to be narrower and steeper than shelves offshore continental landmasses. The shelves of continental settings are on average 4.39 times wider than those of insular settings (108 km compared to 37 km; Two-sample t-test: T-Value=5.29 DF=163 P-Value≤0.001; $N_{continental}$= 167 and $N_{insular}$= 37). Mean overall shelf gradients of insular shelves at the canyon location are 1.8 times greater (0.756° compared to 0.420°; Two-sample t-test: T-Value=-1.88 DF= 24 P-Value= 0.073; $N_{continental}$= 96 and $N_{insular}$= 21).

7.3.2 Interpretations

The results indicate that the association of a submarine canyon with a continental landmass or an island is not reflected in important differences in canyon geomorphology, with the caveat that relationships between S2S system setting and average canyon dimensions remain to be assessed. The similarity in frequency distributions and mean values for individual canyon morphometric parameters across the two groups might reflect how controlling factors are not significantly impacted by the S2S system setting, but also that different controls can generate similar geomorphologic characteristics in canyons across different S2S system settings.

The inherently limited extent of the terrestrial catchment in insular S2S systems compared to continental S2S systems does not appear to be a major factor for submarine canyon geomorphology. In part, this may be linked to the variability of the scale of islands, with large islands having potentially sizable catchments, and smaller catchments also occurring on continental landmasses.

For canyons associated with volcanic islands (97% of the investigated insular canyons in the study), the importance of their terrestrial catchment might be subordinate. Findings from the regional canyon study by Smith et al. (2017) indicate that the prevalence of igneous bedrock lithology in terrestrial source areas might inhibit canyon formation. In volcanic rocks, weathered clay minerals might enhance seafloor cohesion, whereas the lack of mud in plutonic bedrock might inhibit the development of turbidity currents (Smith et al., 2017 and references therein). Hence, the transitioning of hyperpycnal flows (e.g. Zhao et al., 2018), dilute surface river plumes (e.g. Hizzet et al., 2017) and submarine mass failures (e.g. Puig et al., 2014) into turbidity currents might constitute a subordinate evolutionary process in canyons located in front of islands of a volcanic origin. On the other hand, the tendency of volcanic islands to experience slope failures along their flanks (e.g. Le Bas et al., 2007; Chang et al., 2021) and shelf margins (e.g. Quartau et al., 2015) can supply sediment to a canyon by both individual large-scale failures (e.g. Le Bas et al., 2007) and high-frequency

smaller failures (e.g. Chang et al., 2021). The importance of volcanic activity as a trigger for submarine slope failures, however, might be subordinate where other factors prevail, as storm events and onshore failure (Clare et al., 2018). Additionally, sediment transported by oceanic currents can represent a sustained source of sediment to insular canyons, independently of their origin.

Narrow and steep insular shelves promote sediment dispersal to the shelf margin, increased shear stress of sediment gravity flows, and shelfal sediment remobilisation (e.g. Hale et al., 2012; Babonneau et al., 2013). These factors may facilitate canyon activity, countering the effects of the reduced size of terrestrial catchments and limited seafloor erodibility.

A. Length

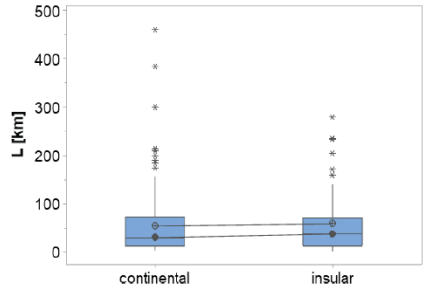

	N	min	mean	StDev	median	max
cont.	**177**	2.70	54.07	65.22	29.62	460.00
insular	**50**	2.00	58.36	67.80	37.28	279.67
T-Value =-0.40 DF = 76 P-Value = 0.691						

B. Maximum width

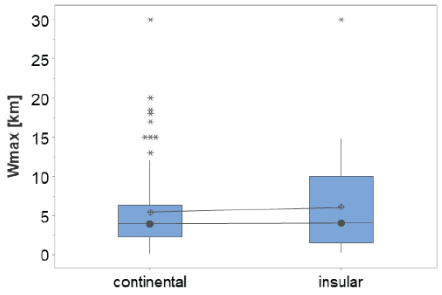

	N	min	mean	StDev	median	max
cont.	**101**	0.15	5.41	4.89	3.91	30.00
insular	**36**	0.25	6.06	6.08	4.00	30.00
T-Value =-0.58 DF = 52 P-Value = 0.565						

C. Average width

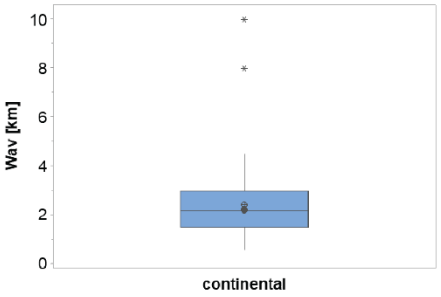

	N	min	mean	StDev	median	max
cont.	**66**	0.58	2.41	1.50	2.18	10.00
insular	**0**	***	***	***	***	***
T-Value =* DF =*** P-Value =***						

D. Maximum depth

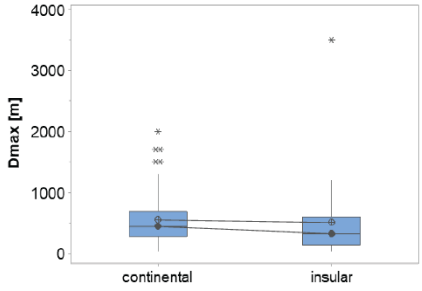

	N	min	mean	StDev	median	max
cont.	**60**	50.00	553.70	426.40	442.50	2000.00
insular	**29**	50.00	511.00	648.00	330.00	3500.00
T-Value = 0.32 DF = 40 P-Value = 0.748						

E. Average depth

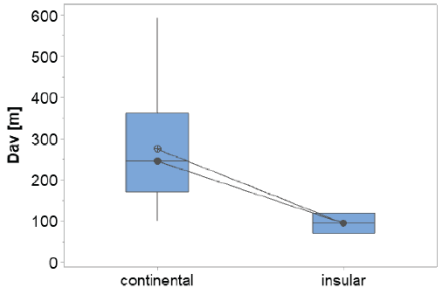

	N	min	mean	StDev	median	max
cont.	**50**	100.00	275.00	123.70	246.00	594.00
insular	**2**	70.00	95.00	35.40	95.00	120.00
T-Value =* DF =*** P-Value =***						

F. Average canyon sinuosity

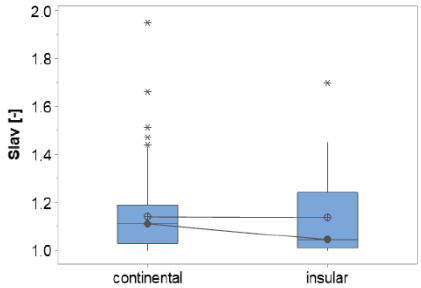

	N	min	mean	StDev	median	max
cont.	**129**	1.00	1.14	0.15	1.11	1.95
insular	**20**	1.00	1.14	0.19	1.05	1.70
T-Value = 0.06 DF = 22 P-Value = 0.949						

G. Average canyon thalweg gradient

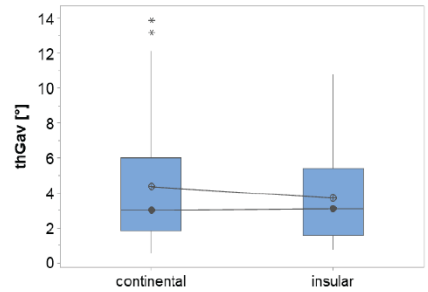

	N	min	mean	StDev	median	max
cont.	**77**	0.60	4.35	3.31	3.00	13.90
insular	**31**	0.78	3.71	2.76	3.09	10.77
T-Value = 1.02 DF = 66 P-Value = 0.309						

H. Maximum canyon sidewall steepness

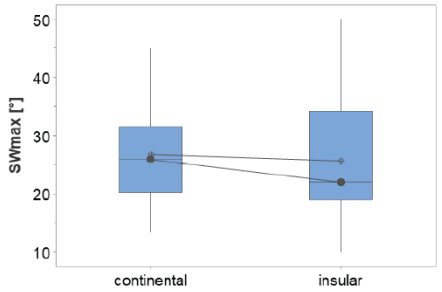

	N	min	mean	StDev	median	max
cont.	**28**	13.40	26.75	7.96	25.90	45.00
insular	**17**	10.00	25.67	10.65	22.00	50.00
T-Value = 0.36 DF = 26 P-Value = 0.721						

Fig. 19a-h: Boxplots of frequency distributions of canyon morphometric parameters for studied canyons classified based on the source-to-sink setting. *** denotes data paucity. See Fig. 17 for legend.

7.4 Oceanographic environment

7.4.1 Observations

Distributions of canyon length (Fig. 20a), maximum width (Fig. 20b), average sinuosity (Fig. 20f) and average thalweg gradient (Fig. 20g) for open-sea canyons and canyons from semi-enclosed or enclosed seas are similar: the mean values of these parameters do not differ to a statistically significant level across the two groups. The average canyon width is greater for canyons located in semi-enclosed and enclosed seas compared to those in open seas, but this observation is based on a small dataset (Fig. 20c); conversely, the average depth of open-sea canyons is higher. In any case, the differences in mean values of average canyon depth and widths across the two groups are not statistically significant. In contrast, marked differences in distributions of maximum canyon depth are seen across the two groups: on average, the maximum canyon depth is 1.91 times higher in open-sea canyons (Fig. 20d). Open-sea canyons also tend to have steeper sidewalls than canyons from semi-enclosed and enclosed seas, by a factor of 1.73 on average (Fig. 20h). These differences are statistically significant.

Continental slopes located in open-sea settings have on average greater slope-break depths than continental slopes associated with semi-enclosed and enclosed seas (3939 m compared to 3072 m, respectively; T-Value=3.50 DF=151 P-Value≤0.001; $N_{open\ sea} = 86$; $N_{se\&e\ seas} = 70$).

7.4.2 Interpretations

The results suggest that conditions associated with the oceanographic environment may exert an influence on maximum canyon depth and the steepness of canyon margins but not on canyon length, maximum width, overall sinuosity and average canyon gradient.

Fundamental differences between the two environments lie in the scale of the water body, in its degree of confinement, and in the presence of thermohaline circulation and major oceanic currents in oceans (e.g. Rahmstorf, 2006; Faugères and Mulder, 2011). Our findings might indicate that controlling factors that predominantly affect canyon geomorphology by acting along directions that are transverse to the canyon axis, like slope-parallel currents and lateral slope failures, might have a greater impact on canyon geomorphology in open seas. Oceanic currents might transport greater volumes of sand-sized sediment due to their greater extent and great depth range (e.g. Faugères and Mulder, 2011) compared to those in semi-enclosed and enclosed seas, which can be deposited onto intracanyon ridges and canyon margins thereby increasing canyon depths and steepening canyon sidewalls by aggradation. Oversteepened margins are in turn more prone to collapse, which can lead to steeper margins over the affected area of the canyon.

The greater sidewall steepness of open-sea canyons might also reflect how the studied high-latitude (sections 5.3 & 7.5) and passive-margin canyons (section 7.2), which tend to have steeper margins, are dominantly located in open-sea settings.

It must be recognised, additionally, that the findings may emerge not because of causal relationships with processes associated with the oceanographic environment, but merely because of positive scaling between canyon depth and sidewall steepness (section 4).

A. Length

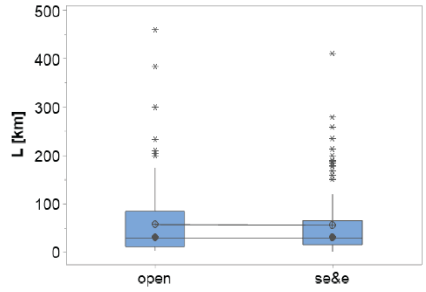

	N	min	mean	StDev	median	max
open	146	2.70	57.10	70.36	29.85	460.00
se&e	117	2.00	55.80	67.91	29.79	411.00
T-Value = 0.15 DF = 252 P-Value = 0.880						

B. Maximum width

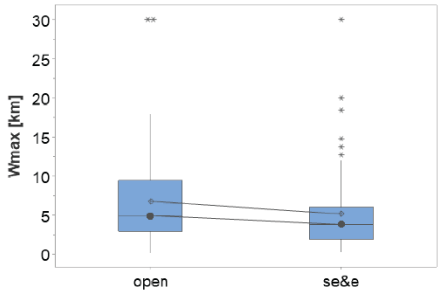

	N	min	mean	StDev	median	max
open	84	0.15	6.73	5.72	4.92	30.00
se&e	80	0.25	5.16	5.02	3.83	30.00
T-Value = 1.87 DF = 160 P-Value = 0.063						

C. Average width

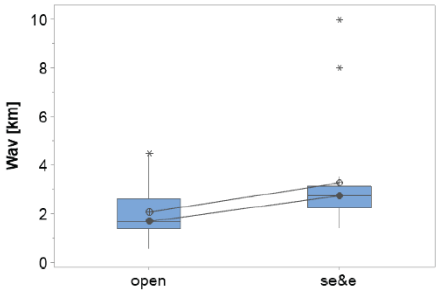

	N	min	mean	StDev	median	max
open	47	0.58	2.06	1.00	1.68	4.48
se&e	19	1.42	3.26	2.118	2.74	10
T-Value =-2.36 DF = 21 P-Value =0.028						

D. Maximum depth

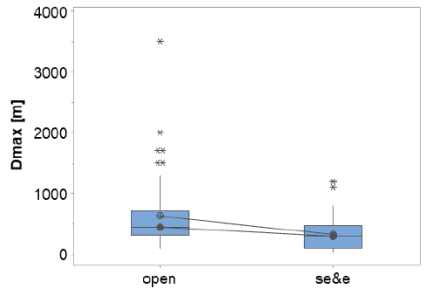

	N	min	mean	StDev	median	max
open	68	100.00	627.50	540.70	450.00	3500.00
se&e	45	35.00	327.40	271.90	297.00	1200.00
T-Value = 3.89 DF = 104 P-Value ≤ 0.001						

E. Average depth

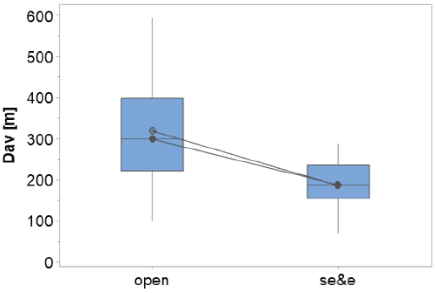

	N	min	mean	StDev	median	max
open	32	100.00	319.00	131.90	299.00	594.00
se&e	20	70.00	186.50	55.20	188.00	289.00
T-Value = 1.34 DF = 134 P-Value = 0.184						

F. Average canyon sinuosity

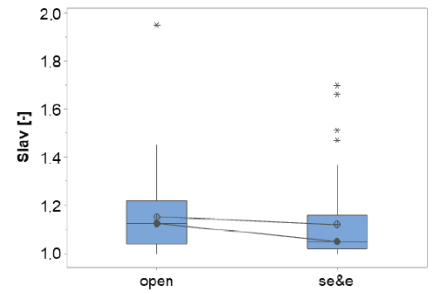

	N	min	mean	StDev	median	max
open	88	1.00	1.15	0.15	1.13	1.95
se&e	63	1.00	1.12	0.15	1.05	1.70
T-Value = 1.34 DF = 134 P-Value = 0.184						

G. Average canyon thalweg gradient

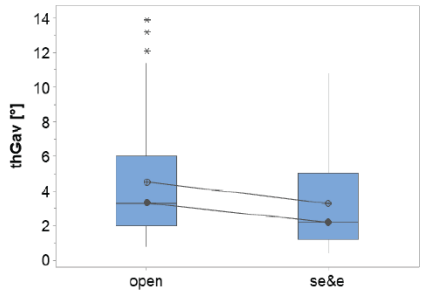

	N	min	mean	StDev	median	max
open	67	0.80	4.53	3.22	3.30	13.90
se&e	53	0.40	3.28	2.79	2.19	10.77
T-Value = 2.26 DF = 116 P-Value = 0.026						

H. Maximum canyon sidewall steepness

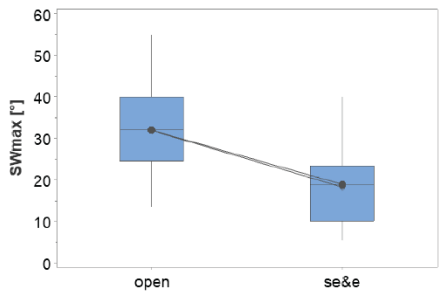

	N	min	mean	StDev	median	max
open	43	13.40	31.93	9.59	32.00	55.00
se&e	26	5.40	18.32	9.17	19.00	40.00
T-Value = 5.87 DF = 54 P-Value ≤ 0.001						

Fig. 20a-h: Boxplots of frequency distributions of canyon morphometric parameters for studied canyons classified based on the oceanographic environment. See Fig. 17 for legend.

7.5 Latitudinal zones

Variations in canyon morphometric parameters are evaluated for latitudinal belts binned into tropical (0-23.5°), temperate (23.5°-66.5°), and arctic (>66.5°) zones. The dataset contains fewer data of canyons from arctic latitudes compared to canyons in tropical and temperate zones; this reflects the paucity of investigations of high-latitude submarine canyons, despite the large number of canyons in the Arctic and Antarctic regions (Harris and Whiteway, 2011). The arctic canyons in this study come from only two regions: the NW Norwegian margin (N=15) and the Barrow Canyon from the N Alaskan margin. Thus, the representativeness of the data is likely to be limited. Because of this geographic bias, differences in mean values of canyon morphometric parameters from tropical and temperate latitudes have been tested separately.

7.5.1 Observations

Results of one-way ANOVA for canyons grouped by latitude range show statistically significant differences in mean values of length (Fig. 21a) and maximum canyon sidewall steepness (Fig. 21h), but not for maximum canyon width (Fig. 21b) and depth (Fig. 21d). Based on two-sample t-tests, statistically significant differences are seen for mean values of length (Fig. 21a) and the average canyon thalweg gradient (Fig. 21g) between canyons of tropical and temperate latitudes.

7.5.2 Interpretations

The results may represent a record of latitude-related controls on aspects of canyon geomorphology. For example, both oversteepening of canyon margins related to high and dispersed sediment supply from glaciated margins (e.g. Martinsen, 2005; Armitage et al.,

2010) and gravitational slope failure from ice loading (Mulder and Moran, 1995) may cause canyon sidewalls to be steeper. Yet any such inference has to be viewed with caution (see section 5.3 for a more detailed discussion). Based on the results of the statistical analyses, submarine canyon geomorphology does not vary markedly with latitude and across latitudinal zones.

A. Length

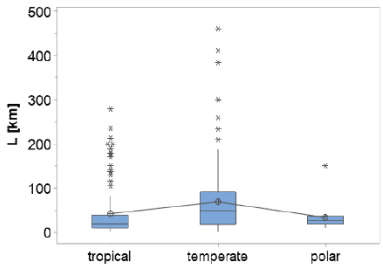

	N	min	mean	StDev	median	max
tropical	108	3.16	42.48	59.48	19.57	279.67
temper.	139	2.00	69.99	76.34	50.93	460.00
polar	16	10.00	34.31	32.30	28.00	150.00
F-Value = 7.43	DF1 = 2 DF2 =57.1562				P-Value = 0.001	
T-Value*=-3.18	DF = 244				P-Value = 0.002	

B. Maximum width

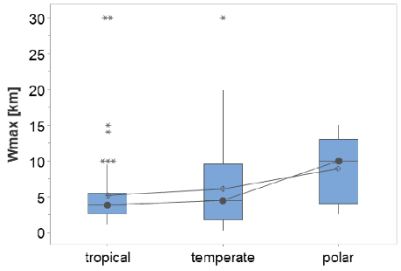

	N	min	mean	StDev	median	max
tropical	70	1.00	5.19	5.12	3.85	30.00
temper.	79	0.15	6.09	5.70	4.49	30.00
polar	15	2.50	8.90	4.61	10.00	15.00
F-Value = 3.79	DF1 = 2 DF2 = 41.8768				P-Value = 0.031	
T-Value*=-1.02	DF = 146				P-Value = 0.311	

C. Average width

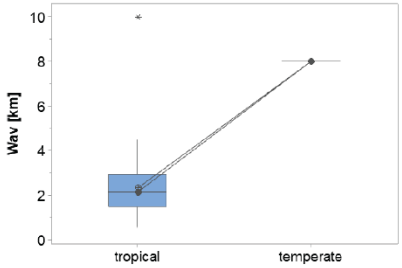

	N	min	mean	StDev	median	max
tropical	65	0.58	2.32	1.339	2.14	10.00
temper.	1	8.00	8.00	***	8.00	8.00
polar	0	***	***	***	***	***
F-Value = ***	DF1 = *** DF2 = ***				P-Value = ***	
T-Value*= ***	DF = ***				P-Value = ***	

D. Maximum depth

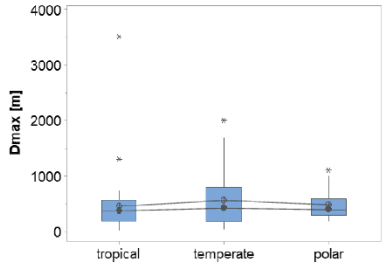

	N	min	mean	StDev	median	max
tropical	49	35.00	458.30	504.20	380.40	3500.00
temper.	49	50.00	564.20	494.60	425.00	2000.00
polar	15	200.00	486.70	274.20	400.00	1100.00
F-Value = 0.59	DF1 = 2 DF2 = 53.2939				P-Value = 0.560	
T-Value*=-1.05	DF = 95				P-Value = 0.297	

E. Average depth

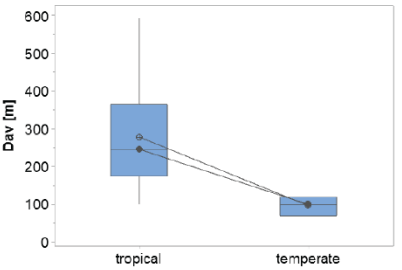

	N	min	mean	StDev	median	max
tropical	49	100.00	278.60	25.20	246.00	594.00
temper.	3	70.00	96.70	25.20	100.00	120.00
polar	0	***	***	***	***	***
F-Value = ***	DF1 = *** DF2 = ***				P-Value = ***	
T-Value*= ***	DF = ***				P-Value = ***	

F. Average canyon sinuosity

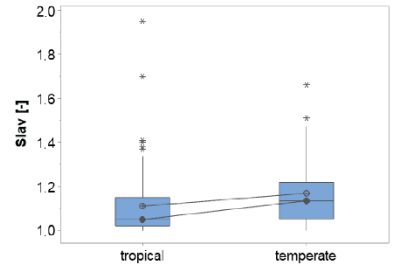

	N	min	mean	StDev	median	max
tropical	79	1.00	1.11	0.16	1.05	1.95
temper.	72	1.00	1.17	0.1395	1.14	1.66
polar	0	***	***	***	***	***
F-Value = ***	DF1 = *** DF2 = ***				P-Value = ***	
T-Value*=-2.43	DF = 148				P-Value = 0.016	

G. Average canyon thalweg gradient

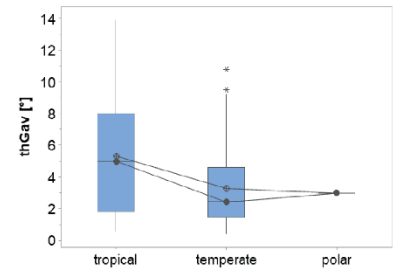

	N	min	mean	StDev	median	max
tropical	41	0.60	5.33	3.78	5.00	13.90
temper.	78	0.40	3.28	2.42	2.42	10.77
polar	1	2.98	2.98	***	2.98	2.98
F-Value = ***	DF1 = *** DF2 = ***				P-Value = ***	
T-Value*= 3.15	DF = 57				P-Value = 0.003	

H. Maximum canyon sidewall steepness

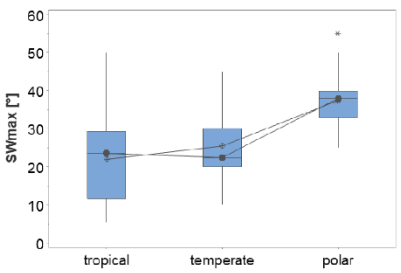

	N	min	mean	StDev	median	max
tropical	26	5.40	22.06	12.02	23.60	50.00
temper.	28	10.00	25.50	8.94	22.50	45.00
polar	15	25.00	37.47	7.82	38.00	55.00
F-Value =14.93	DF1 = 2 DF2 = 39.1479				P-Value ≤ 0.001	
T-Value*=-1.19	DF = 46				P-Value = 0.242	

Fig. 21a-h: Boxplots of frequency distributions of canyon morphometric parameters for studied canyons classified based on latitudinal zones. * indicates that two-sample-t-tests have been conducted for canyons in tropical versus temperate latitudinal zones. N = number of readings; min = minimum value; mean = mean value; StDev = standard deviation; median = median value; max = maximum value. Results of Welch's ANOVA test: DF 1 = degrees of freedom numerator; DF 2 = degrees of freedom denominator. Results of Two-Sample T-test: DF = degrees of freedom; *** denotes data paucity.

7.6 Width-to-depth ratios

To investigate potential relationships between the ratio between maximum canyon width to maximum canyon depth (wdmax) and environmental factors, 100 submarine canyons of the study for which both maximum width and depth values have been obtained have been considered; aspect ratios have been evaluated for canyons across classes of environments (Fig. 22a-f).

7.6.1 Observations

Although wdmax ratios for the studied canyons vary over a broad range (2.45 to 73.33), mean and median values of wdmax ratios are in the order of magnitude of 10^1 both for the whole dataset as well as for canyons grouped according to environmental factors. Mean values range between 11 and 20, and only differ significantly from each other for canyons in open seas versus semi-enclosed and enclosed seas (Fig. 22e). For canyons grouped by the continental-margin type, the difference in mean values yields a p-value of 0.011 (Fig. 22c).

7.6.2 Interpretations

The narrow range in mean and median wdmax ratios and the lack of significant differences in mean values for the majority of canyon environmental classes indicate that maximum width-to-maximum depth ratios in canyons are of limited diagnostic value for inferring the

environmental settings. This might reflect that width-to-depth ratios in canyons are not particularly sensitive to environmental controls and that they may inherently scale with processes that control canyon geomorphology globally. This would imply that width-to-depth ratios in submarine canyons are predominantly controlled by canyon self-organisation and autogenic processes, from the interplay of canyon-floor and margin aggradation and wall failure with intra-canyon sediment gravity flows, as suggested for submarine channels by Shumaker et al. (2018). The findings of this study corroborate the view that channel forms might tend towards common geometries independent of their scale.

The inferred influence of the oceanographic environment on canyon width-to-depth ratios might reflect the way in which both erosional and depositional processes that operate along canyon margins are more strongly affected by the hydrodynamic regime in open seas than semi-enclosed and enclosed ones (see discussion in section 7.4). The tendency for passive-margin canyons to exhibit lower wdmax ratios deserves further investigation.

A. Dataset

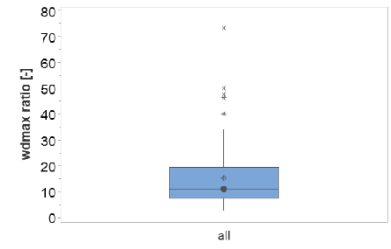

	N	min	mean	StDev	median	max
all	100	2.45	15.25	11.62	11.09	73.33

B. Canyon-apex location

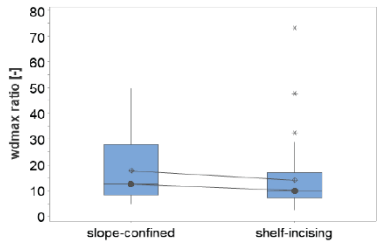

	N	min	mean	StDev	median	max
slope	37	4.65	17.67	12.37	12.50	50.00
shelf	55	2.45	14.05	11.59	10.00	73.33
T-Value = 1.41			DF = 73			P-Value = 0.163

C. Continental-margin type

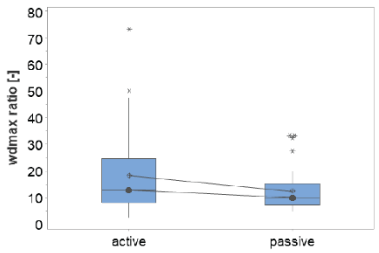

	N	min	mean	StDev	median	max
active	50	2.45	18.20	14.31	12.83	73.33
pass.	50	4.65	12.30	7.07	10.00	33.33
T-Value = 2.61			DF = 71			P-Value = 0.011

D. Source-to-sink setting

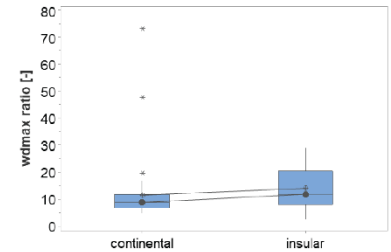

	N	min	mean	StDev	median	max
cont.	48	4.65	11.45	11.16	8.78	73.33
insular	29	2.45	14.00	7.64	11.82	28.86
T-Value =-1.19			DF = 73			P-Value = 0.238

E. Oceanographic environment

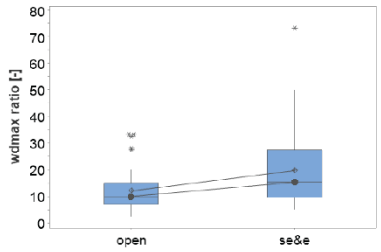

	N	min	mean	StDev	median	max
open	58	2.45	12.06	7.19	10.00	33.33
se&e	42	5.00	19.66	14.82	15.33	73.33
T-Value =-3.07			DF = 54			P-Value = 0.003

F. Latitudinal zones

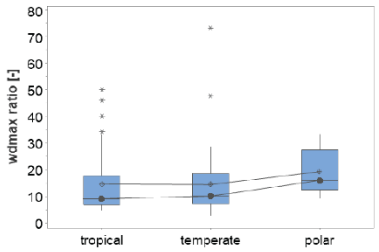

	N	min	mean	StDev	median	max
tropic.	44	4.65	14.65	11.45	9.12	50.00
temp.	41	2.45	14.43	12.67	10.10	73.33
polar	15	9.09	19.27	8.53	16.00	33.33
F-Value = 1.68		DF1 = 2 DF2 = 45.5017				P-Value = 0.198
T-Value*= 0.09		DF = 80				P-Value = 0.931

Fig. 22a-f: Boxplots of frequency distributions of maximum-width-to-maximum-depth (wdmax) ratios in studied canyons A. for the dataset and B.-F. across classes of environments. * indicates that two-sample-t-tests have been conducted for canyons in tropical versus temperate latitudinal zones. See Fig. 21 for legend.

8 Summary and conclusions

To increase understanding of the factors that exert control on canyon geomorphology and their relative importance on a global scale, statistical analyses were conducted to evaluate relationships between canyon morphometric parameters, and between these and attributes describing the physiographic setting of the canyon, including characteristics of elements of the source-to-sink (S2S) system (catchment, shelf and slope), the bathymetric setting of the canyon and its distance to the shoreline, the canyon-apex location relative to the shelf-break, the continental-margin type, the oceanographic environment, and the latitude of the canyon apex. In addition, selected morphometric parameters describing submarine canyons have been quantitatively characterized, both on a global scale and for different environmental settings (canyon-apex location relative to the shelf-break, continental-margin type, source-to-sink system setting, oceanographic environment and climate zones). Certain forms of scaling in attributes of canyon geomorphology are recognisable on a global scale and across different environmental settings and source-to-sink system configurations.

Statistically significant scaling relationships include: (i) Moderate positive scaling between maximum canyon dimensions; strong positive relationships of average canyon width with maximum width, length and maximum depth, and of maximum canyon depth with average depth; modest positive scaling between maximum width and average depth; (ii) for average canyon sinuosity, moderate positive scaling with canyon length and average canyon depth is seen as well as modest, positive scaling with maximum canyon width; weaker inverse scaling exists with the average canyon thalweg gradient; (iii) the average canyon thalweg gradient is inversely related to canyon length and maximum canyon width, but these relationships are

not strong; (iv) positive scaling relationships of maximum canyon sidewall steepness with maximum canyon width and depth are modest; in addition, a weak and positive relationship with canyon length is seen (Fig. 23a&b).

The following significant relationships suggest that some characteristics of canyon geomorphology are scaled to some degree to attributes of the S2S system: (i) Canyon length displays strong positive scaling with slope width, and moderate positive scaling with average annual fluvial discharge, maximum catchment elevation, and shelf-break depth; weaker positive correlations are seen with shelf width and slope-break depth; (ii) maximum canyon width exhibits moderate positive relationships with catchment size, maximum catchment elevation and slope width, and modest positive scaling with shelf-break depth; (iii) average canyon width shows some positive correlations with shelf-break depth, average shelf gradient, and shelf width; the results, however, need to be corroborated by additional data; (iv) maximum canyon depth scales positively, albeit only moderately, with fluvial system length, average annual fluvial discharge, slope width and slope-break depth; modest positive scaling is also seen with shelf width and shelf-break depth; (v) of the considered S2S parameters, the average canyon sinuosity shows some positive relationships with average annual fluvial discharge, maximum catchment elevation and shelf-break depth; (vi) the average canyon thalweg gradient exhibits some inverse relationships with slope width and shelf-break depth, and positive correlation with the average slope gradient; (vii) shelf width and the average slope gradient have moderate positive correlations with the canyon sidewall steepness, which is also inversely related with the slope-break depth (Fig. 23a&b).

The following insights have been gained:

(1) Scaling relationships between canyon morphometric attributes are usually weak, due to the varied influence of environmental controls on allogenic and autogenic processes influencing canyon geomorphology. Nevertheless, despite specific regional or local conditions, some scaling relationships between canyon morphometric attributes are more likely recognisable on a global scale than others;

these include, for example, scaling between maximum canyon dimensions, or between maximum sidewall steepness and maximum canyon width and depth.

(2) The tendency of canyons to have greater maximum widths and depths with increasing canyon-mouth seafloor depth, the overall weakness in scaling of canyon morphometry with the terrestrial catchment and continental shelf, and the steeper canyon walls seen in canyons associated with open-sea settings compared to canyons in semi-enclosed or enclosed seas possibly reflect how hydrodynamic processes such as upwelling, longshore drifts and along-slope currents influence canyon geomorphology.

(3) Canyon morphometric parameters may reflect the interplay of different environmental factors. Hence, controls on canyon geomorphology cannot be described by generic models linking geomorphological characteristics to individual environmental parameters. Potential controls on certain canyon morphometric parameters include: the location of the canyon head relative to the shelf break, the continental-margin type, the oceanographic environment, the absolute latitude of the canyon apex, and the depth of the associated shelf break. Data on canyon length, sinuosity, thalweg gradient and maximum sidewall steepness indicate that these morphometric aspects are likely influenced by several environmental controls.

Key findings regarding relationships between the environmental setting and canyon geomorphology include:

(i) Maximum canyon dimensions and overall canyon sinuosity cannot be used to predict the position of the canyon apex relative to the shelf break and vice versa; this challenges concepts linking higher overall sinuosities in canyons to incision of the canyon into the shelf (e.g. Farre et al., 1983; Jobe et al., 2011; Wiles et al., 2019).

(ii) The tendency of passive-margin canyons to develop steeper sidewalls compared to those of active-margin canyons indicates that slope failure might

be generally less important for canyons from active margins compared to passive-margin ones, perhaps due to recurrent seismic strengthening of the seafloor substrate, which might act to inhibit mass failures, with the exception of cases triggered by high-magnitude earthquakes (e.g. Strozyk et al., 2010; Molenaar et al., 2019).

(iii) Whether a submarine canyon is associated with a continental or insular setting does not exert control on overall canyon geomorphology. Narrow and steep insular shelves might compensate for the impact of smaller associated terrestrial catchments on sediment supply to submarine canyons, and for the potential effect igneous bedrock lithology might have on canyon evolution along volcanic islands by affecting seafloor erodibility and the erosive strengths of flows (Smith et al., 2017 and references therein).

(iv) The complex role of climate influence on sediment sourcing and dispersal along glaciated continental margins, paired with the effect of ice loading on triggering of mass failures, might explain the observed steeper margins and greater average widths of submarine canyons from higher latitudes. However, in view of geographic bias and the limited sample size, it is possible that the results reflect how the studied higher-latitude canyons are coincidentally associated with passive-margin and open-sea settings, which tend to be associated with distinct distributions in sidewall steepness and average canyon width.

(v) Mean values of maximum width-to-maximum depth ratios in canyons are consistently in the order of magnitude of 10^1 for all investigated canyon classes – regardless of canyon-head location relative to the shelf break, the tectonic-margin type, the S2S setting, the oceanographic environment and the latitudinal zone – albeit with significant global variability in documented values. This might reflect how width-to-depth ratios in submarine canyons are

constrained by the interplay of canyon-margin failure and canyon-floor and -margin aggradation by sediment deposition from flows. Our findings suggest that this mechanism of self-organisation, which has been recognised for submarine channels (see Shumaker et al., 2018), also operates in submarine canyons, and that width and depth tend to increase in equal proportion, independently of the scale of the canyon.

Our quantitative characterisation of how canyon morphometric parameters vary as a function of environmental factors demonstrates that the interplay of controls on canyon geomorphology is more complex than hitherto considered in canyon classification schemes (e.g. Jobe et al., 2011), numerical (e.g. Wan et al., 2021) and published conceptual models of canyon evolution (e.g. Chiang & Yu, 2006; Micallef et al., 2014), of deep-water systems and of source-to-sink (S2S) systems (e.g. Sømme et al., 2009; Nyberg et al., 2018). The predictive value of these models can be enhanced by considering the impact of the controlling factors identified in this study – including the hydrodynamic regime of oceans and seas, autogenic canyon processes, characteristics of continental margin physiography and the canyon physiographic setting.

The findings of this study might also aid in estimation of the original geometry of ancient canyons and channel forms whose infills are now preserved in subsurface and outcrop, and in the interpretation of their formative environments, particularly where information on the environmental setting, margin physiography and bathymetry is limited due to scarcity of data (e.g. Martinsen et al., 2010; Helland-Hansen et al., 2016).

Results of this work will aid analyses of source-to-sink systems, i.e., spanning fluvial, paralic and deep-water domains (e.g. Sømme et al., 2009; Nyberg et al., 2018; Wang et al., 2019), by illuminating the response of slope systems to controlling factors on sedimentary processes from terrestrial hinterlands to deep-water environments. Further research is needed to investigate the relative scaling between features of these clastic environments and those of submarine canyons.

A. Relationships between canyon morphometrics

Linear monotonic relationships

	L	Wmax	Wav	Dmax	Dav	Slav	thGav	SWmax
L		0.5	0.8	0.5		0.5	-0.5	
Wmax	0.5		0.8	0.8	0.5	0.4	-0.3	0.4
Wav	0.8	0.8		0.8				
Dmax	0.5	0.8	0.8		1.0			0.4
Dav		0.5		1.0		0.5		***
Slav	0.5	0.4			0.5		-0.3	
thGav	-0.5	-0.3				-0.3		
SWmax		0.4		0.4	***			

Non-linear monotonic relationships

	L	Wmax	Wav	Dmax	Dav	Slav	thGav	SWmax
L		0.6	0.6	0.7		0.5	-0.7	0.3
Wmax	0.6		0.8	0.7		0.4	-0.4	0.4
Wav	0.6	0.8		0.8				
Dmax	0.7	0.7	0.8		1.0			0.4
Dav				1.0		0.5		***
Slav	0.5	0.4			0.5		-0.4	
thGav	-0.7	-0.4				-0.4		
SWmax	0.3	0.4		0.4	***			

B. Relationships between canyon morphometrics and environmental parameters

Linear monotonic relationships & differences between canyon groups

	Lfls	Qfls	Aflsc	Hflsc	Wsh	Dsh	Gsh	Wsl	Dsl	Gsl	Dismin	SDmin	SDmax	Latabs	cnh. location	margin type	S2S setting	ocean. env.	lat. (ANOVA)	lat. (t-test)	sh. depth 120	sh. depth 130
L				0.4	0.2	0.4		0.4					0.6		X				X	X	X	X
Wmax				0.6		0.4		0.4					0.4	0.2								
Wav	***	***	***	***		0.5	0.7							0.5			***		***	***	***	***
Dmax		***		***		0.4		0.4	0.6				0.8					X				
Dav	***	***	***	***		***						-0.4	0.7	-0.4	***	X	***		***	***	***	***
Slav				0.6		0.4		***					0.6		X				***		X	X
thGav		***				-0.3				0.5			-0.3	-0.4		X			***	X	X	X
SWmax	***	***	***	***	0.6					0.8	-0.3		0.4	0.5		X		X	X			

Non-linear monotonic relationships & differences between canyon groups

	Lfls	Qfls	Aflsc	Hflsc	Wsh	Dsh	Gsh	Wsl	Dsl	Gsl	Dismin	SDmin	SDmax	Latabs	cnh. location	margin type	S2S setting	ocean. env.	lat. (ANOVA)	lat. (t-test)	sh. depth 120	sh. depth 130
L		0.7		0.6	0.2	0.5		0.9	0.4				0.7	0.3	X				X	X	X	X
Wmax			0.6	0.6				0.7					0.5	0.2								
Wav	***	***	***	***	0.4	0.6	0.6				0.4			0.5			***		***	***	***	***
Dmax	0.7	***	0.7	***	0.4			0.6	0.5			-0.4	0.8					X				
Dav	***	***	***	***		***						-0.4	0.7	-0.4	***	X	***		***	***	***	***
Slav		0.5		0.6	-0.3	0.4		***			-0.3	-0.3	0.5	0.2	X				***		X	X
thGav		***				-0.3		-0.5		0.5				-0.3		X			***	X	X	X
SWmax	***	***	***	***	0.5				-0.6	0.7			0.4	0.4		X		X	X			

correlation coefficient-value: -1 0 1

p-value: 0 0.005 1

X difference in mean values between canyon groups is statistically significant (p≤0.01)

*** not enough data

Fig. 23a&b: Summary tables displaying relationships of canyon morphometric parameters A. with each other and B. with environmental parameters for results of the correlation analyses and hypothesis testing with a statistical significance ($p \leq 0.01$) and $N \geq 15$ for each parameter and canyon group. *L* = canyon length; *Wmax* = maximum canyon width; *Wav* = average canyon width; *Dmax* = maximum canyon depth; *Dav* = average canyon depth; *SIav* = average canyon sinuosity index; *thGav* = average canyon thalweg gradient; *SWmax* = maximum canyon sidewall steepness; *Lfls* = fluvial system length; *Qfls* = average annual fluvial discharge; *Aflsc* = size of the catchment; *Hflsc* = maximum elevation in the catchment area; *Wsh* = shelf width; *Dsh* = shelf-break depth; *Gsh* = average shelf gradient; *Wsl* = slope width; *Dsl* = slope-break depth; *Gsl* = average slope gradient; Dis_{min} = minimum distance between the canyon and shoreline; SD_{min} = minimum seafloor depth at the canyon; SD_{max} = maximum seafloor depth at the canyon; Lat_{abs} = absolute value of the latitude of the canyon apex; cnh. location= canyon-apex location relative to the shelf-break; margin type = continental-margin type; ocean. env. = oceanographic environment; lat. = latitude at the canyon apex; sh. depth = shelf break depth at the canyon. *** denotes datasets that were deemed too small for statistical analyses.

Acknowledgements

We thank sponsors and partners of the Fluvial, Eolian & Shallow-Marine Research Group (AkerBP, Areva (now Orano), BHPBilliton (now BHP), Cairn India (Vedanta), Chevron, CNOOC International, ConocoPhillips, Equinor, Murphy Oil, Occidental, Petrotechnical Data Systems, Saudi Aramco, Shell, Tullow Oil, Woodside and YPF) and of the Turbidite Research Group (AkerBP, CNOOC, ConocoPhillips, Harbour, Murphy, Occidental, OMV) at the University of Leeds for financial support that has enabled this research.

References

Acosta, J., Canals, M., López-Martínez, Muñoz, A., Herranz, P., Urgeles, R., Palomo, C., Casamor, J.L. 2002. The Balearic promontory geomorphology (western Mediterranean): morphostructure and active processes. Geomorphology. 49, 177-204.

Alford, M. H., MacCready, P. 2014. Flow and mixing in Juan de Fuca Canyon, Washington. Geophys. Res. Lett. 41, 1608–1615. https://doi.org/10.1002/2013GL058967.

Allen, S.E., Vindeirinho, C., Thomson, R.E., Foreman, M.G.G., Mackas, D.L. 2001. Physical and biological processes over a submarine canyon during an upwelling event. Can. J. Fish. Aquat. Sci. 58, 671-684. https://doi.org/10.1139/cjfas-58-4-671.

Allin, J.R., Hunt, J.E., Talling, P.J., Clare, M.A., Pope, E., Masson, D.G. 2016. Different frequencies and triggers of canyon filling and flushing events in Nazaré Canyon, offshore Portugal. Mar. Geol. 371, 89-105. http://dx.doi.org/10.1016/j.margeo.2015.11.005.

Almagor, G. 1993. Continental slope processes off northern Israel and southernmost Lebanon and their relation to onshore tectonics. Mar. Geol. 112, 151-169.

Alonso, B., Ercilla, G. 2003. Small turbidite systems in a complex tectonic setting (SW Mediterranean Sea): morphology and growth patterns. Mar. Pet. Geol. 19, 1225-1240. https://doi.org/10.1016/S0264-8172(03)00036-9.

Amblas, D., Ceramicola, S., Gerber, T.P., Canals, M., Chiocci, F.L., Dowdeswell, J.A., Harris, P.T., Huvenne, V.A.I., Lai, S.Y.J., Lastras, G., Lo Iacono, C., Micallef, A., Mountjoy, J.J., Paull, C.K., Puig, P., Sanchez-Vidal, A. 2017. Submarine canyons and gullies. In: Micallef, A., Krastel, S., Savini, A. (Eds), Submarine Geomorphology, pp- 251-272. Springer.

Amblas, D., Gerber, T.P., De Mol, B., Urgeles, R., Garcia-Castellanos, Canals, M., Pratson, L.F., Robb, N., Canning, J. 2012. Survival of a submarine canyon during long-term outbuilding of a continental margin. Geology. 40(6), 543-546. https://doi.org/10.1130/G33178.1.

Antobreh, A.A., Krastel, S. 2006. Morphology, seismic characteristics and development of Cap Timiris Canyon, offshore Mauritania: a newly discovered canyon preserved-off a major arid climatic region. Mar. Pet. Geol. 23, 37-59. https://doi.org/10.1016/j.marpetgeo.2005.06.003.

Aranguiz, R., Shibayama, T. 2013. Effect of submarine canyons on tsunami propagation; a case study of the Biobio Canyon, Chile. Coast. Eng. J. 55(4), 1350016-1-1350016-23. https://doi.org/10.1142/S0578563413500162.

Armitage, D.A., Piper, D.J.W., McGee, D.T., Morris, W.R. 2010. Turbidite deposition on the glacially influenced, canyon-dominated Southwest Grand Banks Slope, Canada. Sedimentology. 57, 1387-1408. https://doi.org/10.1111/j.1365-3091.2010.01149.x.

Arzola, R.G., Wynn, R.B., Lastras, G., Masson, D.G., Weaver, P.P.E. 2008. Sedimentary features and processes in the Nazaré and Setúbal submarine canyons, west Iberian margin. Mar. Geol. 250, 64-88. https://doi.org/10.1016/j.margeo.2007.12.006.

Azaroff, A., Miossec, C., Lanceleur, L., Guyoneaud, R., Monperrus, M. 2020. Priority and emerging micropollutants distribution from coastal to continental slope sediments: a case study of Capbreton Submarine Canyon (North Atlantic Ocean). Sci. Total Environ. 703, 135057. https://doi.org/10.1016/j.scitotenv.2019.135057.

Babonneau, N., Savoye, B., Cremer, M., Klein, B. 2002. Morphology and architecture of the present canyon and channel system of the Zaire deep-sea fan. Mar. Pet. Geo. 19, 445-467.

Babonneau, N., Delacourt, C., Cancouët, R., Sisavath, E., Bachèlery, P., Mazuel, A., Jorry, S.J., Deschamps, A., Ammann, J., Villeneuve. 2013. Direct sediment transfer form land to deep-sea: insights into shallow multibeam bathymetry at La Réunion Island. Mar. Geol. 346, 47-57. http://dx.doi.org/10.1016/j.margeo.2013.08.006.

Bailey, L.P., Clare, M.A., Rosenberger, K.J., Cartigny, M.J.B., Talling, P.J., Paull, C.K., Gwiazda, R., Parsons. D.R., Simmons, S.M., Xu, J., Haigh, I.D., Maier, K.L., McGann, M.,

Lundstren, E. 2021. Preconditioning by sediment accumulation can produce powerful turbidity currents without major external triggers. Earth Planet. Sci. Lett. 562, 116845. https://doi.org/10.1016/j.epsl.2021.116845.

Baker, E.T., Hickey, B.M. 1986. Contemporary sedimentation processes in and around an active West Coast submarine canyon. Mar. Geol. 71, 15-34.

Baztan, J., Berné, S., Olivet, J.-L., Rabineau, M., Aslanian, D., Gaudin, M., Réhault, J.-P., Canals, m. 2005. Axial incision: The key to understand submarine canyon evolution (in the western Gulf of Lion). Mar. Pet. Geol. 22(6-7), 805-826. http://dx.doi.org/10.1016/j.marpetgeo.2005.03.011.

Benjamin, U., Huuse, M., Hodgetts, D. 2015. Canyon-confirmed pockmarks on the western Niger Delta slope. J. Afr. Earth Sci. 107, 15-27. http://dx.doi.org/10.1016/j.jafrearsci.2015.03.019.

Bernhardt, A., Melnick, D., Jara-Muñoz, J., Argandoña, B., González, J., Strecker, M.R. 2015. Controls on submarine canyon activity during sea-level highstands. The Bíobío canyon system offshore Chile. Geosphere. 11(4), 1226-1255. https://doi.org/10.1130/GES01063.1.

Blum, M.D., Hattier-Womack, J. 2009. Climate change, sea-level change, and fluvial sediment supply to deepwater depositional systems. In: Kneller, B., Martinsen, O.J., McCaffrey, B. (Eds), External Controls on Deep Water Depositional Systems: Climate, Sea-Level, and Sediment Flux. SEPM Spec. Publ. (CD version). 92, 15-39.

Blum, M., Martin, J., Milliken, K., Garvin, M. 2013. Paleovalley systems: insights from Quaternary analogs and experiments. Earth-Sci. Rev. 116, 128-169. http://dx.doi.org/10.1016/j.earscirev.2012.09.003.

Bourget, J., Zaragosi, S., Ellouz-Zimmermann, N., Mouchot, N., Garlan, T., Schneider, J.-L., Lanfumey, V., Lallemant, S. 2010. Turbidite system architecture and sedimentary processes along topographically complex slopes: the Makran convergent margin. Sedimentology. 58(2), 376-406. https://doi.org/10.1111/j.1365-3091.2010.01168.x.

Bosley, K.L., Lavelle, J.W., Brodeur, R.D., Wakefield, W.W., Emmet, R.L., Baker, E.T., Rehmke, K.M. 2004. Biological and physical processes in and around Astoria submarine Canyon, Oregon, USA. J. Mar. Syst. 50, 21-37. https://doi.org/10.1016/j.jmarsys.2003.06.006.

Brunt, R. L., Hodgson, D. M., Flint, S. S., Pringle, J. K., Di Celma, C. N., Prelat, A., Grecula, M. 2013. Confined to unconfined: Anatomy of a base of slope succession, Karoo Basin, South Africa. Mar. Pet. Geol. 41, 206-221.

Budillon, F., Conforti, A., Tonielli, R., De Falco, G., Di Martino, G., Innangi, S., Marsella, E. 2011. The Bulgheria canyon-fan: a small-scale proximal system in the eastern Tyrrhenian Sea (Italy). Mar. Geophys. Res. 32, 83-97. https://doi.org/10.1007/s11001-011-9138-9.

Çağatay, M.N., Uçarkus, G., Eriş, K.K., Henry, P., Gasperini, L., Polonia, A. 2015. Submarine canyons of the Sea of Marmara. In: Briand, F. (Ed), Submarine canyon dynamics in the Mediterranean and tributary seas – an integrated geological, oceanographic and biological perspective. CIESM Workshop Monographs. 47, 123-135.

Canals, M., Puig, P., Durrieu de Madron, X., Heussner, S., Palanques, A., Fabres, J. 2006. Flushing submarine canyons. Nature. 444, 354-357. https://doi.org/10.1038/nature05271.

Carlson, P.R., Bruns, T.R., Fisher, M.A. 1990. Development of slope valleys in the glacimarine environment of a complex subduction zone, Northern Gulf of Alaska. In: Dowdeswell, J.A., Scourse, J.D. (Eds), Glacimarine Environments; Processes and Sediments. Geol. Soc. London Spec. Publ. 53, 139-153.

Carlson, P.R., Karl, H.A. 1984. Discovery of two new large submarine canyons in the Bering Sea. Mar. Geol. 56, 159-179.

Carlson, P.R., Karl, H.A. 1988. Development of large submarine canyons in the Bering Sea, indicated by morphologic, seismic, and sedimentologic characteristics. Geol. Soc. Am. Bull. 100, 1594-1615.

Carson, B., Baker, E.T., Hickey, B.M., Nittrouer, C.A., DeMaster, D.J., Thorbjarnarson, K.W., Snyder, G.W. 1986. Modern sediment dispersal and accumulation in Quinault Submarine Canyon – A summary. Mar. Geol. 71, 1-13.

Carter, L., Gavey, R., Talling, P.J., Liu, J.T. 2014. Insights into submarine geohazards from breaks in subsea telecommunication cables. Oceanography. 27(2), 58–67. http://dx.doi.org/10.5670/oceanog.2014.40.

Carvajal, C., Steel, R., Petter, A. 2009. Sediment supply: the main driver of shelf-margin growth. Earth-Sci. Rev. 96, 221–248. https://doi.org/10.1016/j.earscirev.2009.06.008.

Casalbore, D., Falcini, F., Martorelli, E., Morelli, E., Bosman, A., Calarco, m., Chiocci, F.L. 2018. Characterization of overbanking features on the lower reach of the Gioia-Mesima canyon-channel system (southern Tyrrhenian Sea) through integration of morpho-stratigraphic data and physical modelling. Prog. Oceanogr. 169, 66-78. https://doi.org/10.1016/j.pocean.2018.02.020.

Chang, Y.-C., Mitchell, N. C., & Quartau, R. 2021. Landslides in the upper submarine slopes of volcanic islands: The central Azores. Geochem., Geophys., Geosyst.

22, e2021GC009833. https://doi.org/10.1029/2021GC009833.

Chen, H., Zhan, W., Li, L., Wen, M.-M. 2017. Occurrence of submarine canyons, sediment waves and mass movements along the northern continental slope of the South China Sea. J. Earth Syst. Sci. 126,73. https://doi.org/10.1007/s12040-017-0844-9.

Chiang, C.-S., Yu, H.-S. 2006. Morphotectonics and incision of the Kaoping submarine canyon, SW Taiwan orogenic wedge. Geomorphology. 80, 199-213. https://doi.org/10.1016/j.geomorph.2006.02.008.

Chiang, C.-S., Yu, H.-S., Noda, A., TuZino, T., Su, C.-C. 2012. Avulsion of the Fangliao submarine canyon off southwestern Taiwan as revealed by morphological analysis and numerical simulation. Geomorphology. 177-178, 26-37. https://doi.org/10.1016/j.geomorph.2012.07.011.

Clare, M.A., Le Bas, T., Price, D.M.,Hunt, J.E., Sear, D., Cartigny, M.J.B.,Vellinga, A., Symons, W., Firth, C., Cronin, S. 2018. Complex and cascading triggering of submarine landslides and turbidity currents at volcanic islands revealed from integration of high-resolution onshore and offshore surveys. Front. Earth Sci. 6, 223. https://doi.org/10.3389/feart.2018.00223.

Clark, P.U., Mix, A.C. 2002. Ice sheets and sea level of the Last Glacial Maximum. Quat. Sci. Rev. 21, 1-7.

Coleman, J.M., Prior, D.B., Lindsay, J.F. 1982. Formation of the Mississippi Canyon. GCAGS Transactions. 32, 519-519.

Connolly, T.P., Hickey, B.M. 2014. Regional impact of submarine canyons during seasonal upwelling. J. Geophys. Res. Oceans. 119, 953-975. https://doi.org:10.1002/2013JC009452.

Covault, J.A., Fildani, A., Romans, B.W., McHargue, T. 2011a. The natural range of submarine canyon-and-channel longitudinal profiles. Geosphere. 7(2), 313-332. https://doi.org/10.1130/GES00610.1.

Covault, J.A., Graham, S.A. 2010. Submarine fans at all sea-level stands: tectono-morphologic and climatic controls on terrigenous sediment delivery to the deep sea. Geology. 38(10), 939-942. https://doi.org/10.1130/G31081.1.

Covault, J.A., Normark, W.R., Romans, B.W., Graham, S.A. 2007. Highstand fans in the California borderland: The overlooked deep-water depositional systems. Geology. 35(9), 783-786. https://doi.org/10.1130/G23800A.1.

Covault, J.A., Romans, B.W., Graham, S.A., Fildani, A., Hilley, G.E. 2011b. Terrestrial source

to deep-sea sink sediment budgets at high and low sea levels: insights from tectonically active southern California. Geology. 39(7), 619-622. https://doi.org/10.1130/G31801.1.

Cronin, B.T., Akhmetzhanov, A.M., Mazzini, A., Akhmanov, G., Ivanov, M., Kenyon, N.H., TTR-10 Shipboard Scientists. Morphology, evolution and fill: implications for sand and mud distribution in filling deep-water canyons and slope channel complexes. Sediment. Geol. 179, 71-97. https://doi.org/10.1016/j.sedgeo.2005.04.013.

Crutchley, G.J., Kroeger, K.F., Pecher, I.A., Mountjoy, J.J., Gorman, A.R. 2017. Gas hydrate formation amid submarine canyon incision: Investigations from New Zealand's Hikurangi Subduction Margin. Geochem., Geophys., Geosyst. 18, 4299–4316. https://doi.org/10.1002/2017GC007021.

Cullis, S., Patacci, M., Colombera, L., Bührig, L., McCaffrey, W.D. 2019. A database solution for the quantitative characterisation and comparison of deep-marine siliciclastic depositional systems. Mar. Pet. Geol. 102, 321-339. https://doi.org/10.1016/j.marpetgeo.2018.12.023.

Dadson, S., Hovius, N., Pegg, S., Dade, W.B., Horng, M.J., Chen, H. 2005. Hyperpycnal river flows from an active mountain belt. J. Geophys. Res. 110, F04016. https://doi.org/10.1029/2004JF000244.

Davies, R.J., Thatcher, K.E., Mathias, S.A., Yang, J. 2012. Deepwater canyons: an escape route for methane sealed by methane hydrate. Earth Planet. Sci. Lett. 323-324, 72-78. https://doi.org/10.1016/j.epsl.2011.11.007.

de Almeida, N.M., Vital, H., Gomes, M. P. 2015. Morphology of submarine canyons along the continental margin of the Potiguar Basin, NE Brazil. Mar. Pet. Geol. 68, 307-324. http://dx.doi.org/10.1016/j.marpetgeo.2015.08.035.

De Pippo, T., Ilardi, M., Pennetta, M. 1999. Main observations on genesis and morphological evolution of submarine valleys. Z. Geomorphol. 43(1), 91-111.

Dietz, R.S., Knebel, H.J., Somers, L.H. 1968. Cayar Submarine Canyon. Geol. Soc. Am. Bull.

79, 1821-1828.

Ding, W., Li, J., Li, J., Fang, Y., Tang, Y. 2013. Morphotectonics and evolutionary controls on the Pearl River Canyon system, South China Sea. Mar. Geophys. Res. 34, 221-238. https://doi.org/10.1007/s11001-013-9173-9.

Eittreim, S., Grantz, A., Greenberg, J. 1982. Active geologic processes in Barrow Canyon, Northeast Chukchi Sea. Mar. Geol., 50, 61-76.

Ercilla, G., Alonso, B., Perez-Belzuz, F., Estrada, F., Baraza, J., Farran, M., Canals, M., Masson, D. 1998. Origin, sedimentary processes and depositional evolution of the Agadir turbidite system, central eastern Atlantic. J. Geol. Soc. London. 155(6), 929-939. https://doi.org/10.1144/gsjgs.155.6.0929.

Exon, N.F., Hill, P.J., Mitchell, C., Post, A. 2005. Nature and origin of the submarine Albany canyons off southwest Australia. Aust. J. Earth Sci. 52(1), 101-115. https://doi.org/10.1080/08120090500100036.

Fanelli, E., Bianchelli, S., Danovaro, R. 2018. Deep-sea mobile megafauna of Mediterranean submarine canyons and open slopes: Analysis of spatial and bathymetric gradients. Prog. Oceanogr. 168, 23-34. https://doi.org/10.1016/j.pocean.2018.09.010.

Farre, J.A., McGregor, B.A., Ryan, W.B.F., Robb, J.M. 1983. Breaching the shelfbreak: passage from youthful to mature phase in submarine canyon evolution. In: Stanley, D.J., Moore, G.T. (Eds), The Shelfbreak: Critical Interface on Continental Margins. SEPM Spec. Publ. 33, 25-39.

Faugères, J.-C., Mulder, T. 2011. Chapter 3 – Contour currents and contourite drifts. In: Hüneke, H., Mulder, T. (Eds), Deep-Sea Sediments. Dev. in Sedimentology. 63, 149-214.

Fernandez-Arcaya, U., Ramirez-Llodra, E., Aguzzi, J., Allcock, A.L., Davies, J.S., Dissanayake, A., Harris, P., Howell, K., Huvenne, V.A.I., Macmillan-Lawler, M., Martín, J., Menot, L., Nizinski, M., Puig, P., Rowden, A.A., Sanchez, F., Van den Beld, I.M.J. 2017.

Ecological role of submarine canyons and need for canyon conservation: a review. Front. Mar. Sci. 4, 5. https://doi.org/10.3389/fmars.2017.00005.

Ferry, J.-N., Babonneau, N., Mulder, T., Parize, O., Raillard, S. 2004. Morphogenesis of Congo submarine canyon and valley: implications about the theories of the canyons formation. Geodin. Acta. 17, 241-251.

Fiduk, J.C. 1995. Influence of submarine canyon erosion and sedimentation on allochthonous salt body geometry: the pathway of Bryant canyon in garden banks. GCSSEPM Foundation 16th Annual Research Conference Salt, Sediment and Hydrocarbons. December 3-6, 1995.

Fildani, A. 2017. Submarine canyons: a brief review looking forward. Geology, 45(4), 383-384. https://doi.org/10.1130/focus042017.1.

Fulthorpe, C.S., Carter, R.M. 1991. Continental-shelf progradation by sediment-drift accretion. Geol. Soc. Am. Bull. 103, 300-309. https://doi.org/10.1130/0016-7606(1991)103<0300:CSPBSD>2.3.CO;2.

Gales, J.A., Forwick, M., Laberg, J.S., Vorren, T.O., Larter, R.D., Graham, A.G.C., beaten, N.J., Amundsen, H.B. 2013. Arctic and Antarctic submarine gullies – A comparison of high latitude continental margins. Geomorphology. 201, 449-461. http://dx.doi.org/10.1016/j.geomorph.2013.07.018.

Gardner, J.V., Dartnell, P., Mayer, L.A., Hughes Clarke, J.E. 2003. Mar. Environ. Res. 56, 15-46. https://doi.org/10.1016/S0141-1136(02)00323-9.

Gardner, W.D., Glover, L.K., Hollister, C.D. 1980. Canyons off Northwest Puerto Rico: studies of their origin and maintenance with the nuclear research submarine NR-1. Mar. Geol. 37, 41-70.

Gervais, A., Mulder, T., Savoye, B., Gonthier, E. 2006. Sediment distribution and evolution of sedimentary processes in a small sandy turbidite system (Golo system, Mediterranean Sea): implications for various geometries based on core framework. Geo-Mar. Lett. 26, 373-395.

Gervais, A., Savoye, B., Piper, D.J.W., Mulder, T., Cremer, M., Pichevin, L. 2004. Present morphology and depositional architecture of a sandy confined submarine system: the Golo turbidite system (eastern margin of Corsica). In: Lomas, S.A., Joseph, P. (Eds), Confined Turbidite Systems. Geol. Soc. London Spec. Publ. 222, 59-89.

Gnibidenko, H.S., Svarichevskaya, L.V. 1984. The submarine canyons of Kamchatka. Mar. Geol. 54, 277-307.

Gómez-Ballesteros, M., Druet, M., Muñoz, A., Arrese, B., Rivera, J., Sánchez, F., Cristobo, J., Parra, S., García-Alegre, A., González-Pola, C., Gallastegui, J., Acosta, J. 2014. Geomorphology of the Avilés Canyon System, Cantabrian Sea (Bay of Biscay). Deep Sea Res. Part II Top. Stud. Oceanogr. 106, 99-117. http://dx.doi.org/10.1016/j.dsr2.2013.09.031.

Green, A. 2011. Submarine canyons associated with alternating sediment starvation and shelf-edge wedge development. Northern KwaZulu-Natal continental margin, South Africa. Mar. Geol. 284, 114-126. https://doi.org/10.1016/j.margeo.2011.03.011.

Greene, H.G., Maher, N.M., Paull, C.K. 2002. Physiography of the Montery Bay National Marine Sanctuary and implications about continental margin development. Mar. Geol. 181, 55-82.

Hagen, R.A., Bergersen, D.D., Moberly, R., Coulbourn, W.T. 1994. Morphology of a large meandering submarine canyon system on the Peru-Chile forearc. Mar. Geol. 119, 7-38.

Hagen, R.A., Vergara, H., Naar, D.F. 1996. Morphology of San Antonio submarine canyon on the central Chile forearc. Mar. Geol. 129, 197-205.

Hale, R.P., Nittrouer, C.A., Liu, J.T., Keil, R.G., Ogston, A.S. 2012. Effects of a major typhoon on sediment accumulation in Fangliao Submarine Cayon, SW Taiwan. Mar. Geol. 326-328, 116-130. http://dx.doi.org/10.1016/j.margeo.2012.07.008.

Han, X., Li, J., Chu, F., Li, J., Yang, F. 2010. Geomorphology and tectonic interpretation of Zhujiang Submarine Canyon, in the northern South China Sea. *OCEANS'10 IEEE SYDNEY*,

Conference. May 24-27, 2010. https://doi.org/10.1109/OCEANSSYD.2010.5603638.

Harris, P.T., Macmillan-Lawler, M. 2016. Global overview of continental shelf geomorphology based on the SRTM30_PLUS 30-Arc Second Database. In: Finkl, C., Makowski, C. (Eds), Seafloor Mapping along Continental Shelves: Research and Techniques for Visualizing Benthic Environments. Coastal Research Library. 13, 169-190. https://doi.org/10.1007/978-3-319-25121-9_7.

Harris, P.T., Macmillan-Lawler, M., Rupp, J., Baker, E.K., 2014. Geomorphology of the oceans. Mar. Geol. 352, 4–24. http://dx.doi.org/10.1016/j.margeo.2014.01.011.

Harris, P., Whiteway, T. 2011. Global distribution of large submarine canyons: Geomorphic differences between active and passive continental margins. Mar. Geol. 285, 69-86. https://doi.org:10.1016/j.margeo.2011.05.008.

Helland-Hansen, W., Sømme, T.O., Martinsen, O.J., Lunt, I. 2016. Deciphering Earth's natural hourglasses: perspectives on source-to-sink analysis. J. Sediment. Res. 86, 1008-1033. http://dx.doi.org/10.2110/jsr.2016.56.

Henrich, R., Cherubini, Y., Meggers, H. 2010. Climate and sea level induced turbidite activity in a canyon system offshore the hyperarid Western Sahara (Mauritania): the Timiris Canyon. Mar. Geol. 275, 178-198. https:// doi.org/10.1016/j.margeo.2010.05.011.

Heezen, B.C., Ewing, M. 1952. Turbidity currents and submarine slumps, and the 1929 Grand Banks earthquake. Am. J. Sci. 250, 849-873.

Hereema, C.J., Talling, P.J., Cartigny, M.J., Paull, C.K., Bailey, L., Simmons, S.M., Parsons, D.R., Clare, M.A., Gwiazda, R., Lundsten, E., Anderson, K., Maier, K.L., Xu, J.P., Sumner, E.J., Rosenberger, K., Gales, J., McGann, M., Carter, l., Pope, E., Monterey Coordinated Canyon Experiment (CCE) Team. 2020. What determines the downstream evolution of turbidity currents? Earth Planet. Sci. Lett. 532, 116023. https://doi.org/10.1016/j.epsl.2019.116023.

Hickey, B.M. 1997. The response of a steep-sided, narrow canyon to time-variable wind forcing. J. Phys. Oceanogr. 27(5), 697–726.

Higgins, S.A., Overeem, I., Rogers, K.G., Kalina, E.A. 2018. River linking in India: Downstream impacts on water discharge and suspended sediment transport to deltas. Elem. Sci. Anth. 6(20), 24 p. https://doi.org/10.1525/elementa.269.

Hizzet, J.L., Hughes Clarke, J. E., Sumner, E. J., Cartigny, M. J. B., Talling, P. J., & Clare, M.A. 2018. Which triggers produce the most erosive, frequent, and longest runout turbidity currents on deltas? Geophys. Res. Lett. 45, 855–863. https://doi.org/10.1002/2017GL075751.

Hsiung, K.-H., Kanamatsu, T., Ikehara, K., Shiraishi, K., Horng, C.-S., Usami, K. 2017. Morpho-sedimentary features and sediment dispersal systems of the southwest end of the Ryukyu Trench: a source-to-sink approach. Geo-Mar. Lett. 37, 561-577. https://doi.org/10.1007/s00367-017-0509-3.

Hsiung, K.-H., Yu, H.-S. 2011. Morpho-sedimentary evidence for a canyon-channel-trench interconnection along the Taiwan-Luzon plate margin, South China Sea. Geo-Mar. Lett. 31, 215-226. https://doi.org/10.1007/s00367-010-0226-7.

Hsu, S.-K., Kuo, J., Lo, C.-L., Tsai, C.-H., Doo, W.-B., Ku, C.-Y., Sibuet, J.-C. 2008. Turbidity currents, submarine landslides and the 2006 Pingtung earthquake off SW Taiwan. Terr. Atmos. Ocean. Sci. 19(6), 767-772. https:// doi.org/10.3319/TAO.2008.19.6.767(PT).

Huang, z., Nichol, S.L., Harris, P.T., Caley, M.J. 2014. Classification of submarine canyons of the Australian continental margin. Mar. Geol. 357, 362-383. http://dx.doi.org/10.1016/j.margeo.2014.07.007.

Iglesias, O., Lastras, G., Souto, C., Costa, S., Canals, M. 2014. Effects of coastal submarine canyons on tsunami propagation and impact. Mar. Geol. 350, 39-51. http://dx.doi.org/10.1016/j.margeo.2014.01.013.

Inman, D., Nordstrom, C. 1971. On the tectonic and morphologic classification of coasts. J. Geol. 79(1),1–21.

Itoh, M., Pickart, R.S., Kikuchi, T., Fukamachi, Y., Oshima, K.I., Simizu, D., Arrigo, K.R., Vagle, S., He, J., Ashjian, C., Mathis, J.T., Nishino, S., Nobre, C. Water properties, heat and volume fluxes of Pacific water in Barrow Canyon during summer 2010. Deep Sea Res. Part I Oceanogr. Res. Pap. 102, 43-54. http://dx.doi.org/10.1016/j.dsr.2015.04.004.

Jimoh, R.O., Tang, Y., Li, J., Awosika, L.F., Li, H., Akinnigbage, E.A., Adeleye, A.O. 2018. The architecture of the lower parts of submarine canyons on the western Nigerian continental margin. Acta Oceanol. Sin. 37(7), 28-40. https://doi.org/10.1007/s13131-018-1242-0.

Jipa, D.C., Panin, N. 2020. Narrow shelf canyons vs. wide shelf canyons: Two distinct types of Black Sea submarine canyons. Quat. Int. 540, 120-136. https://doi.org/10.1016/j.quaint.2018.08.006.

Jobe, Z.R., Lowe, D.R., Uchytil, S.J. 2011. Two fundamentally different types of submarine canyons along the continental margin of Equatorial Guinea. Mar. Pet. Geol. 28, 843-860. https://doi.org/10.1016/j.marpetgeo.2010.07.012.

Johnson, S.Y., Hartwell, S.R., Sorlien, C.C., Dartnell, P., Ritchie, A.C. 2017. Shelf evolution along a transpressive transform margin, Santa Barbara Channel, California. Geosphere. 13(6), 2041-2077. https://doi.org/10.1130/GES01387.1.

Jordi, A., Klinck, J.M., Basterretxea, Orfila, A., Tintoré, J. 2008. Estimation of shelf-slope exchanges induced by frontal instability near submarine canyons. J. Geophys. Res. 113, C05016. https://doi.org/10.1029/2007JC004207.

Katz, O., Hamiel, Y. The nature of small to medium earthquakes along the Eastern Mediterranean passive continental margins, and their possible relationships to landslides and submarine salt-tectonic-related shallow faults. 2018. In: Lintern, D.G., Mosher, D.C., Moscardelli, L.G., Bobrowsky, P.T., Campbell, C., Chaytor, J.D., Clague, J.J., Georgiopoulou,

A., Lajeunesse, P., Normandeau, A., Piper, D.J.W., Scherwath, M., Stacey, C., Turmel, D. (Eds), Subaqueous Mass Movements. Geol. Soc. London Spec.Publ. 477, 8 p. https://doi.org/10.1144/SP477.5.

Klaus, A., Taylor, B. 1991. Submarine canyon development in the Izu-Bonin Forearc: a SeaMARC II and seismic survey of Aoga Shima Canyon. Mar. Geophys. Res. 13, 131-152.

Krastel, S., Hanebuth, T.J.J., Antobreh, A.A., Henrich, R., Holz, C., Kölling, M., Schulz, H.D., Wien, K. Eos Trans. Am. Geophys. Union. 85(42), 417-432.

Krastel, S., Wefer, G., Hanebuth, T.J.J., Antobreh, A.A., Freudenthal, T., Preu, B., Schwenk, T., Strasser, M., Violante, R., Winkelmann, D., M78/3 shipboard scientific party. 2011. Sediment dynamics and geohazards off Uruguay and the de la Plata River region (northern Argentina and Uruguay). Geo-Mar. Lett. 31, 271-283. https://doi.org/10.1007/s00367-011-0232-4.

Lastras, G., Acosta, J., Muñoz, A., canals, M. 2011a. Submarine canyon formation and evolution in the Argentine Continental Margin between 44°30'S and 48°S. Geomorphology. 128, 116-136 https://doi.org/10.1016/j.geomorph.2010.12.027.

Lastras, G., Canals, M., Amblas, D., Lavoie, C., Church, I., De mol, B., Duran, R., Calafat, A.M., Hughes-Clarke, J.E., Smith, C.J., Heussner, S., "Euroléon" cruise shipboard party. 2011b. Understanding sediment dynamics of two large submarine valleys from seafloor data: Blanes and La Fonera canyons, northwestern Mediterranean Sea. Mar. Geol. 280, 20-39. https://doi.org/1 0.1016/j.margeo.2010.11.005.

Lastras, G., Arzola, R.G., Masson, D.G., Wynn, R.B., Huvenne, V.A.I., Hühnerbach, V., Canals, M. 2009. Geomorphology and sedimentary features in the Central Portuguese submarine canyons, Western Iberian margin. Geomorphology. 103, 310-329. https://doi.org/10.1016/j.geomorph.2008.06.013.

Lastras, G., Canals, M., Urgeles, R., Amblas, D., Ivanov, M., Droz, L., Dennielou, B., Fabrés,

J., Schoolmeester, T., Akhmetzhanov, A., Orange, D., García-García. 2007. A walk down the Cap de Creus canyon, Northwestern Mediterranean Sea: Recent processes inferred from morphology and sediment bedforms. Mar. Geol. 246, 176-192. https://doi.org/10.1016/j.margeo.2007.09.002.

Laursen, J., Normark, W.R. 2002. Late Quaternary evolution of the San Antonio Submarine Canyon in the central Chile forearc (~33°S). 2002. Mar. Geol. 188, 365-390.

Le Bas, T.P., Masson, R., D.G., Holtom, R.T., Grevemeyer, I. 2007. Slope failures of the flanks of the Southern Cape Verde Islands. In: Lykousis V., Sakellariou D., Locat J. (Eds), Submarine Mass Movements and Their Consequences. Advances in Natural and Technological Hazards Research, vol 27. Springer, Dordrecht. https://doi.org/10.1007.

Le Dantec, N., Hogarth, L.J., Driscoll, N.W., Babcock, J.M., Barnhardt, W.A., Schwab, W.C. 2010. Tectonic controls on nearshore sediment accumulation and submarine canyon morphology offshore La Jolla, Southern California. Mar. Geol. 268, 115-128. https://doi.org/10.1016/j.margeo.2009.10.026.

Lewis, K.B., Barnes, P.M. 1999. Kaikoura Canyon, New Zealand: active conduit from near-shore sediment zones to trench-axis channel. Mar. Geol. 162, 39-69.

Li, M.Z., Prescott, R.H., Robertson, A.G. 2019. Observation of internal tides and sediment transport processes at the head of Logan Canyon on central Scotian Slope, eastern Canada. J. Mar. Syst. 193, 103-125. https://doi.org/10.1016/j.jmarsys.2019.02.007.

Li, W., Li, S., Alves, T.M., Rebesco, M., Feng, Y. 2021. The role of sediment gravity flows on the morphological development of a large submarine canyon (Taiwan Canyon), north-east South China Sea. Sedimentology. 68, 1091-1108. https://doi.org/10.1111/sed.12818.

Liu, J.T., Hsu, R.T., Hung, J.-J., Chang, Y.-P., Wang, Y.-H., Rendle-Bühring, R.H., Lee, C.-L., Huh, C.-A., Yang, R.J. 2016. From the highest to the deepest: The Gaoping River-Gaoping Submarine Canyon dispersal system Earth-Sci. Rev. 153, 274-300.

http://dx.doi.org/10.1016/j.earscirev.2015.10.012.

Liu, J.T., Lin, H.-L. 2004. Sediment dynamics in a submarine canyon: a case of river-sea interaction. Mar. Geol. 207, 55-81.

Lo Iacono, C., Sulli, A., Agate, M. 2014. Submarine canyons of north-western Sicily (Southern Tyrrhenian Sea): variability in morphology, sedimentary processes and evolution on a tectonically active margin. Deep Sea Res. Part II Top. Stud. Oceanogr. 104, 93-105. http://dx.doi.org/10.1016/j.dsr2.2013.06.018.

Lo Iacono, C., Sulli, A., Agate, M., Lo Presti, V., Pepe, F., Catalano, R. 2011. Submarine canyon morphologies in the Gulf of Palermo (Southern Tyrrhenian Sea) and possible implications for geo-hazard. Mar. Geophys. Res. 32, 127-138. https://doi.org/10.1007/s11001-011-9118-0.

Lopez-Fernandez, P., Calafat, A., Sanchez-Vidal, A., Canals, M., Flexas, M.M., Cateura, J., Company, J.B. 2013. Multiple drivers of particle fluxes in the Blanes submarine canyon and southern open slope: results of a year round experiment. Prog. Oceanogr. 118, 95-107. http://dx.doi.org/10.1016/j.pocean.2013.07.029.

Marchès, E., Mulder, T., Cremer, M., Bonnel, C., Hanquiez, V., Gonthier, E., Lecroart, P. 2007. Contourite drift construction influenced by capture of Mediterranean Outflow Water deep-sea current by the Portimão submarine canyon (Gulf of Cadiz, South Portugal). Mar. Geol. 242, 247-260. https://doi.org/10.1016/j.margeo.2007.03.013.

Mart, Y. 1989. Sediment distribution in Akhziv Canyon off Northern Israel. Geo-Mar. Lett. 9, 77-83.

Martín, J., Palanques, A., Puig, P. 2006. Composition and variability of downward particulate matter fluxes in the Palamós submarine canyon (NW Mediterranean). J. Mar. Syst. 60, 75-97. https://doi.org/10.1016/j.jmarsys.2005.09.010.

Martinsen, O.J. 2005. Deep-water sedimentary systems of Arctic and North Atlantic margins:

An introduction. Nor. J. Geol. 85, 261-266.

Martinsen, O.J., Sømme, T.O., Thurmond, J.B., Helland-Hansen, W., Lunt, I. 2010. Source-to-sink systems on passive margins: theory and practice with an example from the Norwegian continental margin. In: Vining, B.A., Pickering, S.C. (Eds), Petroleum Geology: From Mature Basins to New Frontiers – Proceedings of the 7th Petroleum Geology Conference. 7, 913–920. https://doi.org/10.1144/0070913.

Matos, F.L., Ross, S.W., Huvenne, V.A.I., Davies, J.S., Cunha, M.R. 2018. Canyons pride and prejudice: Exploring the submarine canyon research landscape, a history of geographic and thematic bias. Prog. Oceanogr. 169, 6-19. https://doi.org/10.1016/j.pocean.2018.04.010.

Mauffrey, M.A., Berné, S., Jouet, G., Giresse, P., Gaudin, M. 2015. Sea-level control on the connection between shelf-edge deltas and the Bourcart canyon head (western Mediterranean) during the last glacial/interglacial cycle. Mar. Geol. 370, 1-19. http://dx.doi.org/10.1016/j.margeo.2015.09.010.

Mazières, A., Gillet, H., Castelle, B., Mulder, T., Guyot, C., Garlan, T., Mallet, C. 2014. High-resolution morphobathymetric analysis and evolution of Capbreton submarine canyon head (Southeast Bay of Biscay—French Atlantic Coast) over the last decade using descriptive and numerical modelling. Mar. Geol. 351, 1-12. http://dx.doi.org/10.1016/j.margeo.2014.03.001.

McGregor, B.A. 1983. Submarine canyon and slope processes on the U.S. Atlantic continental margin. Open-File Report 83-735. U.S. Geological Survey. https://doi.org/10.3133/ofr83735.

Micallef, A., Mountjoy, J.J., Barnes, P.M., Canals, M., Lastras, G. 2014. Geomorphic response of submarine canyons to tectonic activity: insights from the Cook Strait canyon system, New Zealand. Geosphere. 10(5), 905-929. https://doi.org/10.1130/GES01040.1.

Michaud, F., Proust, J.N., Collot, J.Y., Lebrun, J.F., Witt, C., Ratzov, G., Pouderoux, H., Martillo, C., Hernández, M.J., loayza, G., Penafiel, L., Schenini, L., Dano, A., Gonzalez, M.,

Barba, D., De Min, L., Ponce, G., Urresta, A., Calderon, M. 2015. Quaternary sedimentation and active faulting along the Ecuadorian shelf: preliminary results of the ATACAMES Cruise (2012). Mar. Geophys. Res. 36, 81-98. https:// doi.org/10.1007/s11001-014-9231-y.

Milia, A. 2000. The Dohrn Canyon: a response to the eustatic fall and tectonic uplift of the outer shelf along the eastern Tyrrhenian Sea margin, Italy. Geo-Mar. Lett. 20, 101-108.

Milliman, J., & Farnsworth, K. 2011. River Discharge to the Coastal Ocean: A Global Synthesis. Cambridge University Press, Cambridge. https://doi.org/10.1017/CBO9780511781247.

Mitchell, J.K., Holdgate, G.R., Wallace, M.W., Gallagher, S.J. 2007. Marine geology of the Quaternary Bass Canyon system, southeast Australia: a cool-water carbonate system. Mar. Geol. 237, 71-96. https://doi.org/10.1016/j.margeo.2006.10.037.

Molenaar, A., Moernaut, J., Wiemer, G., Dubois, N., Strasser, M. 2019. Earthquake impact on active margins: tracing surficial remobilization and seismic strengthening in a slope sedimentary sequence. Geophys. Res. Lett. 46, 6015–6023. https://doi.org/10.1029/2019GL082350.

Mondziel, S., Grindlay, N., Mann, P., Escalona, A., Abrams, L. 2010. Morphology, structure, and tectonic evolution of the Mona canyon (northern Mona passage) from multibeam bathymetry, side-scan sonar, and seismic reflection profiles. Tectonics. 29, TC2003. https:// doi.org/10.1029/2008TC002441.

Mougenot, D., Boillot, G., Rehault, J.-P. 1983. Prograding shelfbreak types on passive continental margins: some European examples. In: Stanley, D.J., Moore, G.T. (Eds), The Shelfbreak: Critical Interface on Continental Margins. SEPM Spec. Publ. 33, 25-39.

Mountjoy, J.J., Barnes, P.M., Pettinga, J.R. 2009. Morphostructure and evolution of submarine canyons across an active margin: Cook Strait sector of the Hikurangi Margin, New Zealand. Mar. Geol. 260, 45-68. https://doi.org/10.1016/j.margeo.2009.01.006.

Mountjoy, J.J., Micallef, A., Stevens, C.L., Stirling, M.W. 2014. Holocene sedimentary activity in a non-terrestrially coupled submarine canyon: Cook Strait Canyon system, New Zealand. Deep Sea Res. Part II Top. Stud. Oceanogr. 104, 120-133. http://dx.doi.org/10.1016/j.dsr2.2013.09.001.

Mulder, T., Ducassou, E., Gillet, H., Hanquiez, V., Tournadour, E., Combes, J., Eberli, G.P., Kindler, P., Gonthier, E., Conesa, G., Robin, C., Sianipar, R., Reijmer, J.J.G., François, A. 2012. Canyon morphology on a modern carbonate slope of the Bahamas: evidence of regional tectonic tilting. Geology. 40(9), 771-774. https://doi.org/10.1130/G33327.1.

Mulder, T., Lecroart, P., Hanquiez, V., Marches, E., Gonthier, E., Guedes, J.-C., Thiébot, E., Jaaidi, B., Kenyon, N., Voisset, M., Perez, C., Sayago, M., Fuchey, Y., Bujan, S. 2006. Geo-Mar. Lett. 26(1), 31-41. http://dx.doi.org/10.1007/s00367-005-0013-z.

Mulder, T., Moran, K. 1995. Relationship among submarine instabilities, sea level variations, and the presence of an ice sheet on the continental shelf: an example from the Verrill Canyon Area, Scotian Shelf. Paleoceanography. 1995. 10(1), 137-154.

Mulder, T., Syvitski, J.P.M., Migeon, S., Faugères, J.-C., Savoye, B. 2003. Marine hyperpycnal flows: initiation, behavior and related deposits. A review. Mar. Pet. Geol. 20, 861-882. https://doi.org/10.1016/j.marpetgeo.2003.01.003.

Mulder, T., Zaragosi, S., Garlan, T., Mavel, J., Cremer, M., Sottolichio, A., Sénéchal, N., Schmidt, S. 2012. Present deep-submarine canyons activity in the Bay of Biscay (NE Atlantic). Mar. Geol. 295-298, 113-127. https://doi.org/10.1016/j.margeo.2011.12.005.

Nelson, C.H., Carlson, P.R., Byrne, J.V., Alpha, T.R. 1970. Development of the Astoria Canyon-Fan physiography and comparison with similar systems. Mar. Geol. 8, 259-291.

Nelson, C.H., Escutia, C., Damuth, J.E., Twichell Jr., D.C. 2011. Interplay of mass-transport and turbidite-system deposits in different active tectonic and passive continental margin settings: external and local controlling factors. In: Shipp, R.C., Weimer, P., Posamentier, H.W.

(Eds), Mass-Transport Deposits in Deepwater Settings. SEPM Spec. Publ. 96, 39-66.

Nittrouer, C.A., Wright, L.D. 1994. Transport of particles across continental shelves. Rev. Geophys. 32(1), 85-113.

Noda, A., TuZino, T., Furukawa, R., Joshima, M., Uchida, J. 2008. Physiographical and sedimentological characteristics of submarine canyons developed upon an active forearc slope: the Kushiro Submarine Canyon, northern Japan. Geol. Soc. Am. Bull. 120(5/6), 750-767. https://doi.org/10.1130/B26155.1.

Noda, A., TuZino, T. 2010. Shelf-slope sedimentation during the late Quaternary on the southwestern Kuril forearc margin, northern Japan. Sediment. Geol. 232, 35-51. https://doi.org/10.1016/j.sedgeo.2010.09.008.

Normark, W.R., Piper, D.J.W., Romans, B.W., Covault, J.A., Dartnell, P., Sliter, R.W. 2009. Submarine canyon and fan systems of the California Continental Borderland. In: Lee, H.J., Normark, W.R. (Eds), Earth Science in the Urban Ocean: The Southern California Continental Borderland. Spec. Pap. Geol. Soc. Am. 454, 141–168. https://doi.org/10.1130/2009.2454(2.7).

Nyberg, B., Helland-Hansen, W., Gawthorpe, R.L., Sandbakken, P., Eide, C.H., Sømme, T., Hadler-Jacobsen, F., Leiknes, S. 2018. Revisiting morphological relationships of modern source-to-sink segments as a first-order approach to scale ancient sedimentary systems. Sediment. Geol. 373, 111-133. https://doi.org/10.1016/j.sedgeo.2018.06.007.

Oiwane, H., Tonai, S., Kiyokawa, S., Nakamura, Y., Suganuma, Y., Tokuyama, H. 2011. Geomorphological development of the Goto Submarine Canyon, northeastern East China Sea. Mar. Geol. 288, 49-60. https://doi.org/10.1016/j.margeo.2011.06.013.

Orange, D.L., Anderson, R.S., Breen, N.A. 1994. Regular canyon spacing in the submarine environment: the link between hydrology and geomorphology. GSA Today. 4(2), 35-39.

Osmundsen, P.T., Redfield, T.F. 2011. Crustal taper and topography at passive continental

margins. Terra Nova. 23(6), 349-361. https://doi.org/10.1111/j.1365-3121.2011.01014.x.

Palanques, A., El Khatab, M., Puig, P., Masqué, P., Sánchez-Cabeza, J.A., Isla, E. 2005. Downward particle fluxes in the Guadiaro submarine canyon depositional system (north-western Alboran Sea), a river flood dominated system. Mar. Geol. 220, 23-40. https://doi.org/10.1016/j.margeo.2005.07.004.

Palanques, A., Martín, J., Puig, P., Guillén, J., Company, J.B., Sardá, F. 2006. Evidence of sediment gravity flows induced by trawling in the Palamós (Fonera) submarine canyon (northwestern Mediterranean). Deep Sea Res. Part I Oceanogr. Res. Pap. 53, 201-214.

Paldor, A., Katz, O., Aharonov, E., Weinstein, Y., Roditi-Elasar, M., Lazar, A., Lazar, B. 2020. Deep submarine groundwater discharge—Evidence from Achziv Submarine Canyon at the exposure of the Judea Group confined aquifer, eastern Mediterranean. J. Geophys. Res. Oceans. 125, e2019JC015435. https://doi.org/10.1029/2019JC015435.

Paull, C.K., Caress, D.W., Lundsten, E., Gwiazda, R., Anderson, K., McGann, M., Conrad, J., Edwards, B., Sumner, E.J. 2013. Anatomy of the La Jolla Submarine Canyon system; offshore southern California. Mar. Geol. 335, 16-34. http://dx.doi.org/10.1016/j.margeo.2012.10.003.

Paull, C.K., Talling, P.J., Maier, K.L., Parsons, D., Xu, J., Caress, D.W., Gwiazda, R., Lundsten, E.M., Anderson, K., Barry, J.P., Chaffey, M., O'Reilly, T., Rosenberger, K.J., Gales, J.A., Kieft, B., McGann, M., Simmons, S.M., McCann, M., Sumner, E.J., Clare, M.A., Cartigny, M.J. 2018. Powerful turbidity currents driven by dense basal layers. Nat. Commun. 9, 4114. https://doi.org/10.1038/s41467-018-06254-6.

Peakall, J., Kane, I.A., Masson, D.G., Keevil, G., McCaffrey, W., Corney, R. 2012. Global (latitudinal) variation in submarine channel sinuosity. Geology. 40(1), 11-14. https://doi.org/10.1130/G32295.1.

Peters, S.E., Loss, D.P. 2012. Storm and fair-weather wave base: a relevant distinction?

Geology. 40(6), 511-514. https://doi.org/10.1130/G32791.1.

Pico, T., Mitrovica, J.X., Braun, J., Ferrier, K.L. 2018. Glacial isostatic adjustment deflects the path of the ancestral Hudson River. Geology. 46(7), 591-594. https://doi.org/10.1130/G40221.1.

Pierau, R., Hanebuth, T.J.J., Krastel, S., Henrich, R. 2010. Late Quaternary climatic events and sea-level changes recorded by turbidite activity, Dakar Canyon, NW Africa. Quat. Res. 73, 385-392. https://doi.org/10.1016/j.yqres.2009.07.010.

Pierau, R., Henrich, R., Preiß-Daimler, I., Krastel, S., Geersen, J. 2011. Sediment transport and turbidite architecture in the submarine Dakar Canyon off Senegal, NW-Africa. J. African Earth Sci. 60, 196-208. https://doi.org/10.1016/j.jafrearsci.2011.02.010.

Pierdomenico, M., Martorelli, E., Dominguez-Carrío, C., Gili, J.M., Chiocci, F.L. 2016. Seafloor characterization and benthic megafaunal distribution of an active submarine canyon and surrounding sectors: The case of Gioia Canyon (Southern Tyrrhenian Sea). J. Mar. Syst. 157, 101-117. http://dx.doi.org/10.1016/j.jmarsys.2016.01.005.

Piper, D.J.W., Hiscott, R.N., Normark, W.R. 1999. Outcrop-scale acoustic facies analysis and latest Quaternary development of Hueneme and Dume submarine fans, offshore California. Sedimentology. 46, 47-78.

Piper, D.J.W., Normark, W.R. 2009. Processes that initiate turbidity currents and their influence on turbidites: a marine geology perspective. J. Sediment. Res. 79, 347-362. https://doi.org/10.2110/jsr.2009.046.

Pisareva, M.N., Pickart, R.S., Lin, P., Fratantoni, P.S., Weingartner, T.J. 2019. On the nature of wind-forced upwelling in Barrow Canyon. Deep Sea Res. Part II Top. Stud. Oceanogr. 162, 63-78. https://doi.org/10.1016/j.dsr2.2019.02.002.

Popescu, I., Lericolais, G., Panin, N., Normand, A., Dinu, C., Le Drezen, E. 2004. The Danube submarine canyon (Black Sea): morphology and sedimentary processes. Mar. Geol.

206, 249-265. https://doi.org/10.1016/j.margeo.2004.03.003.

Porcile, G., Pittaluga, M.B., Frascati, A., Sequeiros, O.E. 2020. Typhoon-induced megarips as triggers of turbidity currents offshore tropical river deltas. Commun. Earth & Environ. 1, 2. https://doi.org/10.1038/s43247-020-0002-1.

Posamentier, H. W., Erskine, R. D., Mitchum, R. M., Jr. 1991. Models for submarine-fan deposition within a sequence-stratigraphic framework, in: Weimer, P., Link, M. H. (Eds), Seismic facies and sedimentary processes of submarine fans and turbidite systems. Frontiers in Sedimentary Geology. Springer, New York, pp.127-136.

Post, A.L., Przeslawski, R., Nanson, R., Siwabessy, J., Smith, D., Kirkendale, L.A., Wilson, N.G. 2022. Modern dynamics, morphology and habitats of slope-confined canyons on the northwest Australian margin. Mar. Geol. 444, 106694. https://doi.org/10.1016/j.margeo.2021.106694.

Power, W., Mountjoy, J., Lane, E., Popinet, S., Wang, X. 2016. Assessing landslide-tsunami hazard in submarine canyons, using the Cook Strait Canyon System as an example. J. Tsunami Soc. Int. 35(3), 145-166.

Pratson, L.F., Coakley, B.J. 1996. A model for the headward erosion of submarine canyons induced by downslope-eroding sediment flows. Geol. Soc. Am. Bull. 108 (2), 225-234.

Pratson, L.F., Nittrouer, C.A., Wiberg, P.L., Steckler, M.S., Swenson, J.B., Cacchione, D.A., Karson, J.A., Murray, A.B., Wolinsky, M.A., Gerber, T.P., Mullenbach, B.L., Spinelli, G.A., Fulthorpe, C.S., O'Grady, D.B., Parker, G. Driscoll, N.W., Burger, R.L., Paola, C., Orange, D.L., Field, M.E., Friedrichs, C.T., Fedele, J.J. 2007. Seascape evolution on clastic continental shelves and slopes, in: Nittrouer, C.A., Austin, J.A., Field, M.E., Kravitz, J.H., Syvitski, J.P.M., Wiberg, P.L. (Eds), Continental Margin Sedimentation: From Sediment Transport to Sequence Stratigraphy. Blackwell Publishing, Oxford, pp. 339-380.

Pratson, L.F., Ryan, W.B.F., Mountain, G.S., Twichell, D.C. 1994. Submarine canyon initiation by downslope-eroding sediment flows: evidence in late Cenozoic strata on the New Jersey continental slope. Geol. Soc. Am. Bull. 106, 395-412.

Puga-Bernabéu, A., Webster, J.M., Beaman, R.J., Guilbaud, V. 2011. Morphology and controls on the evolution of a mixed carbonate–siliciclastic submarine canyon system, Great Barrier Reef margin, north-eastern Australia. Mar. Geol. 289, 100-116. https://doi.org/10.1016/j.margeo.2011.09.013.

Puig, P., Durán, R., Muñoz, A., Elvira, E., Guillén, J. 2017. Submarine canyon-head morphologies and inferred sediment transport processes in the Alías-Almanzora canyon system (SW Mediterranean): on the role of the sediment supply. Mar. Geol. 393, 21-34. http://dx.doi.org/10.1016/j.margeo.2017.02.009.

Puig, P., Palanques, A., Guillén, J., García-Ladona. 2000. Deep slope currents and suspended particle fluxes in and around the Foix submarine canyon (NW Mediterranean). 47, 343-366. Deep Sea Res. Part I Oceanogr. Res. Pap. 47, 343-366.

Puig, P., Palanques, A., Martín, J. 2014. Contemporary sediment-transport processes in submarine canyons. Annu. Rev. Mar. Sci. 6, 53-77. https://doi.org/10.1146/annurev-marine-010213-135037.

Quartau, R., Madeira, J., Mitchell, N.C., Tempera, F., Silva, P.F., Brandão, F. 2015. The insular shelves of the Faial-Pico Ridge (Azores archipelago): A morphological record of its evolution. Geochem., Geophys., Geosyst. 16, 1401-1420. https://doi.org/10.1002/2015GC005733.

Rahmstorf, S. Thermohaline Ocean Circulation. 2006, in: Elias, S.A. (Ed), Encyclopedia of Quaternary Sciences. Elsevier, Amsterdam, pp. 739-750.

Rasmussen, E.S. 1994. The relationship between submarine canyon fill and sea-level change: an example from Middle Miocene offshore Gabon, West Africa. Sediment. Geol. 90,

61-75.

Ratzov, G., Sosson, M., Collot, J.-Y., Migeon, S. 2012. Late Quaternary geomorphologic evolution of submarine canyons as a marker of active deformation on convergent margins: The example of the South Colombian margin. Mar. Geol. 315-318, 77-97. https://doi.org/10.1016/j.margeo.2012.05.005.

Restrepo-Correa, I.C., Ojeda, G.Y. 2010. Geologic controls on the morphology of La Aguja submarine canyon. J. South. Am. Earth. Sci. 29, 861-870. https://doi.org/10.1016/j.jsames.2010.07.001.

Ridente, D., Martorelli, E., Bosman, A., Chiocci, F.L. 2014. High-resolution morpho-bathymetric imaging of the Messina Strait (Southern Italy). New insights on the 1908 earthquake and tsunami. Geomorphology. 208, 149-159. http://dx.doi.org/10.1016/j.geomorph.2013.11.021.

Rise, L., Bøe, R., Riis, F., Bellec, V.K., Laberg, J.S., Eidvin, T., Elvenes, S., Thorsnes, T. 2013. Mar. Pet. Geol. 45, 134-149. http://dx.doi.org/10.1016/j.marpetgeo.2013.04.021.

Romans, B.W., Normark, W.R., McGann, M.M., Covault, J.A., Graham, S.A. 2009. Coarse-grained sediment delivery and distribution in the Holocene Santa Monica Basin, California: implications for evaluating source-to-sink flux at millennial time scales. Geol. Soc. Am. Bull. 121(9/10), 1394-1408. https://doi.org/10.1130/B26393.1.

Rona, P.A. 1970. Submarine Canyon Origin on Upper Continental Slope off Cape Hatteras. J. Geol. 78(2), 141-152.

Rona, P., Guida, V., Scranton, M., Gong, D., Macelloni, L., Pierdomenico, M., Diercks, A.-R., Asper, V., Haag, S. 2015. Hudson submarine canyon head offshore New York and New Jersey: a physical and geochemical investigation. Deep Sea Res. Part II Top. Stud. Oceanogr. 121, 213-232. http://dx.doi.org/10.1016/j.dsr2.2015.07.019.

Salmanidou, D.M., Heidarzadeh, M., Guillas, S. 2019. Probabilistic landslide-generated tsunamis in the Indus Canyon, NW Indian Ocean, using statistical emulation. Pure Appl. Geophys. 176, 3099-3114. https://doi.org/10.1007/s00024-019-02187-3.

Santora, J.A., Zeno, R., Dorman, J.G., Sydeman, W.J. 2018. Submarine canyons represent an essential habitat network for krill hotspots in a large marine ecosystem. Sci. Rep. 8, 7579. https://doi.org/10.1038/s41598-018-25742-9.

Schnürle, P., Liu, C.-S., Lallemand, S.E., Reed, D. 1998. Structural controls of the Taitung Canyon in the Huatung Basin East of Taiwan. TAO. 9(3), 453-472.

Sequeiros, O.E., Pittaluga, M.B., Frascati, A., Pirmez, C., Masson, D.G., Weaver, P., Crosby, A.R., Lazzaro, G., Botter, G., Rimmer, J.G. 2019. How typhoons trigger turbidity currents in submarine canyons. Sci. Rep. 9, 9220. https://doi.org/10.1038/s41598-019-45615-z.

Shepard, F.P. 1936. The underlying causes of submarine canyons. Proc. Natl. Acad. Sci. U.S.A. 22(8), 496-502.

Shepard, F.P. 1981. Submarine canyons: multiple causes and long-time persistence. Am Assoc. Pet. Geol. Bull. 65(6), 1062-1077.

Sheng, H., Gao, J.H., Kettner, A.J., Shi, Y., Wang, Y.P., Chen, Y. 2019. Variations in fluvial discharge of rivers over the last millennium along the eastern coast of the Liaodong Peninsula, China. J Asian Earth Sci. 184, 103993. https://doi.org/10.1016/j.jseaes.2019.103993.

Shepard, F.P. 1972. Submarine canyons. Earth-Sci. Rev. 8, 1-12.

Shumaker, L.E., Jobe, Z.R., Johnstone, S.A., Pettinga, L.A., Cai, D.X., Moody, J.D. 2018. Controls on submarine channel-modifying processes identified through morphometric scaling relationships. Geosphere. 14(5), 2171-2187. https://doi.org/10.1130/GES01674.1.

Simmons, S. M., Azpiroz-Zabala, M., Cartigny, M. J. B., Clare, M. A., Cooper, C., Parsons, D. R., Pope, E. L., Sumner, E. J. and Talling, P. J. 2020. Novel Acoustic Method Provides First

Detailed Measurements of Sediment Concentration Structure Within Submarine Turbidity Currents. J. Geophys. Res.: Oceans. 125(5), e2019JC015904. https://doi.org/10.1029/2019JC015904.

Simms, A.R., Lisiecki, L., Gebbie, G. Whitehouse, P.L. 2019. Balancing the last glacial maximum (LGM) sea-level budget. Quat. Sci. Rev. 205, 143-153. https://doi.org/10.1016/j.quascirev.2018.12.018.

Smith, M. E., Finnegan, N. J., Mueller, E. R., Best, R. J. 2017. Durable terrestrial bedrock predicts submarine canyon formation. Geophys. Res. Lett. 44, 10332-10340. https://doi.org/10.1002/2017GL075139.

Smith, M.E., Werner, S.H., Buscombe, D., Finnegan, N.J., Sumner, E.J., Mueller, E.R. 2018. Seeking the shore: evidence for active submarine canyon head incision due to coarse sediment supply and focusing of wave energy. Geophys. Res. Lett. 45,12403-12413. https://doi.org/10.1029/2018GL080396.

Soh, W., Tokuyama, H. 2002. Rejuvenation of submarine canyon associated with ridge subduction, Tenryu Canyon, off Tokai, central Japan. Mar. Geol. 187, 203-220.

Soh, W., Tokuyama, H., Fujioka, K., Kato, S., Taira, A. 1990. Morphology and development of a deep-sea meandering canyon (Boso Canyon) on an active plate margin, Sagami Trough, Japan. Mar. Geol. 91, 227-241.

Sømme, T.O., Helland-Hansen, W., Martinsen, O.J., Thurmond, J.B. 2009. Relationships between morphological and sedimentological parameters in source-to-sink systems: a basis for predicting semi-quantitative characteristics in subsurface systems. Basin Res. 21, 361-387. https://doi.org/10.1111/j.1365-2117.2009.00397.x.

Soutter, E.L., Kane, I.A., Hodgson, D.M., Flint, S. 2021. The concavity of submarine canyon longitudinal profiles. J. Geophys. Res. Earth. Surf. 126, e2021JF006185. https://doi.org/10.1029/2021JF006185.

Stein, S., Cloetingh, S., Sleep, N.H., Wortel, R. 1989. Passive margin earthquakes, stresses and rheology, in: Gregerssen, S., Basham, P.W. (Eds), Earthquakes at North-Atlantic Passive Margins: Neotectonics and Postglacial Rebound, vol 266. Springer, Dordrecht, pp. 231-259.

Straub, K.M., Mohrig, D. 2009. Constructional canyons built by sheet-like turbidity currents: observations from offshore Brunei Darussalam. J. Sediment. Res. 79, 24-39. https://doi.org/10.2110/jsr.2009.006.

Strozyk, F., Strasser, M., Förster, A., Kopf, A., Huhn, K. 2010. Slope failure repetition in active margin environments: constraints from submarine landslides in the Hellenic fore arc, eastern Mediterranean. J. Geophys. Res. Earth. 115, B08103. https://doi.org/10.1029/2009JB006841.

Sweet, M.L., Blum, M.D. 2016. Connections between fluvial to shallow marine environments and submarine canyons: implications for sediment transfer to deep water. J. Sediment. Res. 86, 1147-1162. http://dx.doi.org/10.2110/jsr.2016.64.

Sweet, M.L., Gaillot, G.T., Jouet, G., Rittenour, T.M., Toucanne, S., Marsset, T., Blum, M.D. 2020. Sediment routing from shelf to basin floor in the Quaternary Golo System of Eastern Corsica, France, western Mediterranean Sea. Geol. Soc. Am. Bull. 132(5/6), 1217-1234. https://doi.org/10.1130/B35181.1.

Su, M., Hsiung, K.-H., Zhang, C., Xie, X., Yu, H.-S., Wang, Z. 2015. The linkage between longitudinal sediment routing systems and basin types in the northern South China Sea in perspective of source-to-sink. J. Asian Earth Sci. 111, 1-13. http://dx.doi.org/10.1016/j.jseaes.2015.05.011.

Su, M., Lin, Z., Wang, C., Kuang, Z., Liang, J., Chen, H., Liu, S., Zhang, B., Luo, K., Huang, S., Wu, Q. 2020. Mar. Geol. 424, 106166. https://doi.org/10.1016/j.margeo.2020.106166.

Susanth, S., Kurian, P.J., Bijesh, C.M., Twinkle, D., Tyagi, A., Rajan, S. 2021. Controls on the evolution of submarine canyons in steep continental slopes: geomorphological insights from

Palar Basin, southeastern margin of India. Geo-Mar. Lett. 41, 14. https://doi.org/10.1007/s00367-021-00685-9.

Sylvester, Z., Pirmez, C. 2017. Latitudinal changes in the morphology of submarine channels: reevaluating the evidence for the influence of the Coriolis force. In: Fraticelli ,C.M., Markwick, P.J., Martinius, A.W., Suter, J.W (Eds), Latitudinal Controls on Stratigraphic Models and Sedimentary Concepts. SEPM Spec. Publ. 108. 11 p. https://doi.org/10.2110/sepmsp.108.02.

Tournadour, E., Mulder, T., Borgomano, J., Gillet, H., Chabaud, L., Ducassou, E., Hanquiez, V., Etienne, S. 2017. Submarine canyon morphologies and evolution in modern carbonate settings: The northern slope of Little Bahama Bank, Bahamas. Mar. Geol. 391, 76-97. http://dx.doi.org/10.1016/j.margeo.2017.07.014.

Trumbull, J.V.A., Garrison, L.E. 1973. Geology of a system of submarine canyons South of Puerto Rico. J. Res. U.S. Geol. Survey. 1(3), 293-299.

Tubau, X., Lastras, G., Canals, M., Micallef, A., Amblas, D. 2013. Significance of the fine drainage pattern for submarine canyon evolution: the Foix Canyon System, Northwestern Mediterranean Sea. Geomorphology. 184, 20-37. http://dx.doi.org/10.1016/j.geomorph.2012.11.007.

Tubau, X., Paull, C.K., Lastras, G., Caress, D.W., Canals, M., Lundsten, E., Anderson, K., Gwiazda, R., Amblas, D. 2015. Submarine canyons of Santa Monica Bay, Southern California: variability in morphology and sedimentary processes. Mar. Geol. 365, 61-79. http://dx.doi.org/10.1016/j.margeo.2015.04.004.

TuZino, T., Noda, A. 2010. Architecture and evolution of the Kushiro submarine canyon in the Kurile Trench forearc slope, North-western Pacific. Sedimentology. 57, 611-641. https://doi.org/10.1111/j.1365-3091.2009.01107.x.

Urías Espinosa, J., Bandy, W.L., Mortera Gutiérrez, C.A., Núñez Cornú, F. J., Mitchell, N.C. 2016. Multibeam bathymetric survey of the Ipala Submarine Canyon, Jalisco, Mexico (20°N):

The southern boundary of the Banderas Forearc Block? Tectonophysics. 671, 249-263. http://dx.doi.org/10.1016/j.tecto.2015.12.029.

Valentine, P.C., Uzmann, J.R., Cooper, R.A. 1980. Geology and biology of Oceanographer Submarine Canyon. Mar. Geol. 38, 283-312.

Vardar, D. 2019. Morphological definition of the North İmralı Canyon in the Sea of Marmara. Arab. J. Geosci. 12, 76. https://doi.org/10.1007/s12517-019-4257-8.

Voigt, I., Henrich, R., Preu, B.M., Piola, A.R., Hanebuth, T.J.J., Schwenk, T., Chiessi, C.M. 2013. A submarine canyon as a climate archive – Interaction of the Antarctic Intermediate Water with the Mar del Plata Canyon (Southwest Atlantic). Mar. Geol. 341, 46-57. https://dx.doi.org/10.1016/j.margeo.2013.05.002.

von Rad, U., Tahir, M. 1997. Late Quaternary sedimentation on the outer Indus shelf and slope (Pakistan): evidence from high-resolution seismic data and coring. Mar. Geol. 138, 193-236.

Walsh, J.P., Alexander, C.R., Gerber, T., Orpin, A.R., Sumners, B.W. 2007. Demise of a submarine canyon? Evidence for highstand infilling on the Waipaoa River continental margin, New Zealand. Geophys. Res. Lett. 34, L20606. https://doi.org/10.1029/2007GL031142, 2007.

Wang, H., Bi, N., Wang, Y., Saito, Y., Yang, Z. 2010. Tide-modulated hyperpycnal flows off the Huanghe (Yellow River) mouth, China. Earth Surf. Process. Landf. 35, 1315-1329. https://doi.org/10.1002/esp.2032.

Wang, R., Colombera, L., Mountney, N.P. 2019. Geological controls on the geometry of incised-valley fills: insights from a global dataset of late-Quaternary examples. Sedimentology. 66(6), 2134-2168. https://doi.org/10.1111/sed.12596.

Wang, X., Zhuo, H., Wang, Y., Mao, P., He, M., Chen, W., Zhou, J., Gao, S., Wang, M. 2018. Controls of contour currents on intra-canyon mixed sedimentary processes: Insights from the Pearl River Canyon, northern South China Sea. Mar. Geol. 406, 193-213.

https://doi.org/10.1016/j.margeo.2018.09.016.

Waterhouse, A.F., Allen, S.E., Bowie, A.W. 2009. Upwelling flow dynamics in long canyons at low Rossby number. J. Geophys. Res. 114, C05004. https://doi.org/10.1029/2008JC004956.

Warratz, G., Schwenk, T., Voigt, I., Bozzano, G., Henrich, R., Violante, R., Lantzsch, H. 2019. Interaction of a deep-sea current with a blind submarine canyon (Mar del Plata Canyon, Argentina). Mar. Geol. 417, 106002. https://doi.org/10.1016/j.margeo.2019.106002.

Wiles, E., Green, A., Watkeys, M., Botes, R., Jokat, W. 2019. Submarine canyons of NW Madagascar: a first geomorphological insight. Deep Sea Res. Part II Top. Stud. Oceanogr. 161, 5-15. https://doi.org/10.1016/j.dsr2.2018.06.003.

Wiles, E., Green, A., Watkeys, M., Jokat, W., Krocker, R. 2013. The evolution of the Tugela canyon and submarine fan: a complex interaction between margin erosion and bottom current sweeping, southwest Indian Ocean, South Africa. Mar. Pet. Geol. 44, 60-70. http://dx.doi.org/10.1016/j.marpetgeo.2013.03.012.

Wolin, E., Stein, S., Pazzaglia, F., Meltzer, A., Kafka, A., Berti, C. 2012. Mineral, Virginia, earthquake illustrates seismicity of a passive-aggressive margin. Geophys. Res. Lett. 39, L02305. https://doi.org/10.1029/2011GL050310.

Wynn, R.B., Weaver, P.P.E., Masson, D.G., Stow, D.A.V. 2002. Turbidite depositional architecture across three interconnected deep-water basins on the north-west African margin. Sedimentology. 49, 669-695.

Xu, J.P. 2011. Measuring currents in submarine canyons: technological and scientific progress in the past 30 years. Geosphere. 7(4), 868-876. https://doi.org/10.1130/GES00640.1.

Xu, J.P., Noble, M.A. 2009. Currents in Monterey Submarine Canyon. J. Geophys. Res. 114, C03004. https://doi.org/10.1029/2008JC004992.

Xu, S., Wang, Y., Peng, X., Zou, H., Qiu, Y., Gong, C., Zhuo, H. 2014. Origin of Taiwan

Canyon and its effects on deepwater sediment. Sci. China Earth Sci. 57(11), 2769-2780. https://doi.org/10.1007/s11430-014-4942-0.

Yin, S., Li, J., Ding, W., Gao, J., Ding, W., Wang, Y. 2018. Migration of the lower North Palawan submarine canyon: characteristics and controls. Int. Geol. Rev. 6287-8), 988-1005. https://doi.org/10.1080/00206814.2018.1522519.

Yin, S., Lin, L., Pope, E.L., Li, J., Ding, W., Wu, Z., Ding, W., Gao, J., Zhao, D. 2019. Continental slope-confined canyons in the Pearl River Mouth Basin in the South China Sea dominated by erosion, 2004–2018. Geomorphology. 344, 60-74. https://doi.org/10.1016/j.geomorph.2019.07.016.

Yin, S., Wang, L., Guo, Y, Zhong, G. 2015. Morphology, sedimentary characteristics, and origin of the Dongsha submarine canyon in the northeastern continental slope of the South China Sea. Sci. China Earth Sci. 58, 971–985. https://doi.org/10.1007/s11430-014-5044-8.

Yu, H.-S., Chiang, C.-S. 1995. Morphology and origin of the Hongtsai Submarine Canyon West of the Hengchun Peninsula, Taiwan. J. Geol. Soc. China. 38(1), 81-93.

Yu, H.-S., Chang, J.-F. 2002. The Penghu Submarine Canyon off Southwestern Taiwan: morphology and origin. TAO. 13(4), 547-562.

Yu, H.-S., Liu, C.S., Lee, J.-T. 1992. The Kaohsiung Submarine Canyon: a modern aborted canyon and its morphology and echo character. Acta Oceangr. Taiwan. 28, 19-30.

Yu, H.-S., Lu, J.C. 1995. Development of the shale diapir-controlled Fangliao Canyon on the continental slope off southwestern Taiwan. J. Asian Earth Sci. 11(4), 265-276.

Zhang, Y., Liu, Z., Zhao, Y., Colin, C., Zhang, X., Wang, M., Zhao, S., Kneller, B. 2018. Long-term in situ observations on typhoon-triggered turbidity currents in the deep sea. Geology. 46(8), 675-678. https://doi.org/10.1130/G45178.1.

Zhao, L., Ouillon, R., Vowinckel, B., Meiburg, E., Kneller, B., He, Z. 2018. Transition of a hyperpycnal flow into a saline turbidity current due to differential diffusivities. *Geophys. Res.*

Lett. *45*,11875-11884. https://doi.org/10.1029/2018GL080150.

Zhong, G., Peng, X. 2021. Transport and accumulation of plastic litter in submarine canyons – The role of gravity flows. Geology. 49, 581-586. https://doi.org/10.1130/G48536.1.

Website

https://www.ncei.noaa.gov/maps/bathymetry/ (accessed 20 October 2021).